ADSORPTION, DESORPTION, AND STABILIZATION OF

ARSENIC ON ALUMINUM SUBSTITUTED FERRIHYDRITE

A Thesis

by

YOKO MASUE

Submitted to the Office of Graduate Studies of
Texas A&M University
in partial fulfillment of the requirements for the degree of

MASTER OF SCIENCE

December 2004

Major Subject: Soil Science

ADSORPTION, DESORPTION, AND STABILIZATION OF

ARSENIC ON ALUMINUM SUBSTITUTED FERRIHYDRITE

A Thesis

by

YOKO MASUE

Submitted to Texas A&M University
in partial fulfillment of the requirements
for the degree of

MASTER OF SCIENCE

Approved as to the style and content by:

Richard H. Loeppert (Chair)	Timothy A. Kramer (Member)
Charles T. Hallmark (Member)	Mark Hussey (Head of Department)

December 2004

Major Subject: Soil Science

ABSTRACT

Adsorption, Desorption, and Stabilization of Arsenic

on Aluminum Substituted Ferrihydrite.

(December 2004)

Yoko Masue, B.S., Texas A&M University

Chair of Advisory Committee: Dr. Richard H. Loeppert

Because of As toxicity, the complexity of its chemistry, and the recent lowering of the maximum contaminant level of As in municipal drinking water, there has been considerable interest for improved methods to remove As from water. Although Al and Fe hydroxides have been extensively studied as adsorbents for As removal during water treatment, coprecipitated Al:Fe hydroxides have received only minimal attention. The theoretical and experimental feasibility of coprecipitated Al:Fe hydroxide systems were evaluated by studying their mineralogy, stability, and As adsorption and desorption behavior.

The broad XRD peaks revealed that Al was substituted into the ferrihydrite structure and that this was the only major product up to about a 2:8 Al:Fe molar ratio. Gibbsite and bayerite were identified when Al content was higher. The rate of recrystallization of ferrihydrite into goethite and hematite was significantly reduced as Al substitution was increased.

In general, adsorption capacity of both As^V and As^{III} decreased with increase in Al:Fe molar ratio; however, similar As^V adsorption capacities were observed with Fe and

Al:Fe hydroxides with Al:(Al+Fe) molar ratios $\leq$ 0.20. Both As^{III} and As^{V} adsorption isotherms were effectively described by Langmuir and Freundlich equations. Adsorption maxima of As^{V} on Fe and Al:Fe hydroxides were observed at pH 3 to 7, and that of As^{V} on Al hydroxide was observed at pH 5.2, with significant decreases in adsorption with increase and decrease in pH. Adsorption maxima of As^{III} decreased by approximately 4 % for each 10 % increase in Al substitution up to 5:5 Al:Fe molar ratio. Adsorption maxima of As^{III} on Fe and Al:Fe hydroxides were observed at pH 8 to 9. As^{III} adsorption on Al hydroxide was negligible. Counterion Ca^{2+}, compared to Na^{+}, enhanced the retention of As^{V}, especially at pH > 7. Counterion concentration did not significantly affect As^{V} adsorption. Though phosphate desorbed both As^{V} and As^{III} from all Al:Fe hydroxides, quantitative desorption was never observed.

The results of this study indicate the possible utility of coprecipitated Al:Fe hydroxide in wastewater treatment. Based on adsorption/desorption behavior and stability of the Al:Fe hydroxide product, the preferred Al:Fe molar ratio was 2:8.

ACKNOWLEDGEMENTS

I wish to express my gratitude to all of the people who supported me through this study. I would like to thank Dr. R. H. Loeppert, chair of my advisory committee, for his enduring encouragement and support. I would especially like to express my appreciation to Dr. C. T. Hallmark for his support as my undergraduate advisor, soil judging coach, and a committee member. I would also like to thank my committee member Dr. Timothy Kramer for his time and assistance in understanding water treatment from the engineering point of view. I also thank Dr. B. K. Biswas for analytical support, and Dr. G. N. White and Dr. J. B. Dixon for assistance with mineral characterization and TEM study respectively. I also thank Lea Dell Morris for her assistance in obtaining library resources. I also acknowledge the help of my colleagues Brandon Lafferty and Sujin Yean. Thank you also to Joe Stobaugh and his family for their continuous support and encouragement. Most of all, I would like to thank my family in Japan for their enduring love. Without each of these people, this research would not have been possible.

TABLE OF CONTENTS

Page

LIST OF TABLES

LIST OF FIGURES

INTRODUCTION

Arsenic (As) introduced by natural processes or human activities can result in the contamination of water. Arsenic is sufficiently toxic that its removal from contaminated water is necessary if the water is to be consumed by humans. Many areas worldwide are facing serious health problems due to As in drinking water, and the U.S. is not an exception (Nriagu, 2002).

In October of 2001, the United States Environmental Protection Agency (USEPA) lowered the maximum contaminant level (MCL) of As in municipal drinking water to 10 μg_{As} L^{-1} from the previous 50 μg_{As} L^{-1} standard (USEPA, 2001). Due to this new regulation, the concentration of As in sludge and volume of As-containing sludge from water-treatment plants are expected to increase as more As is removed from water. This regulation has created demands for improved methods to remove As from water and to control As in sludge.

Al or Fe hydroxides are used traditionally as adsorption agents in water-treatment systems (Hammer and Hammer, 2001; Hering et al., 1996). Fe hydroxide is usually considered to be a superior As adsorbent compared to Al hydroxide (Cheng et al., 1994; Edwards, 1994; Gulledge and O'Connor, 1973; Hering et al., 1997; Tokunaga et al., 1999); however, Fe and As compounds in contaminated residue from water treatment can transform into soluble forms due to the redox processes involving Fe (Meng et al., 2001), while solubilities of Al-hydroxide minerals are not as strongly affected by redox processes. Al^{3+} substituted Fe^{3+} hydroxide might be able to combine the individual

---

This thesis follows the style and format of the Soil Science Society of America Journal.

advantages that the Al and Fe systems offer. An improved understanding of As

chemistry in mixed Al:Fe hydroxides could lead to improved methods of As treatment

and waste management. In addition, an improved understanding of As retention on Al^{3+}

substituted Fe^{3+} hydroxides is necessary to fully understand As retention in soil, since the

majority of soil Fe hydroxides are known to be Al substituted (Schwertmann and Taylor,

1989).

OBJECTIVES

The purpose of this study is to examine the potential application of mixed Al:Fe hydroxides in water treatment and residual stabilization by studying:

i.   the mineralogy of Al^{3+} substituted Fe^{3+} hydroxides and their stabilities against transformation, and

ii. the comparison of As^{V} and As^{III} adsorption/desorption behavior on mixed Al:Fe hydroxides as affected by Al substitution level, pH , and counterion (Ca^{2+} versus Na^{+}).

LITERATURE REVIEW

Arsenic in the Environment

The natural occurrence of As is typically associated with igneous and sedimentary rocks either containing or derived from sulfidic compounds, geothermal areas, and fossil fuels (Cullen and Reimer, 1989). Anthropogenic sources of As include by-products of mining, metal refining, fossil fuels, and agriculture (Cullen and Reimer, 1989). Extensive agricultural use of As in the U.S. has contributed to widespread contamination of the environment (Nriagu, 2000). The agricultural utilization of As has decreased drastically; however, traces of As can be found in food, water, air, and soil (Nriagu, 2000).

Chemical Properties of Arsenic

Arsenic has several possible oxidation states (-3, 0, +3, and +5), and its speciation is strongly influenced by redox potential. Both inorganic and organically-bound As are found in natural ecosystems; however, inorganic As species dominate in most aqueous systems (Francesconi and Kuehnelt, 2002). Dissolved inorganic As exists mostly as As^{III} (arsenite) or As^V (arsenate) oxyanions in natural systems. As^V usually dominates under oxidizing conditions, and As^{III} is stable under reducing conditions (Cherry et al., 1979; Smedley and Kinniburgh, 2002). Nonetheless, As^{III} and As^V often coexist in both reduced and oxidized environments due to the relatively slow kinetics of transformation between oxidation states. Transformation of As^{III} to As^V or vice versa can be either

abiotically or biotically mediated because the half cell potential of the As^V/As^{III} couple is within the redox-potential range of natural environments (Inskeep et al., 2002). For example, the logK^o of the As^V/As^{III} redox couple resides between those of NO_3^-/N_2 and $Fe(OH)_3/Fe^{2+}$. The logK^o values indicate that As^V will be reduced after N^V, but before Fe^{III} (Table 1).

In addition to redox potential, pH influences the predominant inorganic As species in aqueous systems (Table 2, Figure 1, and Figure 2). The pKa values indicate that inorganic As^{III} exists predominately as $H_3AsO_3^o$ and inorganic As^V exists as $H_2AsO_4^-$ and $HAsO_4^{2-}$ in most natural aqueous environments (Sadiq, 1997). Both As^{III} and As^V must be considered in the design of effective wastewater-treatment and waste-management systems. The speciation of As in soil is spatially variable and seasonally dependent, because pH, organic matter, biological activity, and redox potential, which are also spatially and seasonally variable, influence the localized distribution of As species (Inskeep et al., 2002; Masscheleyn et al., 1991b).

Table 1. Selected reduction half-reactions and thermodynamic constants (Sparks, 2003).

Half-reaction	$\log K^o$
$1/5NO_3^- + e^- + 6/5H^+ = 1/10N_2 + 3/5H_2O$	21.1
$1/2AsO_4^{3-} + e^- + 2H^+ = 1/2AsO_2^- + H_2O$	16.5
$Fe(OH)_3 + e^- + 3H^+ = Fe^{2+} + 3H_2O$	15.8

Table 2. The pKa values of As^{III} (H_3AsO_3) and As^V (H_3AsO_4) (Wagman et al., 1982).

	pKa_1	pKa_2	pKa_3
As^{III}	9.22	12.13	13.4
As^V	2.2	6.97	11.53
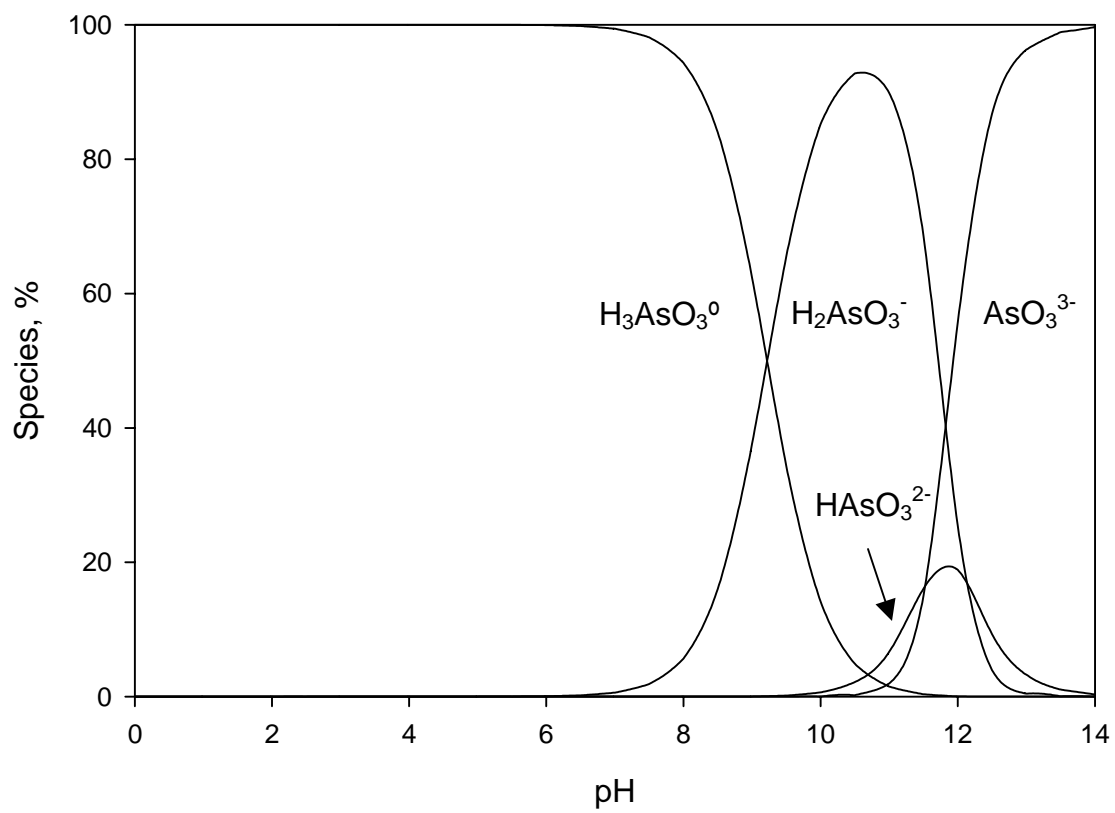
Figure 1. Speciation of As^{III} as a function of pH.
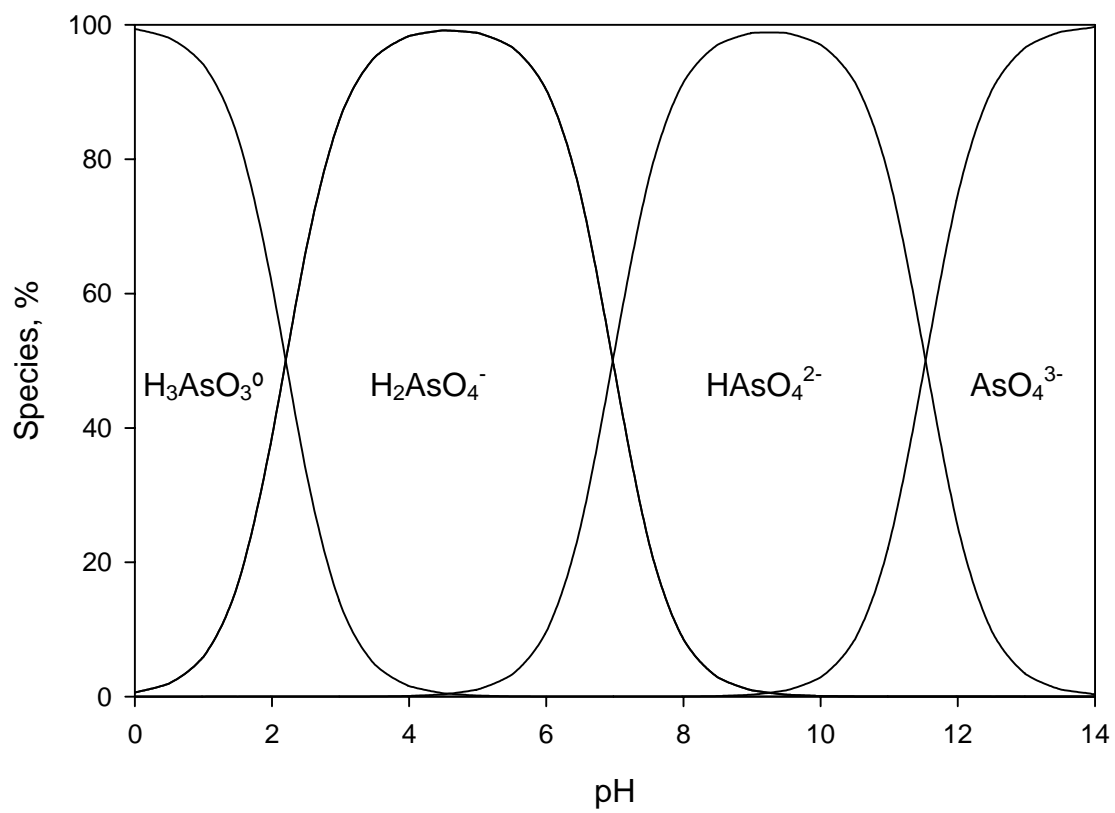
Figure 2. Speciation of As^V as a function of pH.

Arsenic Toxicity

Epidemiological evidence indicates that As intake is detrimental to humans (Smith et al., 2002a). Human response to As intake is highly variable as a result of numerous intrinsic or extrinsic factors such as As dose, genetic variants, nutritional status, age, pre-existing health conditions, and recreational habits (Anawar et al., 2002; NRC, 2001). Both cancer and noncancer health effects have been observed due to ingestion of As (NRC, 2001). The proposed mode of action for As carcinogenicity is through induction of chromosomal aberration without direct interaction with DNA (NRC, 2001). Chronic exposure of As can cause skin, liver, kidney, bladder, and lung cancers (NRC, 2001; Smith et al., 1992). Inhibition of cellular respiration is known to be the predominant mode of action for the noncancer effects of As (NRC, 2001). Several symptoms of acute non-cancerous As-related illnesses include fever, anorexia, hepatomegaly, melanosis, and cardiac arrhythmia. Neurotoxicity of both the peripheral and central nervous system is observed as a result of chronic exposure of As (Goyer and Clarkson, 2001).

The main source of inorganic As ingestion by humans is drinking water (Smith et al., 1992); therefore, the assurance of safe drinking water is critical. Effective water treatment is essential, because, at the previous MCL (50 μg_{As} L^{-1}), human health could be affected. Risk assessment by Smith et al. (1992) showed that the cancer mortality risk was as high as 13 per 1000 persons from the lifetime ingestion of 1 L/day of water containing 50 μg_{As} L^{-1}.

Critical Problems

In order to achieve the new MCL, some water-treatment plants will need to upgrade or install new treatment systems for effective As removal. The increase in cost to meet the new As standard in the U.S. is expected to be approximately $200 million annually (Smedley and Kinniburgh, 2002). Arsenic removal from water is challenging because of the complex reaction of As.

Not only As removal, but also disposal and stabilization of the residual materials generated from removing As, present technical challenges. Arsenic in sludge might be remobilized due to possible change in pH and redox potential, especially when Fe is used during the coagulation process. Meng et al. (2001) studied the effect of reductive transformations of As^V and Fe^{III} on As mobility from sludge generated by coprecipitation with $FeCl_3$. Upon reduction of the sludge, soluble As^{III} and As^V concentrations were increased, as reactive sites of the Fe hydroxide in the sludge were decreased as a result of dissolution. The reactive surface sites of Fe hydroxide controlled the adsorption and solubility of As^{III} and As^V in the sludge. The results of this study indicate that the biological reduction of sludge at land disposal sites might create a problem.

Bonding Mechanisms of Arsenic

The mode of As bonding on Fe hydroxides has been examined by extended X-ray absorption fine-structure spectroscopy (EXAFS) as well as Fourier transform infrared (FTIR) spectroscopy by various scientists (Fendorf et al., 1997; Goldberg and Johnson, 2001; Harrison and Berkheiser, 1982; Manceau, 1995; Manning et al., 1998; Sun and Doner, 1996; Waychunas et al., 1993). Waychunas concluded from EXAFS studies that As^V predominantly forms inner-sphere bidentate complexes on the ferrihydrite surface

(Figure 3), although about 30 % of all As-O-Fe complexes were monodentate complexes.

A bidentate-bridging bond of As^V on freshly prepared hydrous Fe oxide was also

observed by infrared spectroscopy (Harrison and Berkheiser, 1982). Goldberg and

Johnson (2001) utilized Raman and FTIR spectroscopy to detect inner-sphere

complexation of As^V and As^{III} with amorphous Fe oxides; however, outer-sphere

complexation of As^{III} was also detected. EXAFS results have shown that As^{III} also forms

inner-sphere, bidentate binuclear-bridging complexes at the goethite surface (Manning et

al., 1998).

EXAFS results have indicated that both As^{III} and As^V form inner-sphere bidentate

binuclear complexes with γ-Al_2O_3 (Arai et al., 2001). XANES spectra indicated the

formation of both inner-sphere and outer-sphere complexes of As^{III} on γ-Al_2O_3. As pH

was increased and ionic strength was decreased, outer-sphere As^{III} complexation

increased (Arai et al., 2001). Goldberg and Johnson (2001) observed in their Raman and

FTIR spectroscopy study that As^V forms inner-sphere complexes, and conversely that

As^{III} forms only outer-sphere complexes with amorphous Al oxide.
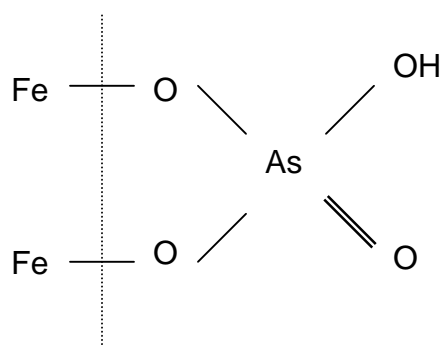
Figure 3. Schematic illustration of the bidentate binuclear surface structure of As^V on Fe hydroxide.

Macroscopic Adsorption Behavior of Arsenic

Adsorption of anions on metal oxide has been of great interest because of the importance of their removal during water treatment (Anderson et al., 1976). These adsorption processes are pH dependent, and protons in solution and on the colloid surface impact the rate of ligand exchange. Protons are available on the oxide surface below the point of zero charge (pzc) or they could originate from free H^+ at low pH or dissociation of the conjugate acid of an inorganic or organic anion (Hingston et al., 1971).

An understanding of As adsorption on poorly crystalline Al and Fe hydroxides is important because the solubility of As in natural environments is strongly influenced by reactions at these highly reactive surfaces. In addition, poorly crystalline Al and Fe hydroxides are expected to form during the coagulation processes of wastewater treatment with Fe salts [e.g., $FeCl_3$ and $Fe_2(SO_4)_3$] and Al salts [e.g., $Al_2(SO_4)_3$] (Hammer and Hammer, 2001).

Fe hydroxide has a high affinity for As, but the reaction is highly dependent on pH and the oxidation state of As. Studies have confirmed that As^V retention is usually higher at low pH, and maximum As^V retention is usually achieved in the pH range of 4 to 5 (Dixit and Hering, 2003; Hingston et al., 1971; Hsia et al., 1992; Pierce and Moore, 1982; Raven et al., 1998). The Fe-hydroxide surface is positively charged below the pzc (approximately at pH 8) due to increased protonation; therefore, conditions are favorable for adsorption of negatively charged As^V species (Hsia et al., 1992). In the case of As^{III}, adsorption on a Fe hydroxide increases as pH increases up to the adsorption maximum at approximately pH 8 to 10 (Ferguson and Anderson, 1974; Raven et al., 1998).

Negatively charged species dominate only above pH 9.2, due to the pKa of $H_3AsO_3^o$, and repulsive forces between As^{III} and Fe-hydroxide surfaces are only appreciable at pH>9.

As^V adsorbs on Al hydroxides, whereas, As^{III} is less readily adsorbed (Ferguson and Anderson, 1974). The adsorption of As^V by Al hydroxide is dependent on pH (Anderson et al., 1976; Ferguson and Anderson, 1974; Goldberg, 1986; Hingston et al., 1971). Retention of As^V was greater at lower pH; however, As^V adsorption decreased at pH<4.3 due to dissolution of amorphous Al hydroxide (Anderson et al., 1976).

In summary, the oxidation state of As and pH of the system are the most critical factors affecting the inorganic As adsorption behavior on poorly crystalline Al and Fe hydroxides.

Counterion Effect on Arsenic Adsorption

Counterions can strongly impact anion adsorption by soils and pure minerals (Bowden et al., 1977). Increase in valency of the cation contributes to a less negatively charged surface at pH values above the pzc of the mineral; therefore, under these conditions, anion sorption increases with increasing valency of the counterion (Bowden et al., 1977). An improved understanding of the counterion effect on As adsorption would be valuable in the design of improved methods for water treatment.

The presence of Ca^{2+} compared to Na^+ as the counterion has been reported to significantly enhance the retention of As^V in soils, due to decrease in negative charge character at the surfaces of soil minerals; however, As^{III} adsorption by soil was little affected by valency of the counterion (Smith et al., 2002b). Parks et al. (2003) observed that the presence of dissolved Ca^{2+} enhanced the retention of As by Fe hydroxide and Al hydroxide, and proposed that increased retention of As was due to reduced electrostatic

repulsion between the negatively charged surfaces and the As oxyanions. Reduction of

soluble As concentration was observed due to Ca arsenate precipitation at pH > 12 in a

mixture of $CaCl_2$ and Na arsenate with no sludge; however, improved retention of As was

also observed at pH < 12 in a sludge suspension with lime. Although a considerable

amount of Ca^{2+} was adsorbed on the Fe hydroxide surface, the possibility of cation

bridging was eliminated as a reason for the differences, by diffuse layer modeling (Parks

et al., 2003). Jing et al. (2003) observed the reduced mobility of As from Fe sludge upon

cement treatment, due to the formation of Ca arsenate. The pH of the cement-treated, As-

containing sludge was reported to be 11.32. Ca-arsenate precipitation in the cement-

treated sample and inner-sphere complexation of As^V with Fe oxide in the non cement-

treated sample were detected by both FTIR and EXAFS (Jing et al., 2003). Formation of

Ca-arsenate solid was especially evident at pH > 7.3 in the mixture of $Ca(OH)_2$ and the

As^V salt (Bothe and Brown, 1999). Depending on Ca/As molar ratio and pH, several

forms of Ca arsenate were formed (Table 3). The precipitation of Ca arsenate contributed

to reduce As leaching.

These results suggest that the use of Ca^{2+} for removal and stabilization of residual

materials could improve As retention.

Table 3. Ca arsenate hydrate precipitates (Bothe and Brown, 1999).

Solid-phase assemblage	Ca/As	pH
$Ca_4(OH)_2(AsO_4)_2 \cdot 4H_2O$	2.2 ~ 2.5	12.23 ~ 12.54
$Ca_5(AsO_4)_3OH$	1.9 ~ 1.67	12.63 ~ 9.77
$Ca_3(AsO_4)_2 \cdot 32/3H_2O$ $Ca_3(AsO_4)_2 \cdot 41/4H_2O$	1.67 ~ 1.5	11.18 ~ 7.32

Effect of Ionic Strength on Arsenic Adsorption

A strong dependence of ionic strength is typically shown by anions forming outer-sphere complexes (McBride, 1997). The adsorption of an anion (e.g., selenate) by outer-sphere complexation is suppressed by competition with non-specifically adsorbed anions, such as Cl^- and NO_3^- (McBride, 1997). Inner-sphere complexes are less affected by ionic strength Adsorption of anion (e.g., selenite) might be independent of ionic strength due to strong bonding. Increase in anion adsorption (e.g., borate) with increase in ionic strength has also been observed (McBride, 1997). This phenomenon is explained by the contraction of the diffuse double layer, which allows the anion to more readily approach the negatively charged oxide surface.

Goldberg and Johnson (2001) studied As adsorption on amorphous Fe and Al oxides in 0.01 to 1.0 M NaCl by mean of adsorption envelopes. As^V adsorption by amorphous Fe and Al oxides was independent of ionic strength, which is indicative of inner-sphere complexation. As^{III} adsorption by amorphous Al oxide decreased as ionic strength was increased, but was only slightly dependent on ionic strength above pH 6. In summary, As^{III} adsorption on Al and Fe oxide surfaces was more strongly influenced by ionic strength than is As^V adsorption.

Gupta and Chen (1978) studied the effect of ionic strength on adsorption of As by activated alumina. Adsorption isotherms of As^{III} at pH 6.5 to 8.5 and As^V at pH 6 to 7 were obtained in fresh water, diluted seawater, 0.67 M NaCl, and seawater. As^V and As^{III} adsorption on activated alumina decreased as the ionic strength was increased. For example, As^V adsorption capacity of alumina was 4.11 $mg_{As^V} g^{-1}$ adsorbent in fresh water,

whereas, adsorption capacity was 0.81 $mg_{As^V} g^{-1}$ adsorbent in seawater. In addition, the kinetics of As^{III} and As^V adsorption by alumina was slower with higher ionic strength.

Goldberg and Johnson (2001) and Gupta and Chen (1978) obtained different results with As^V adsorption on Al oxides as affected by ionic strength. Their results indicate the complexity of the systems. The observed differences in adsorption might be due to differences in experimental conditions such as adsorbent mineralogy, counterion, pH, and As to adsorbent ratio. As^V adsorption by Al oxides should not be affected by ionic strength, since the predominant mode of bonding between As^V and Al oxide is known to be inner-sphere complexation according to the spectroscopic studies discussed previously.

Adsorption Modeling

Adsorption reactions have been described using a variety of models such as the Langmuir and Freundlich equations. The Langmuir equation was first developed in 1918 by Irving Langmuir to describe the adsorption of gaseous molecules on a homogeneous planar surface, using several assumptions (Sparks, 2003). Most of these assumptions are not met in heterogonous soil systems (Veith and Sposito, 1977). Although the Langmuir equation has been widely used to model adsorption in soil systems, it should only be used for qualitative purposes. In the Langmuir expression, the free energy of adsorption is assumed to be independent of surface coverage (Reed and Matsumoto, 1993). Monolayer coverage of the adsorbate at high C values and linear adsorption at low C values can be described by the Langmuir isotherm. The Langmuir equation is presented as Equation [1], and it can be transformed into a linear expression Equation [2] with 1/b as the slope and $1/K_L b$ as the intercept (Sparks, 2003). The K_L and b parameters are usually

$$Q = (K_L C b) / (1 + K_L C) \qquad [1]$$

$$C/q = (1 / K_L b) + (C / b) \qquad [2]$$

,where

C = concentration of As in solution
q = amount of As adsorbed
b = calculated adsorption maximum
K_L = constant related to binding strength

considered to be a function of pH, ionic composition, and ionic strength. The K_L and b

values are influenced by the electric double layer and the amphoteric behavior of the

surface (Reed and Matsumoto, 1993).

The Freundlich equation was first developed to describe gas-phase adsorption and

solute adsorption (Sparks, 2003). Unlike the Langmuir equation, the Freundlich equation

is not theoretically based. The Freundlich equation is presented as Equation [3], and it

can be transformed into a linear Equation [4] with N as the slope and $\log K_F$ as the

intercept (Essington, 2004). In a broad sense, both K_F and N are considered as constants

$$q = K_F C^N \qquad [3]$$

$$\log q = N \log C + \log K_F \qquad [4]$$

where,

C = concentration of As in solution
q = amount of As adsorbed
K_F = adjustable parameter
N = adjustable parameter ($0 \leq N \leq 1$)

characterizing the adsorption capacity (Yang, 1998). The constants K_F and N are also

related to the strength of the adsorptive bond and bond distribution, respectively (Reed

and Matsumoto, 1993). It has been shown mathematically that N can be regarded a

measure of heterogeneity of adsorption sites (Yang, 1998). For example, surface site

heterogeneity increases as N approaches 0 (Essington, 2004). When N > 1, bond energies increase with surface density (Reed and Matsumoto, 1993). When N < 1, bond energies decrease with surface density. When N = 1, all surface sites are equivalent, and the function is mathematically equivalent to the Langmuir isotherm with b approaching infinity or K_L << 1. Adsorption behavior with N < 1 is most common due to decreased adsorption with increasing surface density (Reed and Matsumoto, 1993). In natural systems, N is considered to be in between 0 and 1. The disadvantage of the Freundlich equation is that it cannot be used to predict an adsorption maximum (Sparks, 2003). K_F and N values are also influenced by the electric double layer and the amphoteric behavior of the surface.

Mineralogy of Mixed Al:Fe Hydroxides

The mineralogy of the adsorbent is a critical factor for As removal and stabilization of residuals. Hematite and goethite are commonly found as products of recrystallization of ferrihydrite (Schwertmann and Murad, 1983). Hematite formation results from solid-phase transformation, while goethite formation occurs via dissolution of ferrihydrite followed by reprecipitation, usually from $Fe(OH)_2^+$ and $Fe(OH)_4^-$. Formation of hematite as opposed to goethite is preferred at pH 7 to 8, where the solubility of ferrihydrite is at the approximate minimum, whereas, maximum formation of goethite as opposed to hematite has been reported at pH 4 and pH 12 (Schwertmann and Murad, 1983). Preferential formation of hematite over goethite from Al-substituted ferrihydrite has been reported by Schwermann et al. (2000), which indicates relatively slow dissolution of the Al-substituted ferrihydrite.

Colombo and Violante (1996) synthesized a series of mixed Al:Fe hydroxides at various Al:Fe molar ratios, by titrating mixtures of dissolved $Fe(NO)_3$ and $Al(NO)_3$ with NaOH to pH 5, and studied the recrystallization of the products. Upon incubation of the mixed Al:Fe hydroxides, changes in mineralogy were observed depending on the initial Al:Fe molar ratio and temperature. Gibbsite, hematite, and goethite were detected as products of the incubation; however, high stabilities against transformation were observed at Al:Fe molar ratios of 2:8 to 5:5. This trend indicates a significant advantage of Al:Fe hydroxides as an adsorbent in water treatment, since higher surface area is favorable for anion adsorption, and the increased stability of the poorly crystalline phases would decrease the potential for As release with time.

Arsenic Removal by Coagulation of Al and Fe Salts

Several techniques, such as ion exchange, adsorption by activated alumina and activated carbon, ultrafiltration, reverse osmosis, and precipitation with or adsorption by metal oxides followed by coagulation, have been used for removal of As from waste water (Leist et al., 2000). Coagulation by Al or Fe salts is commonly used to remove As in conventional water-treatment plants (Cheng et al., 1994; Hammer and Hammer, 2001; Hering et al., 1996).

Arsenic is removed from wastewater much more efficiently as As^V than as As^{III} (Cheng et al., 1994; Gupta and Chen, 1978; Hering et al., 1997; Tokunaga et al., 1999). As^{III} is not as effectively removed by Al compared to Fe systems; however, As^V can be removed by coagulation with Al hydroxide (Tokunaga et al., 1999). Fe coagulation compared to Al coagulation is generally more effective in removing As (Cheng et al., 1994; Edwards, 1994; Gulledge and O'Connor, 1973; Hering et al., 1997; Tokunaga et

al., 1999). Batch studies of the removal of As^V by coagulation with $Fe_2(SO_4)_3$ and alum have suggested that As^V is more effectively removed by $Fe_2(SO_4)_3$ than by alum; however, a larger coagulant dose improved the removal of As^V in both scenarios (Cheng et al., 1994; Gulledge and O'Connor, 1973). As^V removal by Fe coagulation was most effective at pH < 7, and its removal was independent of pH between 5.5 and 7.0 (Cheng et al., 1994; Gulledge and O'Connor, 1973). Removal of As^V by Al hydroxide was highly pH dependent at pH < 7 (Cheng et al., 1994; Gulledge and O'Connor, 1973). These observations are consistent with the adsorption studies of As^{III} and As^V on Fe and Al hydroxides discussed above.

Desorption of Arsenic by Phosphate

Phosphate and As^V have similar chemical properties, and compete for the binding sites of Al and Fe hydroxides; therefore, a reduction of As^V retention on Al and Fe hydroxides has been reported in the presence of phosphate (Hingston et al., 1971; Jackson and Miller, 2000; Jain and Loeppert, 2000; Liu et al., 2001; Manning and Goldberg, 1996; Violante et al., 2002). Because of this phenomenon, extraction by high phosphate solution has been utilized to assess As in soil (Alam et al., 2001; Davenport and Peryea, 1991; Woolson et al., 1973). In waste disposal sites, the presence of phosphate can significantly impact leaching of As from residual materials due to this phenomenon.

Desorption of As by phosphate is dependent on oxidation state of As, pH, and adsorbent. The kinetics of As^{III} and As^V desorption from goethite exhibited different trends. As^{III} desorption reached an approximate maximum within 4 h; however, As^V was continuously desorbed up to 100 h (Loeppert et al., 2002). Liu et al. (2001) studied the

desorption of As^V by phosphate and desorption of phosphate by As^V from goethite at an As^V to phosphate molar ratio of 1:1 in the pH range of 3.0 to 8.5. The efficiency of phosphate desorption by As^V was higher than that of As^V desorption by phosphate at any given pH, and the effect of pH on desorption was greater with phosphate desorption by As^V. This result is indicative of a stronger affinity of As^V on goethite relative to that of phosphate.

The efficiency of As^V desorption is also affected by adsorbent, since more phosphate than As^V was adsorbed on goethite, whereas, more As^V than phosphate was adsorbed on gibbsite at an As^V to P molar ratio of 1:1 at both pH 4 and 7 (Violante et al., 2002). This result indicates that there could be a difference in As-release potential from residual material generated from Al and Fe coagulation.

Arsenic Analysis by Flow-Injection Hydride-Generation Flame-Atomic-Absorption Spectroscopy

Flow-injection hydride-generation atomic-absorption spectroscopy is a widely accepted analytical technique to analyze As at trace levels. The method involves reaction of the sample in an acid medium with sodium borohydride ($NaBH_4$) to convert As^{III} into gaseous arsine (AsH_3) as summarized in Equation [5] (Masscheleyn et al., 1991a). Arsine is transported by an inert gas such as argon to an atomizer of an atomic-absorption spectrophotometer, where gas-phase atoms are generated. As^V species are reduced to As^{III} when solution pH is less than 1, which is then converted to AsH_3. Because As^V must be reduced to As^{III} before the formation of AsH_3, the kinetics of AsH_3 formation from As^V is slower than that from As^{III}. The formation of AsH_3 from As^V versus As^{III} is pH dependent, since As species must to be fully protonated to allow the reduction

reaction for the formation of AsH_3 (Carrero et al., 2001). The advantage of As analysis by this technique is the low detection limit.

$$NaBH_4 + H_3AsO_3 + HCl \rightarrow AsH_3(g) + H_3BO_3 + H_2 + NaCl \qquad [5]$$
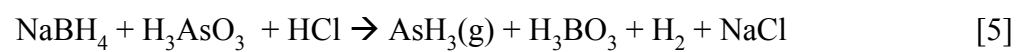
MATERIALS AND METHODS

Chemicals

Reagent grade chemicals were used in all studies. As^V and As^{III} were obtained

from Alpha Aesar (Ward Hill, MA) as As_2O_5 and As_2O_3, respectively. As^V stock

solution was prepared in gently heated deionized water. As^{III} stock solution was prepared

under N_2 atmosphere with a minimum amount of NaOH added to ensure complete

dissolution of As_2O_3 at room temperature.

Synthesis of Ferrihydrite and Al-substituted Analogs

A series of Al-substituted hydroxides were prepared at 0:1, 3:97, 1:9, 2:8, 3:7, 4:6,

5:5, and 1:0 Al:Fe molar ratios. The two-line ferrihydrite method of Schwertmann and

Cornell (1991) was used except ferric nitrate $[Fe(NO_3)_3]$ and aluminum nitrate $[Al(NO_3)_3]$

were hydrolyzed using sodium hydroxide (NaOH) rather than potassium hydroxide

(KOH).

In order to examine the counterion effect, 0:1 and 2:8 Al:Fe hydroxides were

prepared using saturated calcium hydroxide $[Ca(OH)_2]$ or 0.1 M NaOH to adjust the

appropriate $Al(NO_3)_3 : Fe(NO_3)_3$ mixtures to pH 7 to 8, to obtain systems with calcium

(Ca) or sodium (Na) as the only counterion. The initial concentrations of the hydroxides

were 0.004 mol_{Al+Fe} L^{-1}. The volumes of saturated $Ca(OH)_2$ or 0.1 M NaOH solution

needed were recorded to determine the accurate concentrations of Ca and Na in the

systems. The saturated $Ca(OH)_2$ solution was prepared under nitrogen (N_2) atmosphere

at room temperature with boiled deionized water to avoid the formation of calcium

carbonate $(CaCO_3)$ in the presence of carbon dioxide (CO_2). The $Ca(OH)_2$ solution was

immediately filtered through a 0.2 μm nominal pore-size membrane filter to remove any

precipitated $CaCO_3$. The concentration of $Ca(OH)_2$ was determined by titration with hydrochloric acid (HCl). The $Ca(OH)_2$ solution was prepared as close to the time of hydroxide synthesis as possible to minimize $CaCO_3$ formation.

Characterization of Synthesized Ferrihydrite and Al-substituted Analogs

X-ray Diffraction

Each hydroxide in a Nalgene bottle was shell frozen with liquid nitrogen. Samples were then freeze-dried. X-ray diffraction analyses were performed on front loaded power mounts with graphite monochromatized CuKα radiation from a Philip's X-ray diffraction unit, using a 0.05º step collected for 5 s from 2 to 65 º2θ.

Transmission Electron Microscopy

The morphology and aggregation of the hydroxides were examined using transmission electron microscopy, on a JEOL 2010 TEM. To prepare the samples for examination, dilute suspensions of hydroxides were sonicated in an ice bath for 1 h, and mounted on silicon grids, which were first treated with chloroform.

Point of Zero Salt Effect

The point of zero salt effect (PZSE) and charge characteristics of each product were determined using a batch titration procedure (Van Raij and Peech, 1972). During the PZSE determination, the hydroxides were suspended in 1, 0.01, and 0.0001 M NaCl. The concentration of Al+Fe in the suspensions was fixed at 0.01 mol_{Al+Fe} L^{-1}. The pH values of separate samples were adjusted from 3 to 11 in 0.4 pH unit intervals, using HCl and NaOH. Following 2 h equilibration on a platform shaker, samples were centrifuged, and equilibrium pH values were obtained while purging with N_2 gas. The PZSE curve was formed using the amount of HCl or NaOH added on the y-axis and pH on the x-axis.

Following filtration, the supernatant was analyzed by AAS to determine the concentration of dissolved Al and Fe to allow for correction of H^+ and OH^- consumption due to dissolved Al and Fe species.

Stability of Ferrihydrite and Al-substituted Analogs

The tendency of the 0:1 and 2:8 Al:Fe hydroxides to transform into crystalline materials, and the mineralogy of the precipitated phases were examined following incubation at pH 4 and 10, using the procedure summarized in Figure 4. Samples were prepared with no added As^V and with an As:(Al+Fe) molar ratio of 0.05:1, and the pH adjusted by adding HCl or NaOH. Samples were then incubated at 70^oC, and subsamples were taken after 12, 24, 48, and 96 h. The solution of As^V was added to the subsamples which were incubated without As^V, and deionized water was added to the samples which were incubated with As^V to ensure equal concentrations of As, Al and Fe in the two sets of samples. The subsamples were adjusted to pH 7.0 with HCl or NaOH, and they were aged at room temperature for 2 h to allow adsorption of As^V. Samples were centrifuged, filtered, and analyzed for total dissolved As by FI-HG-AAS. The residual hydroxides were washed with deionized water, freeze dried and then analyzed using XRD. Samples were also extracted in the dark for 2 h with 0.2 M ammonium oxalate at pH 3.0 to determine the proportion of poorly crystalline Fe hydroxide (Loeppert and Inskeep, 1996).

Hydroxides

Incubate with As^V at pH 4 and 10 at 70°C

Incubate without As^V at pH 4 and 10 at 70°C

Subsamples- 12, 24, 48, and 96 h

Subsamples- 12, 24, 48, and 96 h

Add DI water, then adjust pH to 7
Age at RT for 2 h.

Add As^V, then adjust pH to 7
Age at RT for 2 h.

Centrifuge, filter, then total As analysis

Centrifuge, filter, then total As analysis

XRD analysis of residual, and
ammonium oxalate extraction
of residual at pH 3 in the dark

XRD analysis of residual, and
ammonium oxalate extraction
of residual at pH 3 in the dark

Figure 4. Experimental procedure for determination of stability of the 0:1 and 2:8 Al:Fe hydroxides.

Analysis

Arsenic was analyzed by FI-HG-FAAS using a Perkin Elmer AA400 atomic absorption spectrophotometer (Perkin Elmer Corporation, Norwalk, CT), with an electrodeless discharge lamp (EDL) as the source of radiation. $NaBH_4$ (1.5 %) in 0.5 % NaOH was used as the reductant, and 5 M HCl was used as the eluent during flow injection, to convert the As species in solution to AsH_3 (Samanta et al., 1999). Gaseous AsH_3 was separated from the aqueous eluent using an ice water cooling system and a gas/liquid separator, and transported to a quartz cell in FAAS. An air-acetylene flame was used with a 10-cm burner head. The atomized As was analyzed at 193.7 nm wavelength. The As detection limit was 0.5 μg_{As} L^{-1} with a 95 % confidence level. Analysis of Al and Fe was also conducted using the Perkin Elmer AA400 atomic absorption spectrophotometer. Nitrous oxide-acetylene and air-acetylene flames were used for Al and Fe analyses, respectively. The matrix of the standard solutions was matched to that of the samples in all cases.

Arsenic Adsorption Isotherms

Adsorption isotherms are used to present the adsorbate/adsorbent relationship and are often represented as plots of the quantity of adsorbate retained by solid adsorbent as a function of the equilibrium concentration of that adsorbate at fixed pH and ionic strength (McBride, 1994). The capacities of 0:1, 2:8, 5:5, and 1:0 Al:Fe hydroxides to adsorb As^{III} and As^{V} were studied by means of adsorption isotherms at pH 5 and 8. The reactions were conducted in 0.1 M NaCl ionic strength buffer, as a batch experiment with As:(Al+Fe) molar ratios ranging from 0.0125:1 to 0.5:1. The Al+Fe concentration was fixed at 267 μmol_{Al+Fe} L^{-1} and As concentrations ranged from 3 to 133 μmol_{As} L^{-1}, in

order to achieve the desired range of As:(Al+Fe) molar ratios. The pH values of separate

samples were adjusted by adding HCl or NaOH, and each sample was brought to 30 mL

final volume. Following equilibration for 24 h on a rotary shaker, the samples were

centrifuged and filtered through 0.2 μm nominal pore-size membrane filters. Supernates

were analyzed for total As by FI-HG-FAAS.

Arsenic Adsorption Modeling

Langmuir Adsorption Isotherms

Adsorption isotherm data were evaluated using the Langmuir equation (Equation

[2]). C/q versus C was plotted, and linear regression analyses were performed. The

calculated As adsorption maximum, b, and the constant related to binding strength, K_L,

were examined. Because there is a large potential of analytical error with higher

As:(Al+Fe) molar ratios, all of the points over 0.2 As:(Al+Fe) molar ratio were excluded

for the Langmuir calculations.

Freundlich Adsorption Isotherms

Adsorption isotherm data were also evaluated using the Freundlich equation

(Equation [4]). Log q versus log C was plotted, and linear regression analyses were

performed. The calculated empirical constants, N and K_F, were examined. All of the

points over 0.2 As:(Al+Fe) molar ratio were excluded for the Freundlich calculations.

Arsenic Adsorption Envelopes

Adsorption envelope is used to evaluate the influence of pH on adsorption at ionic

strength and constant adsorbent and adsorbate concentrations. The effect of pH and Al

substitution on As^{III} and As^V adsorption was examined using adsorption envelopes.

Adsorption envelopes of As^{III} and As^V on 0:1, 2:8, 5:5, and 1:0 Al:Fe hydroxides were

obtained in 0.1 M NaCl ionic strength buffer, as a batch experiment at a As:(Al+Fe) molar ratio of 0.05:1 (13.35 μmol_{As} L^{-1} and 267 μmol_{Al+Fe} L^{-1}). The pH values of individual samples were adjusted between 3 and 11 at 0.4 pH unit intervals by adding HCl or NaOH, and each sample was brought to 30 mL final volume with deionized water. Following 24 h equilibration on a platform shaker, samples were centrifuged, and the pH values of the supernate were obtained. The samples were filtered through 0.2 μm nominal pore-size membrane filters and analyzed by FI-HG-FAAS. The adsorption envelopes were plotted using the proportion of the total adsorbed As (%) on the y-axis and pH on the x-axis.

Arsenic Adsorption as Affected by Counterion

Adsorption envelopes and adsorption isotherms of As^V on 0:1 and 2:8 Al:Fe hydroxides in Ca and Na systems were obtained to examine the counterion effect. The procedures discussed previously were used, except the hydroxides prepared with $Ca(OH)_2$ and NaOH were used to maintain exclusively Ca and Na systems. The concentration of counterion, Ca^{2+} and Na^+, were adjusted using $Ca(NO_3)_2$ and $NaNO_3$ salt solutions.

For the adsorption envelopes, the suspensions were fixed at 0.1, 0.01, and 0.001 mol_{Ca} L^{-1} and mol_{Na} L^{-1} to examine the effect of counterion concentration. The adsorption envelopes were obtained at both 0.025:1 and 0.1:1 As:(Al+Fe) molar ratios by varying As^V concentration (3.35 and 13.35 μmol_{As} L^{-1}, respectively) with fixed Al+Fe concentration (133.5 μmol_{Al+Fe} L^{-1}). For adsorption isotherms, the suspensions were fixed at 0.1 mol_{Ca} L^{-1} and mol_{Na} L^{-1}. Nitrate salts were used since $Fe(NO_3)_3$ and $Al(NO_3)_3$ were used to prepare the hydroxides. The Al+Fe concentration was fixed at

267 μmol_{Al+Fe} L^{-1}, and As concentrations ranged from 3 to 133 μmol_{As} L^{-1} in order to achieve the desired As:(Al+Fe) molar ratios. Separate samples were adjusted by adding HNO_3 or NaOH to obtain pH values within the range of 3 to 11 in 0.4 pH unit intervals for adsorption envelopes and at pH 5 and 8 for adsorption isotherms. The amount of NaOH used to adjust pH in Ca systems was considered to be insignificant.

Arsenic Desorption Envelopes

The effect of pH and Al substitution on As^{III} and As^V desorption by competitive ligand change with phosphate was examined by mean of desorption envelopes. Arsenic was first adsorbed on 0:1, 2:8, 5:5, and 1:0 Al:Fe hydroxides in a 0.1 M NaCl ionic strength buffer at an As:(Fe+Al) molar ratio of 0.05:1 (26.7 μmol_{As} L^{-1} and 534 μmol_{Al+Fe} L^{-1}) for 24 h. As^V was adsorbed at pH 5.2, and As^{III} was adsorbed at pH 8.5. These pH values were used since the adsorption maxima of As^V and As^{III} were found at approximately pH 5.2 and pH 8.5, respectively, for all hydroxides in the adsorption envelope study. Sub-samples were taken from each suspension before the addition of phosphate to determine the amount of As adsorbed after 24 h. Following As adsorption, desorption envelopes were obtained as a batch experiment. Ten milliliters of 0.2 M sodium phosphate solution, with pH preadjusted from 3 to 11 in 0.4 pH unit intervals, were added to each bottle containing 10 ml of As-treated hydroxide suspension. Deionized water was added to a separate As-treated hydroxide suspension as a control to evaluate whether desorption of As was due to mechanical agitation. The total concentration of As during the desorption reaction was 13.35 μmol_{As} L^{-1}, and sodium phosphate concentration was 0.1 M (1:7491 As:P molar ratio). Each sample was allowed to react for 24 h on a rotary shaker. Upon completion of the reaction, samples were

centrifuged, and the pH values of the supernatant solutions were obtained. The samples were filtered through 0.2 μm nominal pore-size membrane filters, and analyzed by FI-HG-FAAS. The desorption envelopes were plotted using the percent of As desorbed on the y-axis and pH on the x-axis.

RESULTS AND DISCUSSION

Characterization of Synthesized Ferrihydrite and Al-substituted Analogs

X-ray Diffraction

Differences in XRD patterns of synthesized Al:Fe hydroxides were observed with the varying Al:Fe molar ratios. The 2:8 Al:Fe hydroxide resulted in an XRD pattern almost identical to that of ferrihydrite, except the peaks were boarder (Figure 5). The peak widths at half height were 7.55, 8.35, and 9.37 º2θ for the 0:1, 2:8, and 3:7 Al:Fe hydroxides, respectively. XRD line broadening can be indicative of both smaller crystal size and a reduction in long-range order of the materials. The XRD pattern of the 2:8 Al:Fe hydroxide suggests that this material has a smaller particle size than that of the 0:1 Al:Fe hydroxide. A smaller particle size of goethite (α-FeOOH) was observed with increasing Al substitution, by both XRD and TEM analysis (Fey and Dixon, 1981; Schulze and Schwertmann, 1984). The ionic radius of Al^{3+} (0.53 Å) is slightly smaller compared to that of Fe^{3+} (0.65 Å); therefore, isomorphous substitution of Al^{3+} for Fe^{3+} would result in a decrease in average size of the unit cell (Schulze, 1984), which would result in peak shifts in the XRD pattern. In the current study, there was a small tendency toward shift to higher º2θ at the higher Al contents. The broad peak at approximately 62 º2θ also shifted towards higher º2θ with the higher Al contents. With the 4:6 and 5:5 Al:Fe hydroxides, there was an indication of the peak splitting of the 35 º2θ peak, which is probably due to the presence of a separate Al-rich phase at the higher Al contents. Heterogeneous distribution of Al^{3+} within the structure could also contribute to peak broadening. Small peaks of gibbsite [γ-Al(OH)$_3$], which increased in size with time,
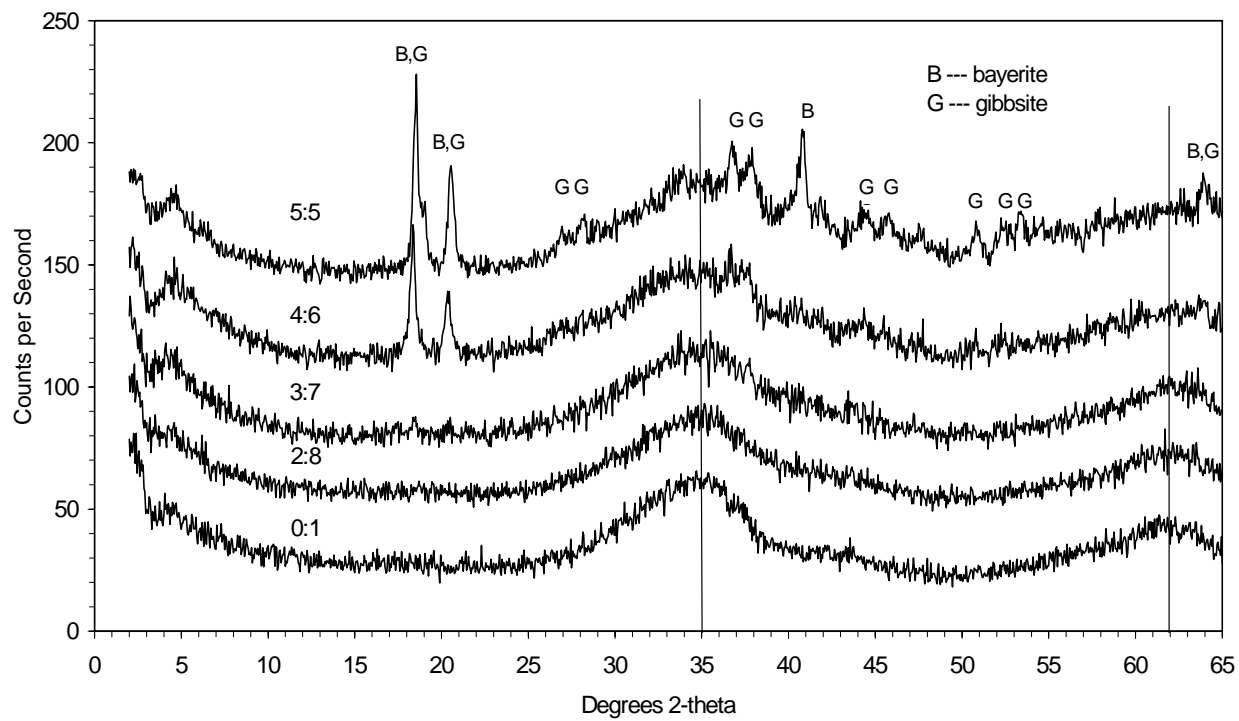
Figure 5. XRD patterns of freshly prepared hydroxides at various Al:Fe molar ratios.

were observed with the 3:7 Al:Fe hydroxide (Figure 6). After 1 month aging at 2ºC, a white precipitate was observed in the storage bottle. Only poorly crystalline material was detected with the 0:1 and 2:8 Al:Fe hydroxides, even upon aging. Bayerite and gibbsite were both identified as products of the synthetic systems with Al:(Al+Fe) molar ratios greater than 0.4 (Figure 5 and Figure 7). At 0.4 Al:(Al+Fe) molar ratio, only a small peak of bayerite was observed at 40.7 º2θ (Figure 5), which indicates that the predominant crystalline product was gibbsite. Although the 1:0 Al:Fe hydroxide contained significant amounts of both bayerite and gibbsite, the broad background peaks were indicative of poorly crystalline Al hydroxide (Figure 7). Crystalline Fe hydroxide minerals were not found in any of the synthesized materials. In summary, Al incorporates quantitatively into the poorly crystalline ferrihydrite structure, with no evidence of a crystalline Al hydroxide phase, up to approximately 0.20 Al:(Al+Fe) molar ratio.

Gibbsite and bayerite are composed of identical structural units, that is, two planes of close-packed OH^- with Al^{3+} between them (Hsu, 1989). These $Al(OH)_3$ sheets are held together by hydrogen bonding. Two-thirds of the octahedral sites are filled with Al^{3+}, to form a planar hexagonal ring structure, in which each Al^{3+} shares six OH^- with three other Al^{3+} ions, and each OH^- is bridged between two Al^{3+} ions. In gibbsite, one-half of the OH^- groups point away, perpendicularly, from the octahedral sheet, while half of the OH^- groups on adjacent sheets reside directly opposite from the perpendicular OH^-
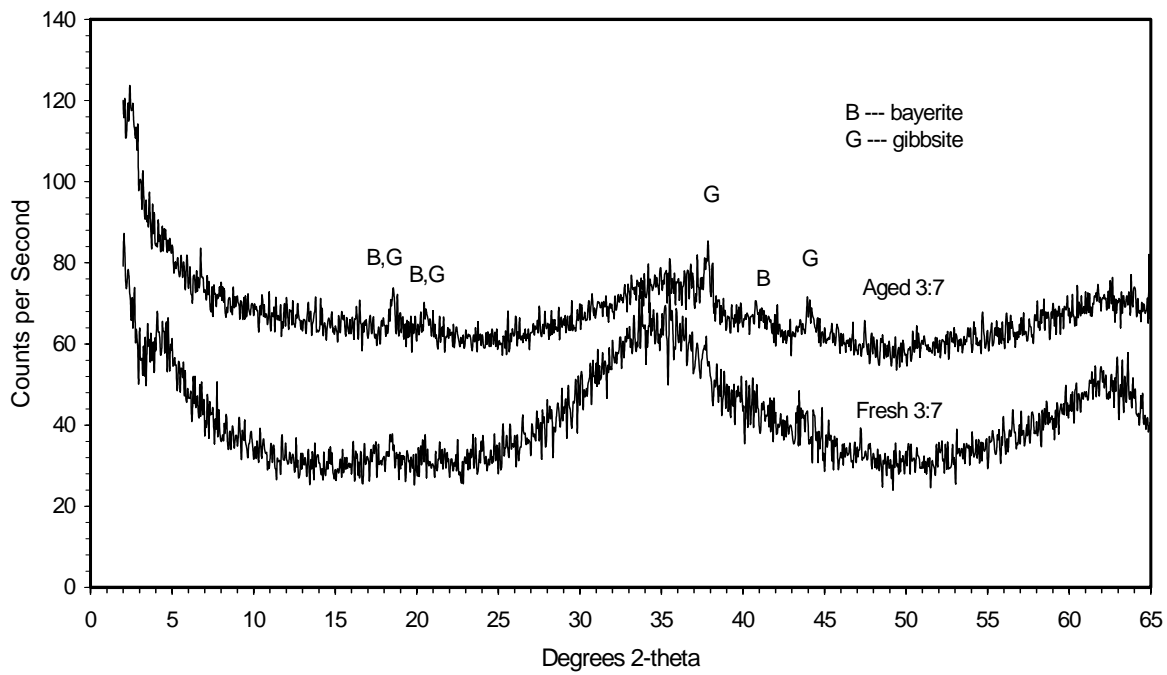
Figure 6. XRD patterns of fresh 3:7 Al:Fe hydroxides and 3:7 Al:Fe hydroxides aged at 2ºC for 1 month.
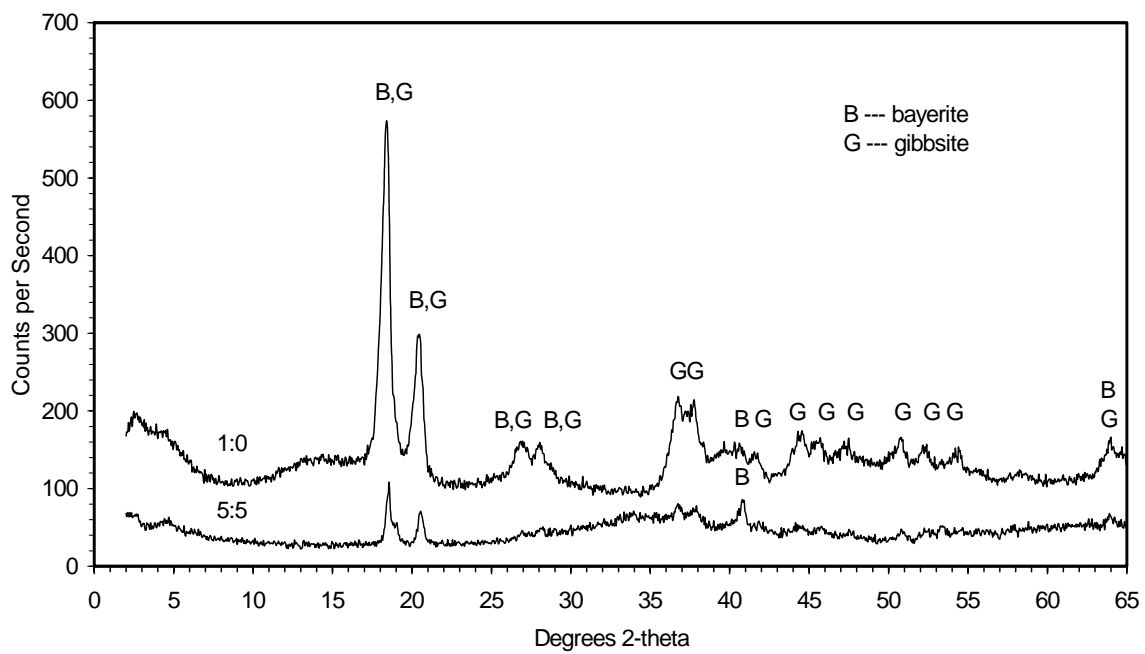
Figure 7. XRD patterns of 1:0 and 5:5 Al:Fe hydroxides.

groups but parallel to the basal plane. The OH^- planes of gibbsite have an AB-BA-AB-BA stacking arrangement (Figure 8) (Wefers and Bell, 1972). Gibbsite has zero net permanent charge because there is no significant isomorphous substitution of Al^{3+} by divalent cations (Huang et al., 2002). In bayerite, the perpendicular OH^- groups in one plane lie in the depression of the adjacent plane (Wefers and Bell, 1972). As a result, the crystal lattice of bayerite is composed of layers of OH^- with an AB-AB-AB stacking arrangement, as opposed to the AB-BA-AB-BA sequence for gibbsite (Figure 9).

The hue of the hydroxides became less red (10R to 5YR), and value and chroma increased as Al substitution increased (Figure 10). In the case of hematite (α-Fe_2O_3), both value and chroma increased as Al substitution increased; however, hue was independent of Al substitution (Kosmas et al., 1986). For goethite, value and hue decreased as Al substitution increased, although chroma was independent of Al substitution (Kosmas et al., 1986). The variation in color of the Fe oxides and hydroxides are often indicative of differences in mineral structure (Schwertmann and Taylor, 1989). Darker colors (low values) are often exhibited with condensed masses (Schwertmann and Taylor, 1989), which indicates that the 0:1 Al:Fe hydroxide was likely to be most condensed compared to the Al substituted hydroxide.
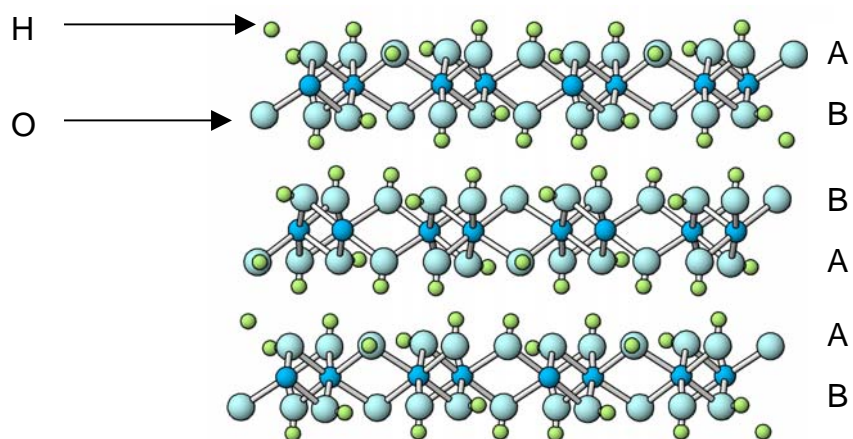
Figure 8. Structure of gibbsite.
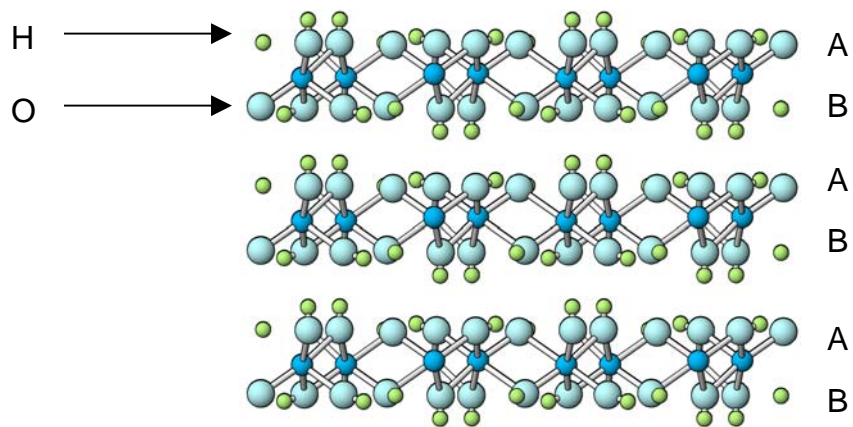
Figure 9. Structure of bayerite.
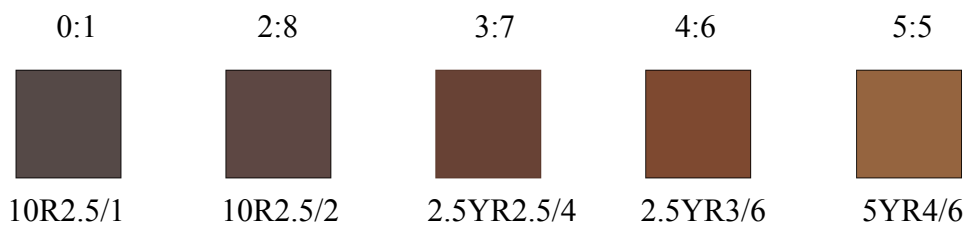
Figure 10. Colors of freeze dried ferrihydrite and its Al-substituted analogs.

Transmission Electron Microscopy

In TEM micrographs, differences in aggregation were observed with change in Al:Fe molar ratio. The 0:1 Al:Fe hydroxide was observed only as aggregates of varying density (Figure 11 and Figure 12). The 2:8 Al:Fe hydroxide was generally more dispersed than the 0:1 Al:Fe hydroxide (Figure 11 versus Figure 13). Low-density regions were observed with the 2:8 Al:Fe hydroxide (Figure 13 and Figure 14); however, high-density aggregates similar to those found with the 0:1 Al:Fe hydroxide were also observed (Figure 13). Hexagonal gibbsite and pyramidal bayerite crystals along with small aggregates of poorly crystalline hydroxide were observed with the 5:5 Al:Fe hydroxide (Figure 15 and Figure 16-a). The aggregates with the 5:5 Al:Fe hydroxide were generally smaller and less dense than those observed with the 0:1 and 2:8 Al:Fe hydroxides. Crystalline products in the 5:5 Al:Fe hydroxide were identified as gibbsite (hexagonal plates) and bayerite (triangular pyramidal) (Hsu, 1989). Smaller gibbsite and bayerite crystals were observed with the 1:0 Al:Fe hydroxide than with the 5:5 Al:Fe hydroxide (Figure 15-a versus Figure 16-b). Determination of the crystal size was difficult because Al hydroxides in the 1:0 Al:Fe hydroxide sample were unstable under the TEM electron beam, and the image was distorted due to the evolution of water vapor. Aggregates of poorly crystalline Al hydroxide were also found in the 0:1 Al:Fe hydroxide.
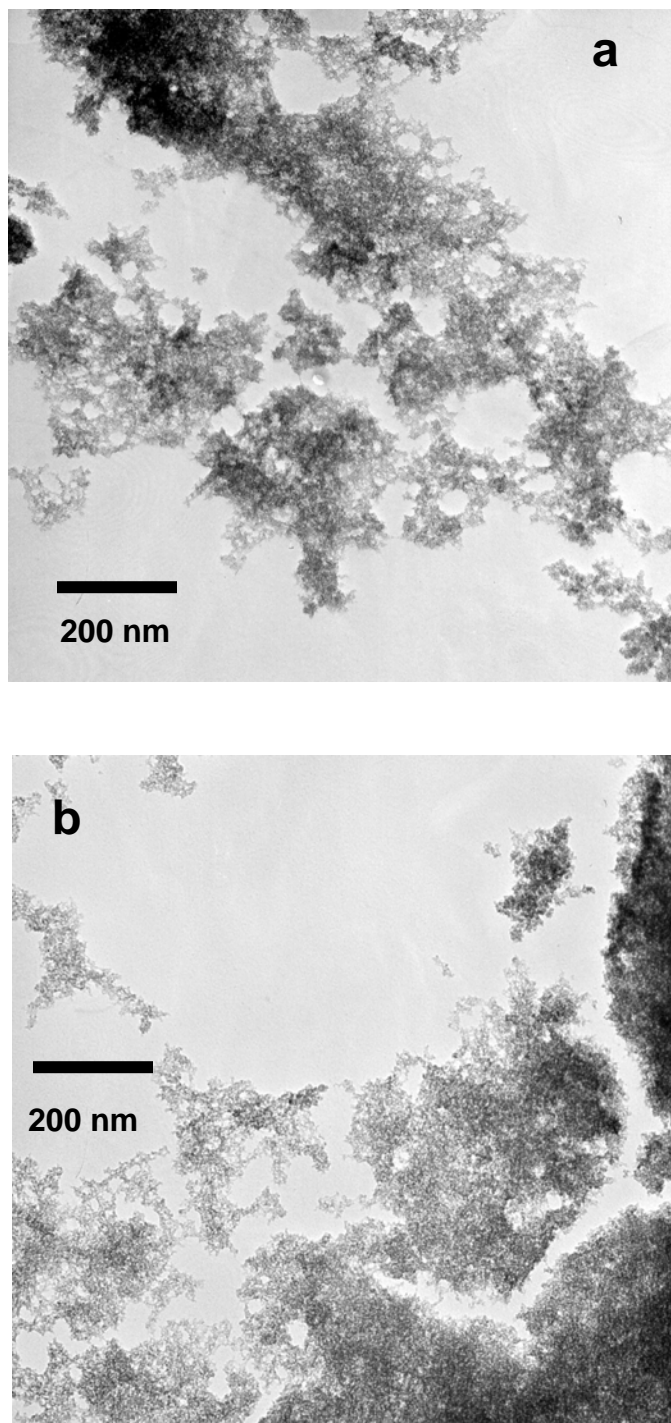
Figure 11. TEM micrographs of the 0:1 Al:Fe hydroxides. (a) Aggregates of 0:1 Al:Fe hydroxide. (b) Dense aggregates of 0:1 Al:Fe hydroxide.
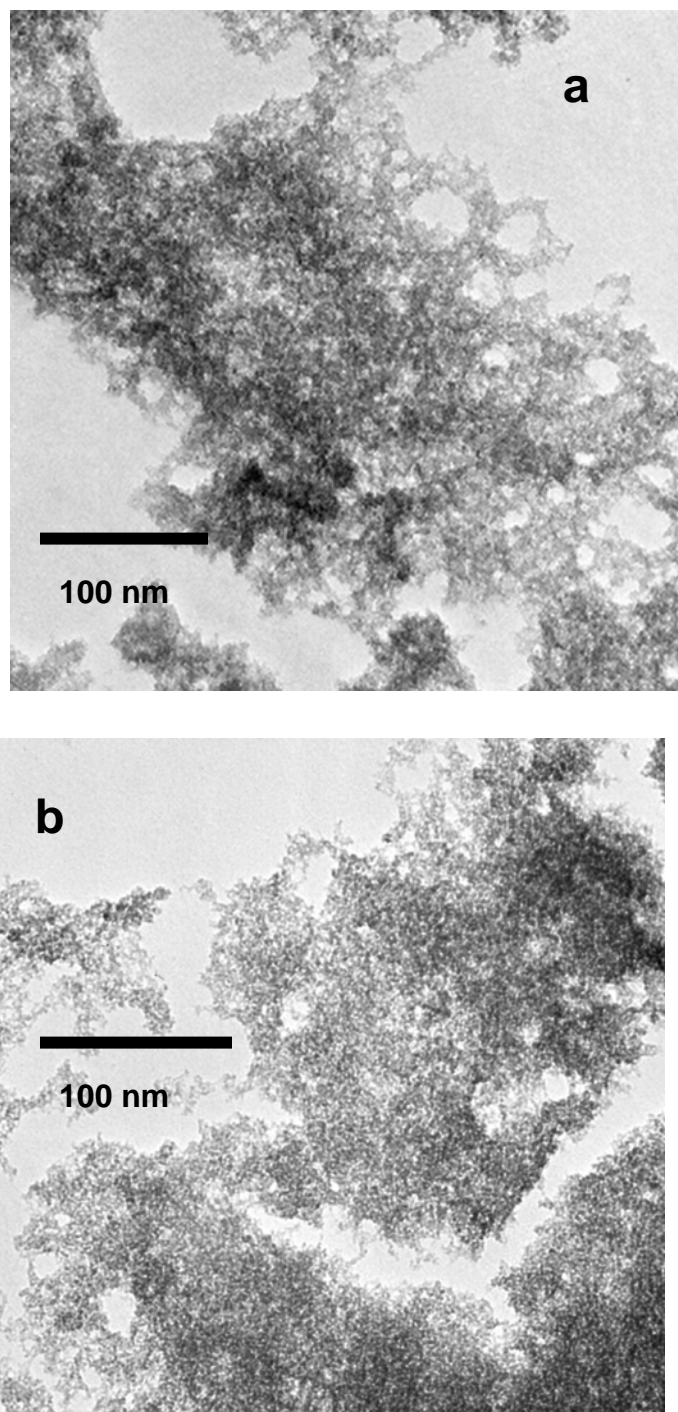
Figure 12. TEM micrographs of the 0:1 Al: Fe hydroxides. (a) Aggregates of 0:1 Al:Fe hydroxide (magnified picture of Figure 11-a). (b) Dense aggregates of 0:1 Al:Fe hydroxide (magnified picture of Figure 11-b).
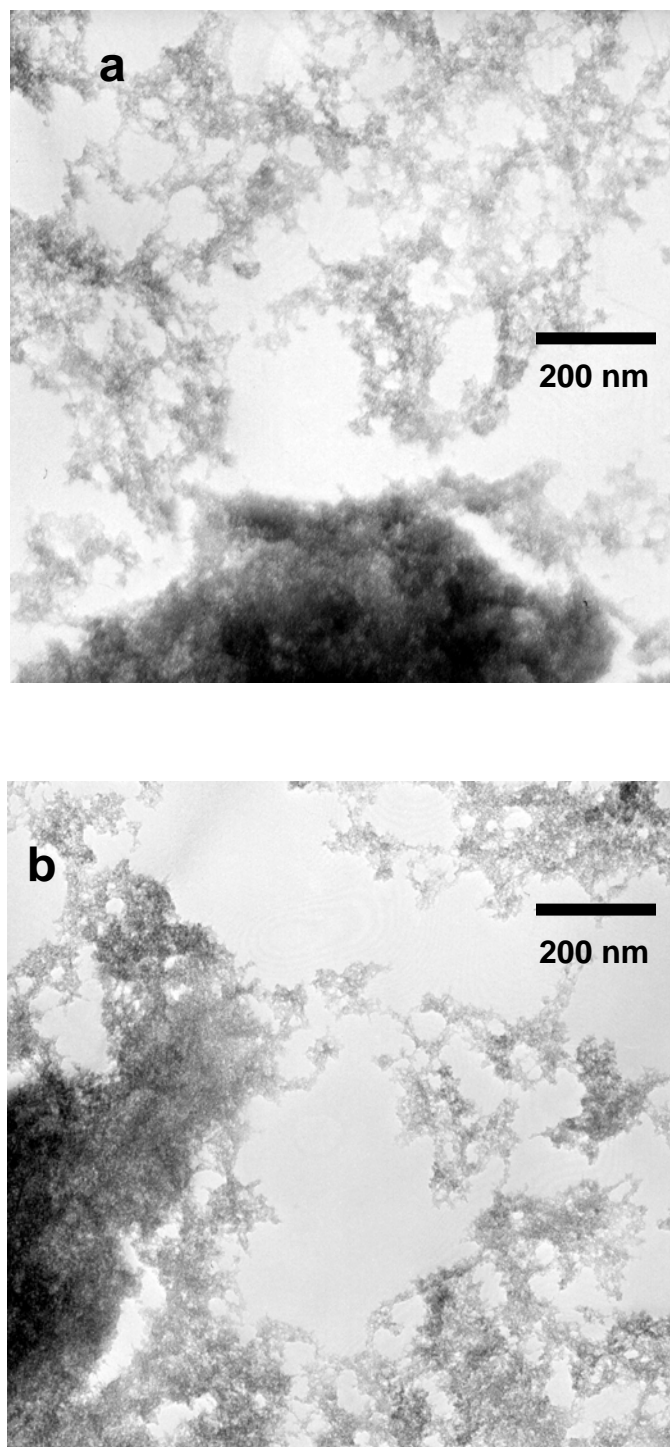
Figure 13. TEM micrographs of the 2:8 Al:Fe hydroxides. (a) Dense aggregates of the 2:8 Al:Fe hydroxide and porous surrounding. (b) Dense aggregates of 2:8 Al:Fe hydroxide with dispersed aggregates.
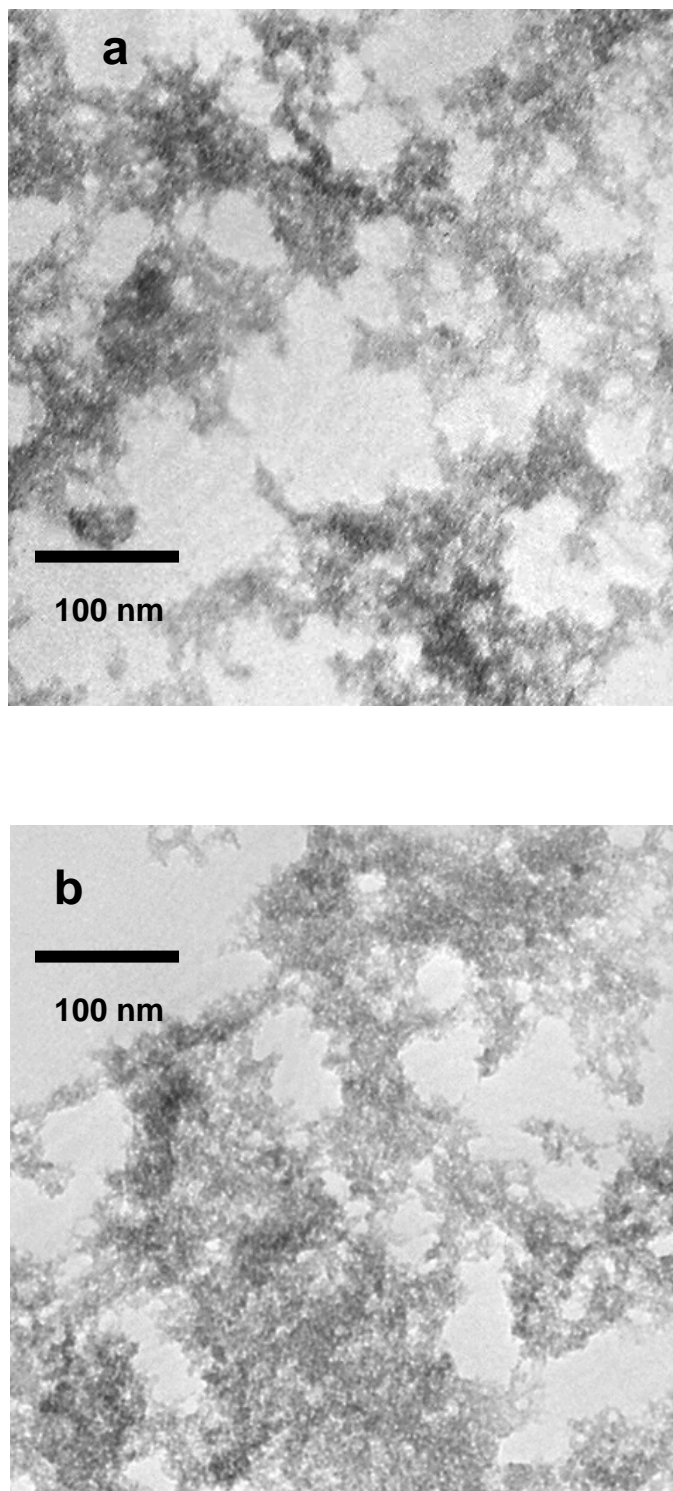
Figure 14. TEM micrographs of the 2:8 Al:Fe hydroxides. (a) Aggregates of 2:8 Al:Fe hydroxide (magnified from Figure 13-a). (b) Aggregates of 2:8 Al:Fe hydroxide (magnified from Figure 13-b).
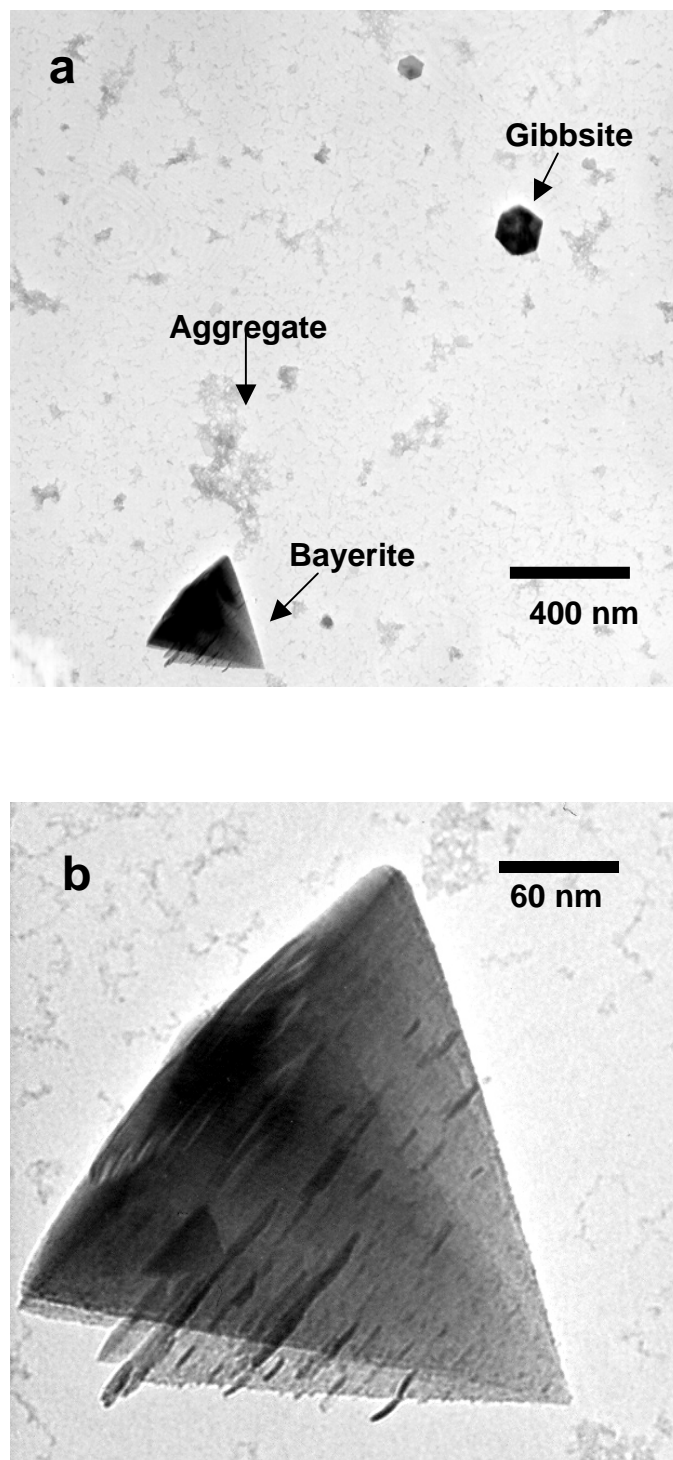
Figure 15. TEM micrographs of the 5:5 Al:Fe hydroxides. (a) Gibbsite, bayerite, and small aggregates of the 5:5 Al:Fe hydroxide. (b) Magnified image of bayerite crystal found in the 5:5 Al:Fe hydroxide.
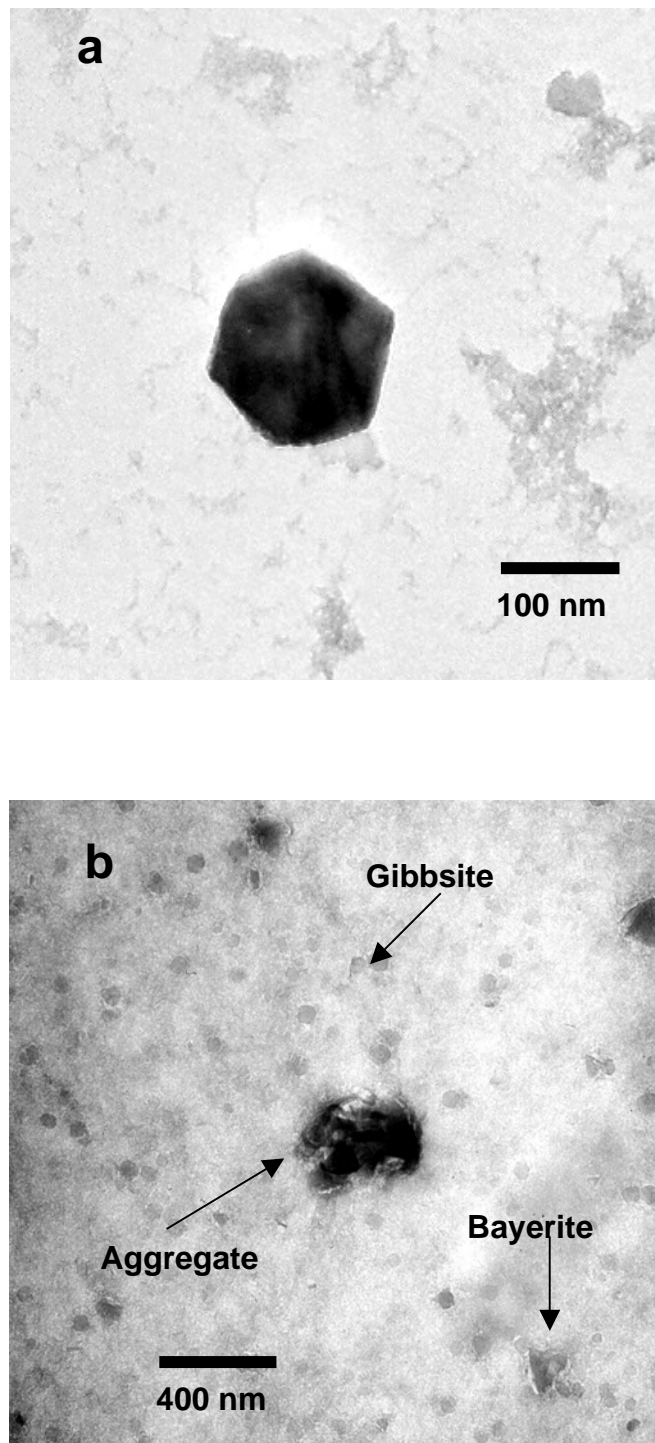
Figure 16. TEM micrographs of the 5:5 and 0:1 Al:Fe hydroxides. (a). Magnified image of gibbsite crystal found in the 5:5 Al:Fe hydroxide. (b) Gibbsite, bayerite, and aggregate of Al hydroxide found in the 0:1 Al:Fe hydroxide.

The TEM study further confirmed that 0:1 and 2:8 Al:Fe hydroxides are poorly crystalline and highly aggregated; however, the TEM images revealed that the 2:8 Al:Fe hydroxide was generally more dispersed. Due to the tendency of the poorly crystalline hydroxides to aggregate, quantitative determination of surface area is challenging. Multiple phases (gibbsite, bayerite, and poorly crystalline product) were observed in the 5:5 and 1:0 Al:Fe hydroxides, which confirms the XRD data.

Point of Zero Salt Effect

The PZSEs of 0:1, 2:8, 5:5, and 1:0 Al:Fe hydroxides were approximately 7.6, 8.2, 8.7, and 8.9, respectively (Figures 17 – 20). Titration curves followed similar trends regardless of Al:Fe molar ratio; however, pH values at PZSE increased as Al:Fe molar ratio was increased. This trend indicates the reversal in the net charge of the surface occurs at higher pH with higher Al:Fe molar ratio. The charge characteristics of the 1:0 Al:Fe hydroxide were not as strongly influenced by ionic strength compared to the other hydroxides.
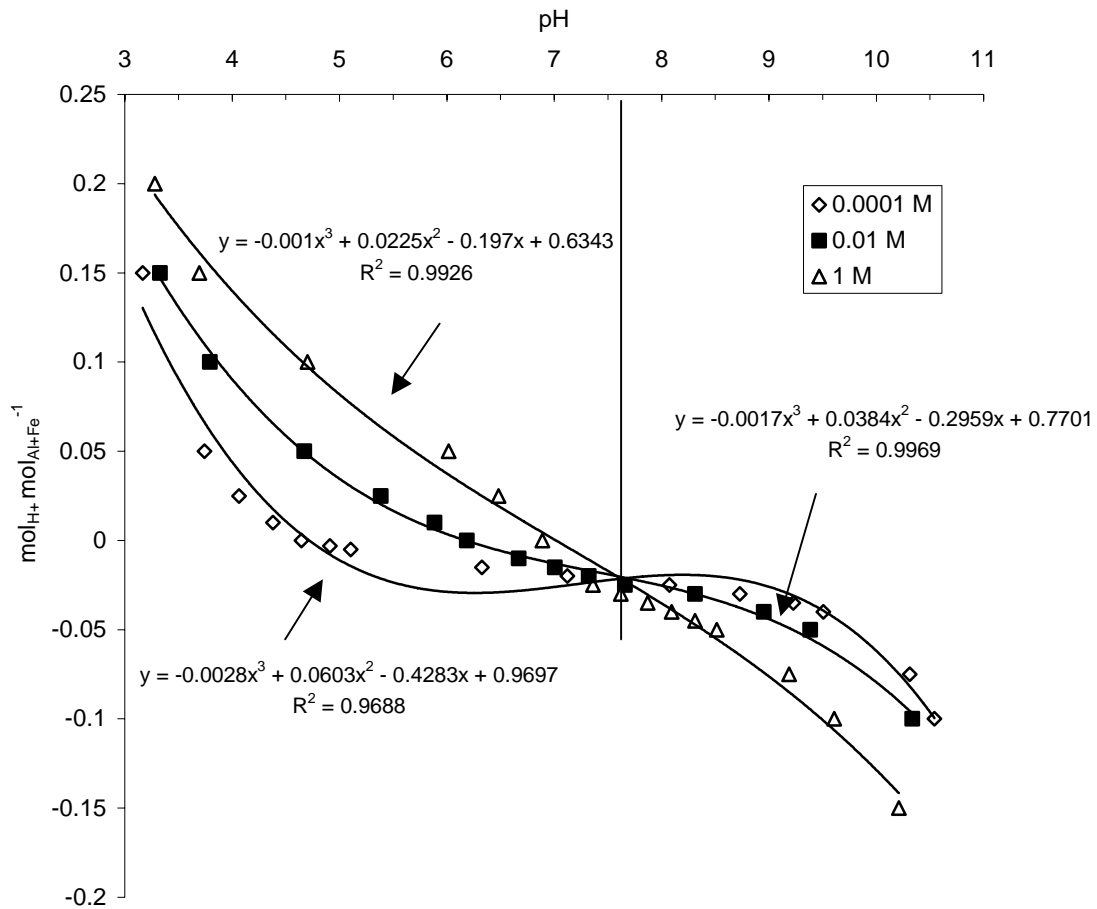
Figure 17. Titration curves for the 0:1 Al:Fe hydroxide at three ionic strengths.
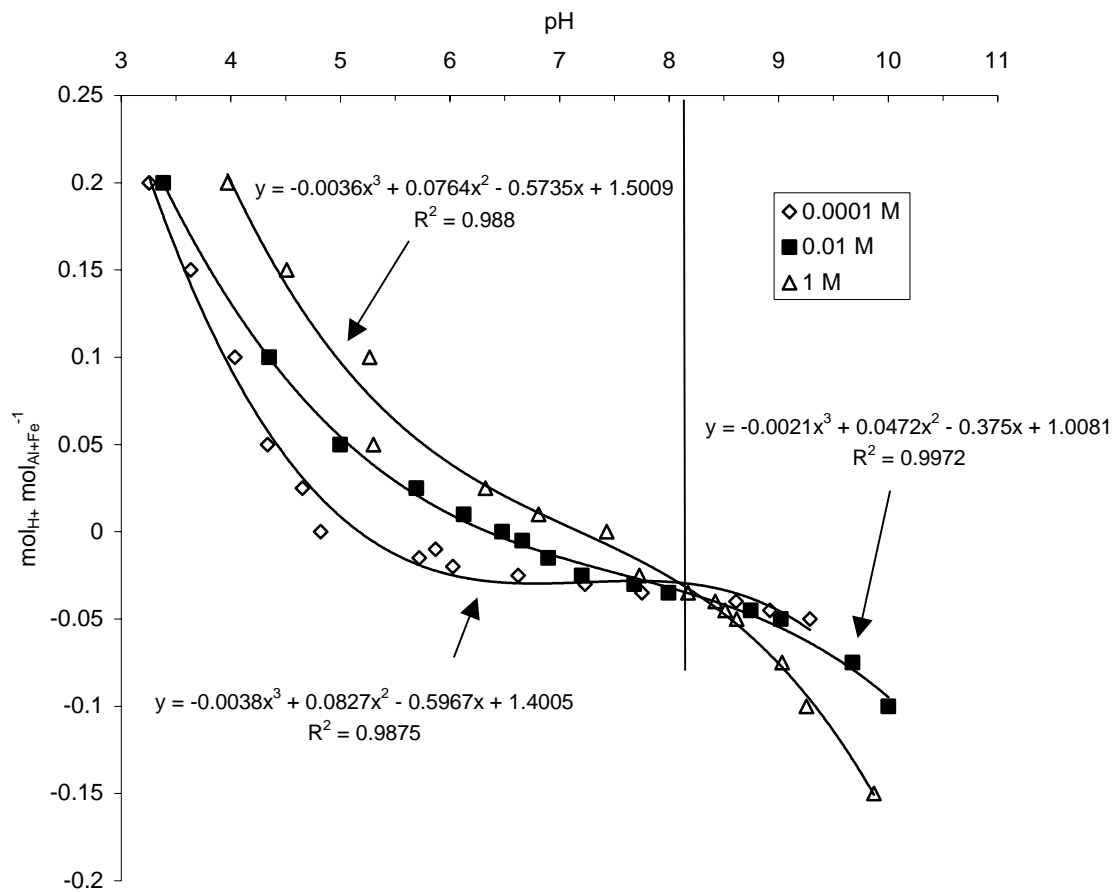
Figure 18. Titration curves for the 2:8 Al:Fe hydroxide at three ionic strengths.
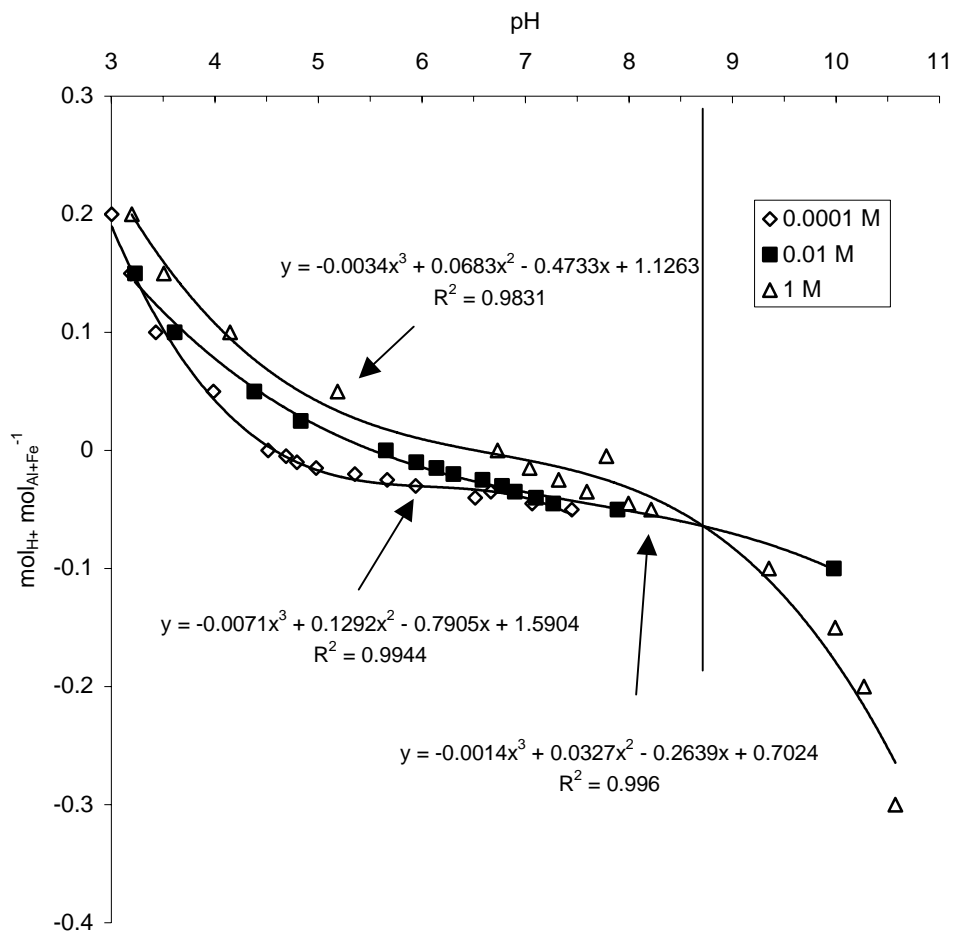
Figure 19. Titration curves for the 5:5 Al:Fe hydroxide at three ionic strengths.
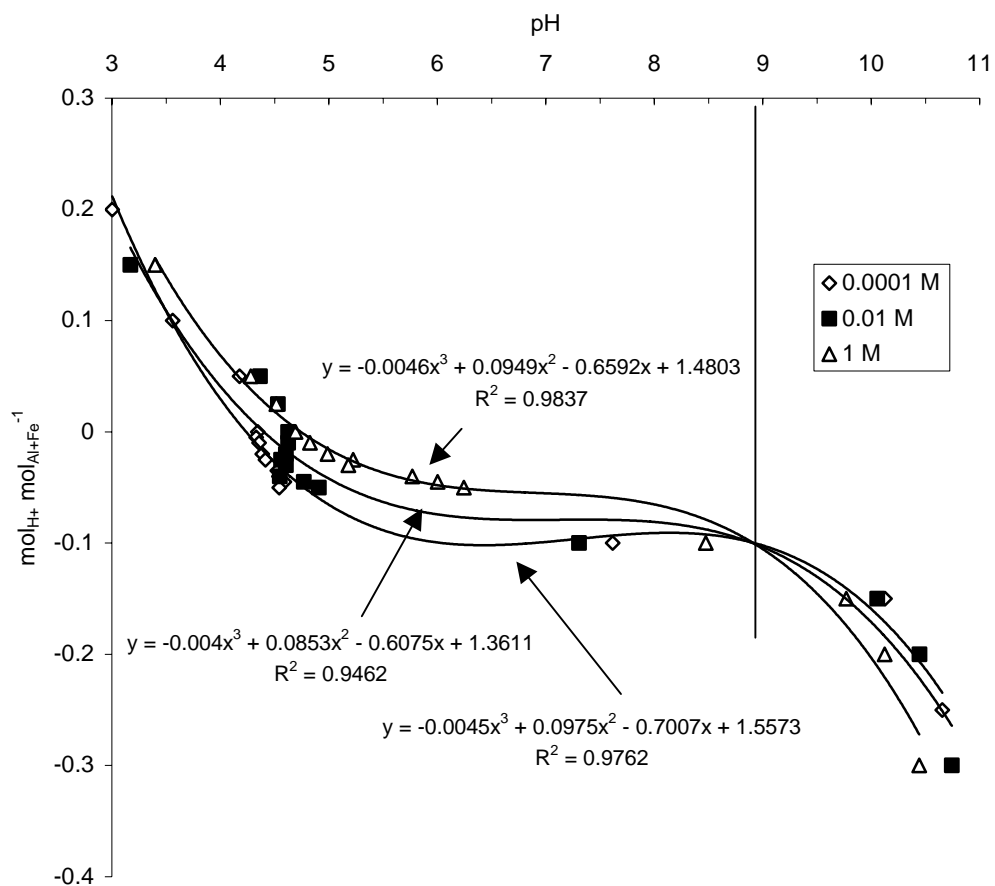
Figure 20. Titration curves for the 1:0 Al:Fe hydroxide at three ionic strengths.

Stability of Ferrihydrite and Its Al-substituted Analogs

Effect of Al Substitution and pH

After 70°C incubation at pH 10 for 96 h without As^V, no poorly crystalline Fe hydroxide remained in the 0:1 Al:Fe hydroxide, as detected by pH 3 ammonium-oxalate extraction in the dark; however, 64 % of the poorly crystalline Fe hydroxide remained in the 2:8 Al:Fe hydroxide (Table 4). Also, 53 % of the Fe hydroxide was poorly crystalline in the 0:1 Al:Fe hydroxides following incubation at pH 4, although transformation of the 2:8 Al:Fe hydroxide at pH 4 into a crystalline hydroxide was not evident by pH 3 ammonium-oxalate extraction in the dark (Table 4). The proportion of crystalline Fe hydroxide to poorly crystalline phase is known to increase with increasing incubation pH (Schwertmann and Murad, 1983). The results of ammonium oxalate extraction indicate that differences in stability of the originally synthesized poorly crystalline phases against transformation into crystalline phases are influenced by Al substitution.

Table 4. Percent of ammonium oxalate extractable (AOE) Fe to total Fe following incubation at 70 ^{o}C for 96 h.

Treatment	Incubated with As	Incubated without As
	Ammonium oxalate extractable Fe/Total Fe	
	%	
0:1 Al:Fe pH 10	97	0
0:1 Al:Fe pH 4	95	53
2:8 Al:Fe pH 10	99	64
2:8 Al:Fe pH 4	100	100

The influence of Al substitution and incubation pH on incubation product mineralogy was also determined by XRD (Figure 21). Following incubation at pH 10 for 96 h, hematite and goethite were detected by XRD analysis of the 0:1 Al:Fe hydroxide; however, only hematite was detected with the 2:8 Al:Fe hydroxide. The broad background peak of the incubated 2:8 Al:Fe hydroxide is an indication that the sample still contained considerable poorly crystalline hydroxide. Following pH 4 incubation of the 0:1 Al:Fe hydroxide, hematite and goethite were detected, although no crystalline material was found in the incubation product of the 2:8 Al:Fe hydroxide. XRD analyses of the final products were compatible with the result of the pH 3 ammonium-oxalate extractions in the dark (Table 4 and Figure 21).

The formation of goethite and hematite from ferrihydrite at pH 10 versus the formation of only hematite at pH 4 is influenced by Al substitution and pH, because the mechanisms of formation of these phases differ. Goethite is formed by dissolution of ferrihydrite, followed by reprecipitation, usually from $Fe(OH)_2^+$ and $Fe(OH)_4^-$; however, hematite is formed by internal rearrangement and dehydration within the ferrihydrite (Schwertmann and Murad, 1983). The solubility of ferrihydrite is pH dependent, and the
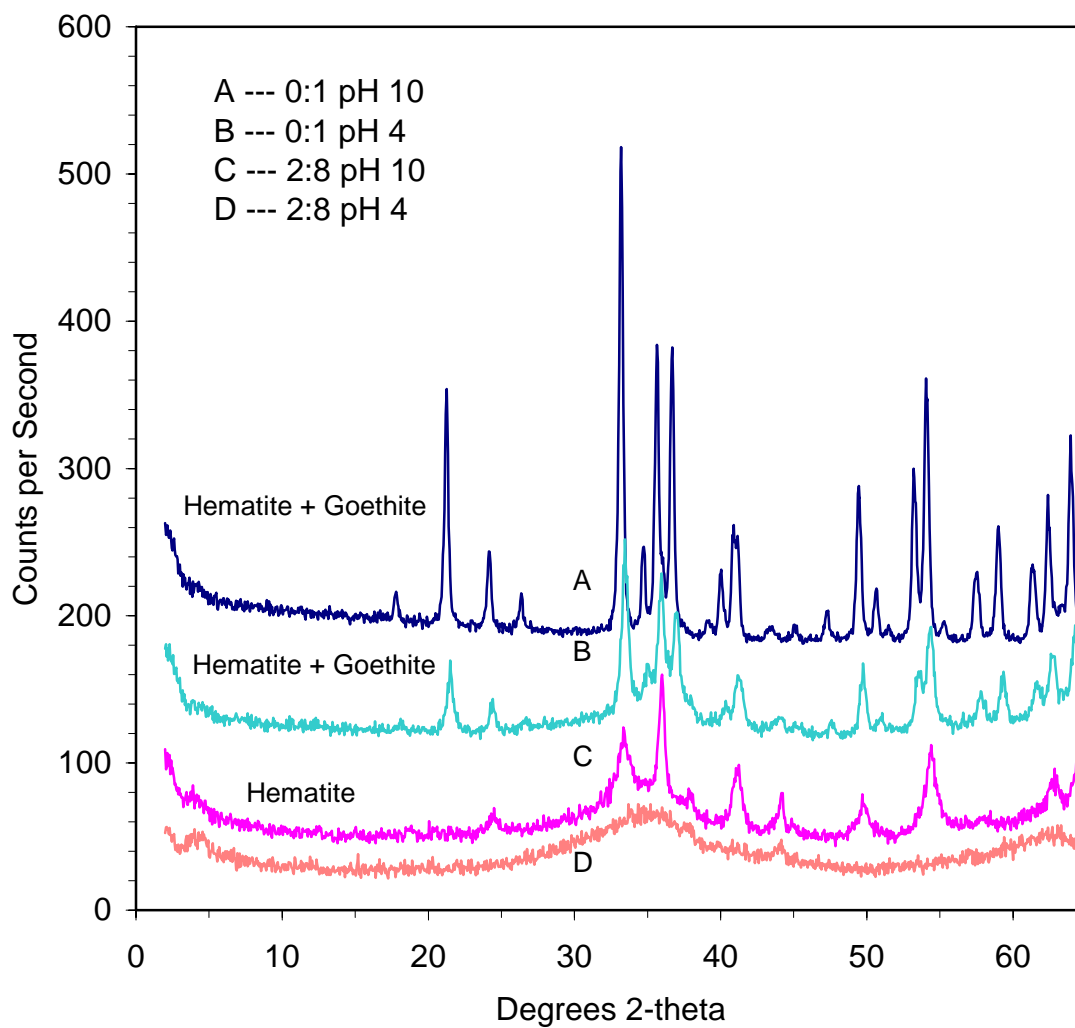
Figure 21. XRD patterns of the hydroxides incubated without As^V at 70 ^{o}C for 96 h.

minimum solubility of ferrihydrite occurs at pH 7.5 to 8.5 (Figure 22) (Lindsay, 1979).

Maximum formation of hematite as opposed to goethite has been reported at pH 7 to 8,

where the solubility of ferrihydrite is at an approximate minimum; maximum formation

of goethite as opposed to hematite has been reported at pH 4 and pH 12, where the

principal dissolved species are $Fe(OH)_2^+$ and $Fe(OH)_4^-$, respectively (Schwertmann and

Murad, 1983). The formation of hematite only was observed with the 2:8 Al:Fe

hydroxide at pH 10, where goethite formation should be favored (Figure 21). This

phenomenon indicates that the 2:8 Al:Fe hydroxide might be less soluble compared to the

0:1 Al:Fe hydroxide (Schwertmann et al., 2000). Preferential formation of hematite over

goethite from Al-substituted ferrihydrite was also observed by Schwermann et al. (2000).

Kinetics of Mineral Transformation

The kinetics of mineral transformation was also affected by Al substitution and

pH. The hydroxides equilibrated at pH 4 transformed more slowly than those

equilibrated at pH 10 (Figure 23 versus Figure 24). The decrease in the rate of

ferrihydrite transformation with decrease in pH was also observed by Schwertmann and

Murad (1983). The relationship between the proportion of As^V not adsorbed and the

proportion of the crystalline Fe hydroxide is summarized in Figure 25. The proportion of

As^V not adsorbed increased as the surface area decreased, due to the formation of

crystalline hydroxides. In addition, the slower increase in As^V concentration in solution

with the 2:8 Al:Fe hydroxides relative to the 0:1 Al:Fe hydroxide indicates that the

mineral transformation was slower with the 2:8 Al:Fe hydroxide. Schwertmann et al.

(2000) also showed that the transformation of poorly crystalline Fe hydroxide was slower

when Al substitution of ferrihydrite was increased.
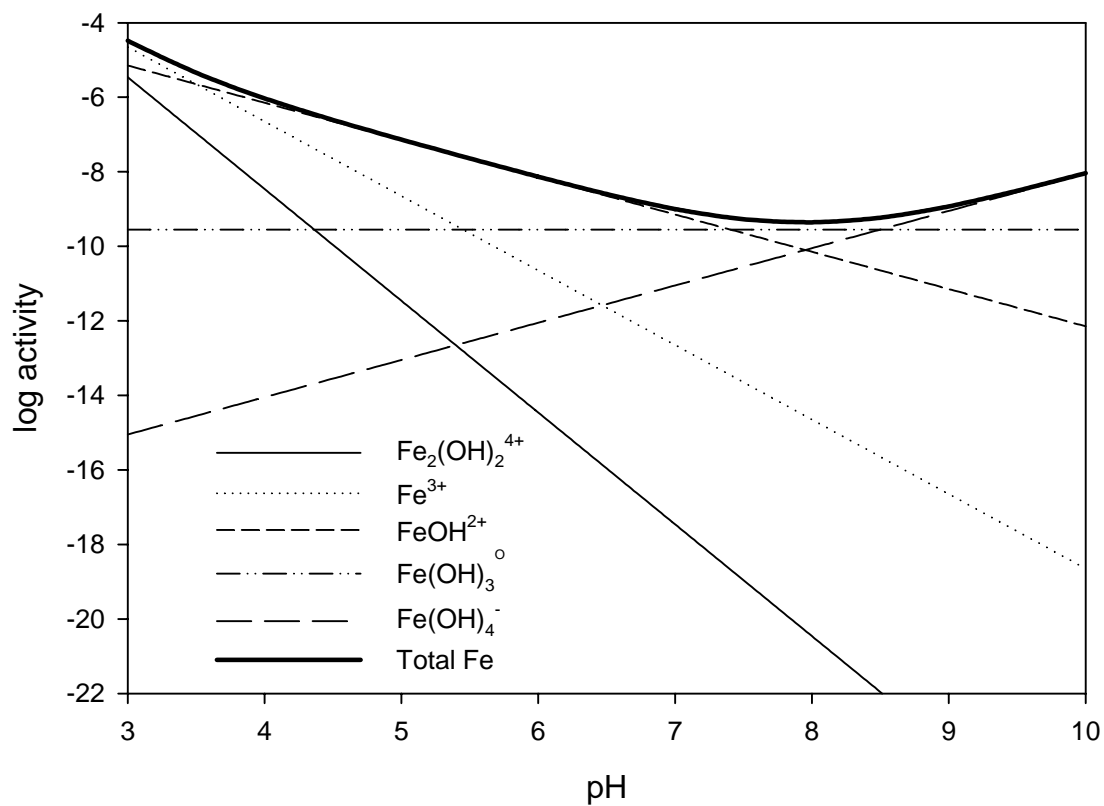
Figure 22. The activities of hydrolysis species of Fe^{3+} in equilibrium with amorphous Fe hydroxide as a function of pH, calculated using thermodynamic constants from Lindsay (1979).
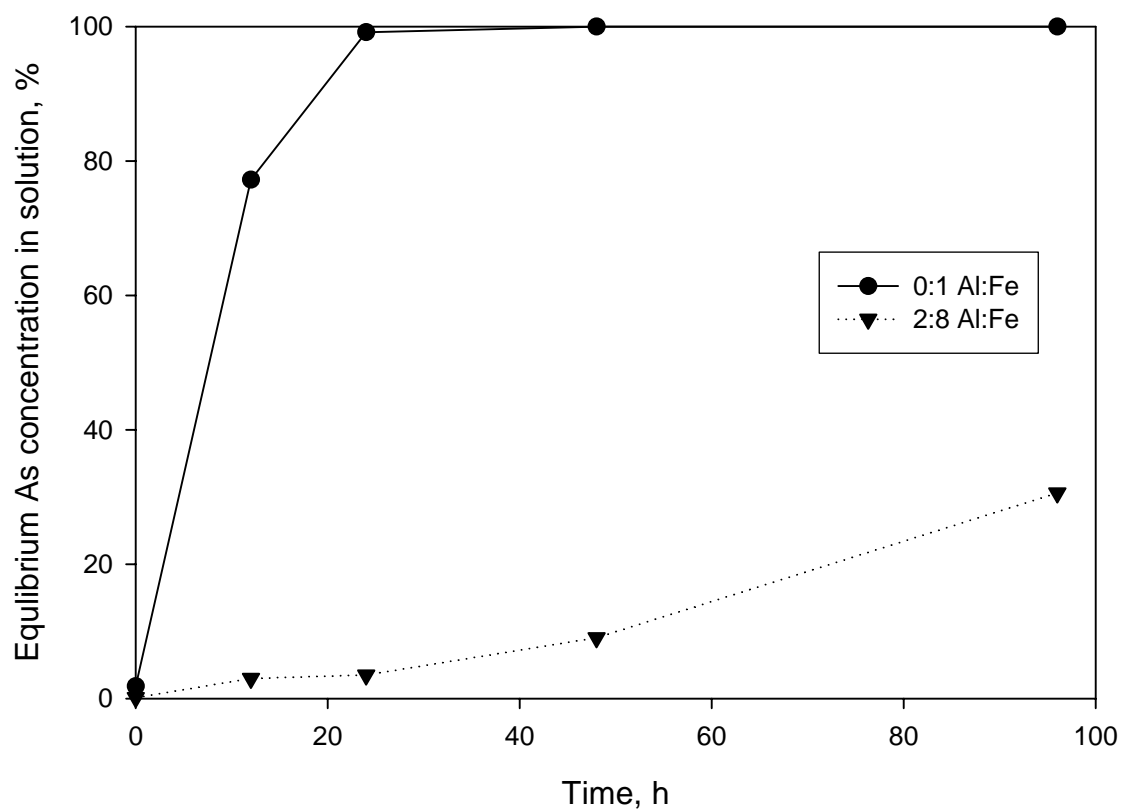
Figure 23. The influence of incubation time on the proportion of added As^V not adsorbed. The incubation was at pH 10 and 70 ^{o}C. The As^V (0.05 $mmol_{As}$ $mmol_{Al+Fe}^{-1}$) was added to the suspension following incubation and was allowed to equilibrate at pH 7 and 23 ^{o}C for 2 h.

Figure 24. The influence of incubation time on the proportion of added As^V not adsorbed. The incubation was at pH 4 and 70 ^{o}C. The As^V (0.05 mmol$_{As}$ mmol$_{Al+Fe}^{-1}$) was added to the suspension following incubation and was allowed to equilibrate at pH 7 and 23 ºC for 2 h.

Figure 25. As^V remaining in solution from the final incubation products as a function of proportion of crystalline Fe not extracted by pH 3 ammonium oxalate from the products. The As^V was added to the suspension following incubation and was allowed to equilibrate at pH 7 and 23 °C for 2 h.

Effect of Arsenic

The transformation of both 0:1 and 2:8 Al:Fe hydroxides into crystalline products was retarded in the presence of As^V (Table 4). There are two possible factors by which As^V might contribute to this overall relationship. Adsorbed As^V at the surface of nuclei might poison the crystal growth of the transformation product of both 0:1 and 2:8 Al:Fe hydroxides. Also, dissolution of ferrihydrite might be reduced by the presence of As^V (Paige et al., 1996). In the latter case, transformation to goethite might be limited because goethite formation is dependent on ferrihydrite dissolution. The presence of coprecipitated or adsorbed As^V on amorphous Fe hydroxide slowed the rate of transformation into crystalline products at pH 12 (Paige et al., 1996). This trend indicates that the As^V-contaminated sludge would be more resistant to transformation than the non-contaminated adsorbent.

The results of this study indicate that coprecipitation of Al during precipitation of poorly crystalline Al:Fe hydroxide resulted in a product that was more resistant to transformation into well crystalline goethite or hematite. In the water treatment scenario, the use of Al with Fe during coagulation might contribute to the maintenance of higher surface areas for As adsorption.

Arsenic Adsorption Isotherms

Effect of Mineralogy

There were differences in the adsorption of As^V on poorly crystalline hydroxides (0:1 and 2:8 Al:Fe hydroxides) versus the 5:5 Al:Fe hydroxide at both pH 5 and 8 (Figure 26 and Figure 27). Furthermore, adsorption of As^V on the 1:0 Al:Fe hydroxide was
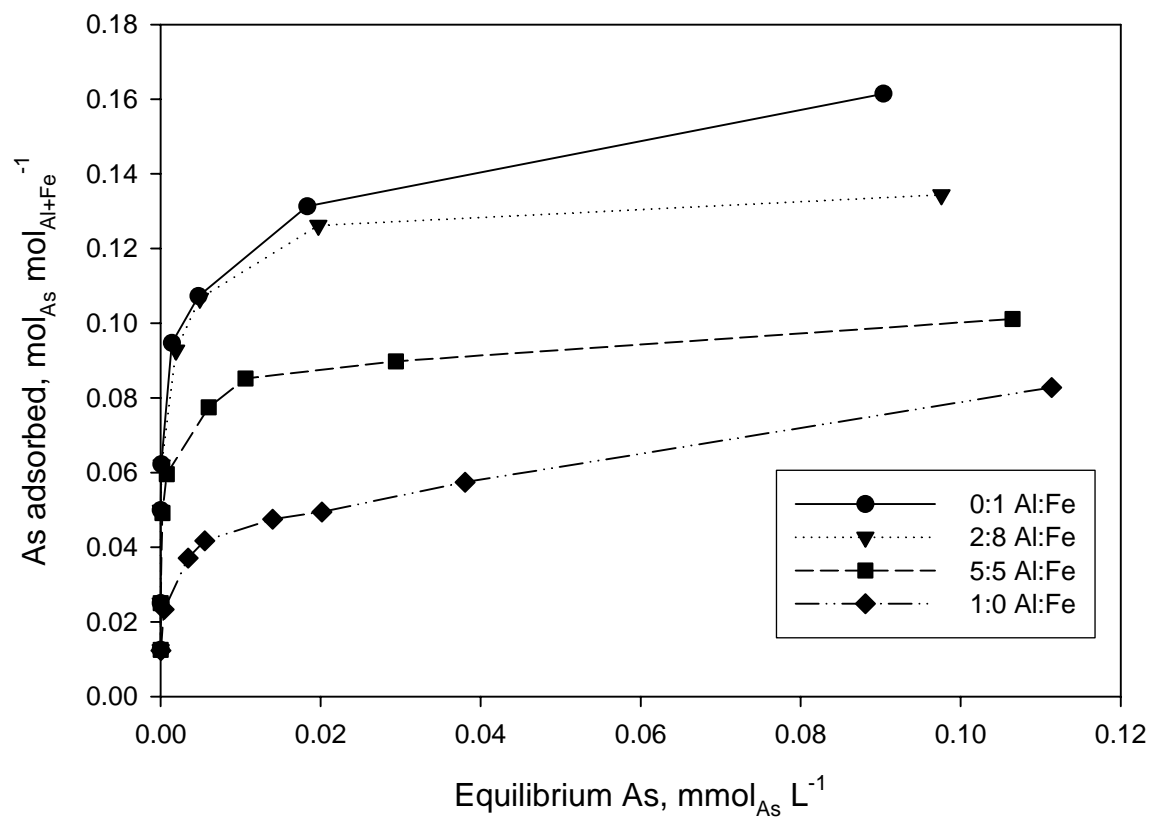
Figure 26. Adsorption isotherms of As^V at pH 5 on precipitated products of various Al:Fe molar ratio.
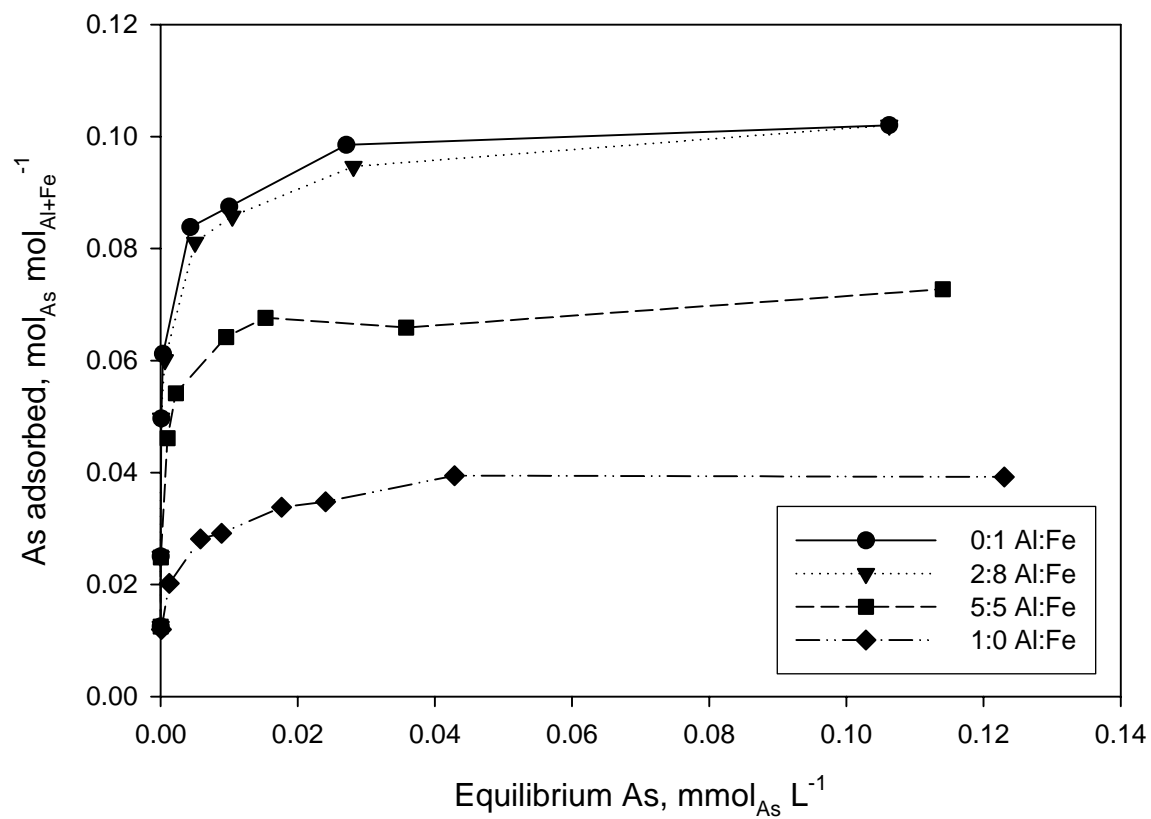
Figure 27. Adsorption isotherms of As^V at pH 8 on precipitated products of various Al:Fe molar ratio.

substantially lower than that on the Fe-containing adsorbents, regardless of pH. This difference in As^V adsorption is primarily due to the differences in surface area. The XRD and TEM study revealed the presence of crystalline bayerite and gibbsite in the 5:5 and 1:0 Al:Fe hydroxides; therefore, a lower concentration of surface adsorption sites would be expected with these hydroxides compared to the poorly crystalline 0:1 and 2:8 Al:Fe hydroxides. The low reactivity of gibbsite and bayerite can be explained by their relatively inert structures. Since there is no significant isomorphous substitution of Al^{3+} by divalent cation, the net permanent charge approaches zero in gibbsite and bayerite. The only sites for As adsorption are the edge sites, because all OH^- groups on the planar surfaces are charge satisfied. Even at the edge site, one half of the OH^- groups are charge satisfied since they are doubly coordinated to two Al^{3+} ions. The only reactive sites are the other half of the OH^- groups, which are undercoordinated (Essington, 2004). In addition, Al hydroxide has a strong tendency to grow in the X and Y plane, but crystal growth is often limited in the Z direction, which also contributes to a lower concentration of surface adsorption sites. The crystal growth of gibbsite and bayerite is influenced by strong Al-OH-Al bonding within the layer structure and weak bonding between layers via hydrogen bonding (Hsu, 1989). Because the poorly crystalline hydroxides have higher concentrations of surface adsorption sites, it is predictable that higher concentrations of As would be adsorbed. At both pH 5 and 8, As^V was quantitatively adsorbed by the 5:5 Al:Fe hydroxide up to approximately 0.025 As:(Fe+Al) molar ratio, although the 0:1 and 2:8 Al:Fe hydroxides adsorbed As^V quantitatively up to approximately 0.05 As:(Al+Fe) molar ratio (Figure 28 and Figure 29). The 0:1 and 2:8 Al:Fe hydroxides exhibited a
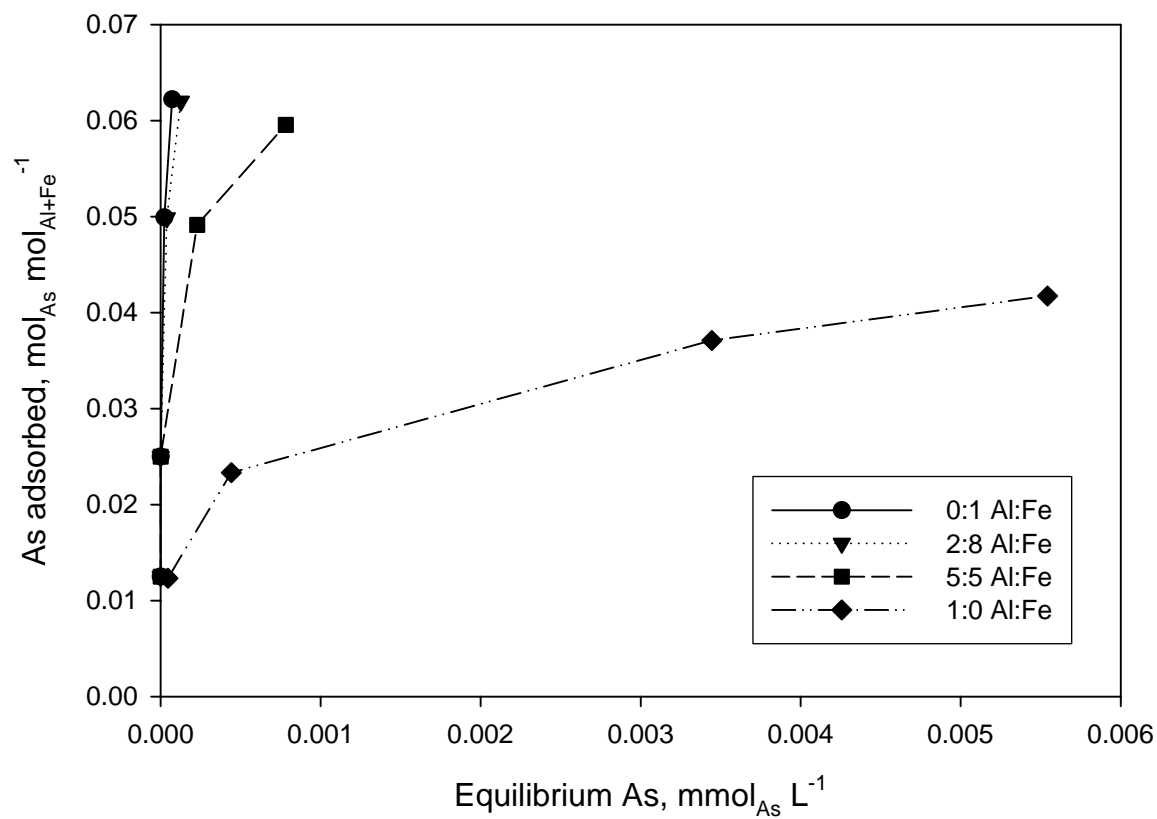
Figure 28. Adsorption isotherms of As^V at low equilibrium As^V concentrations at pH 5 on precipitated products of various Al:Fe molar ratio.
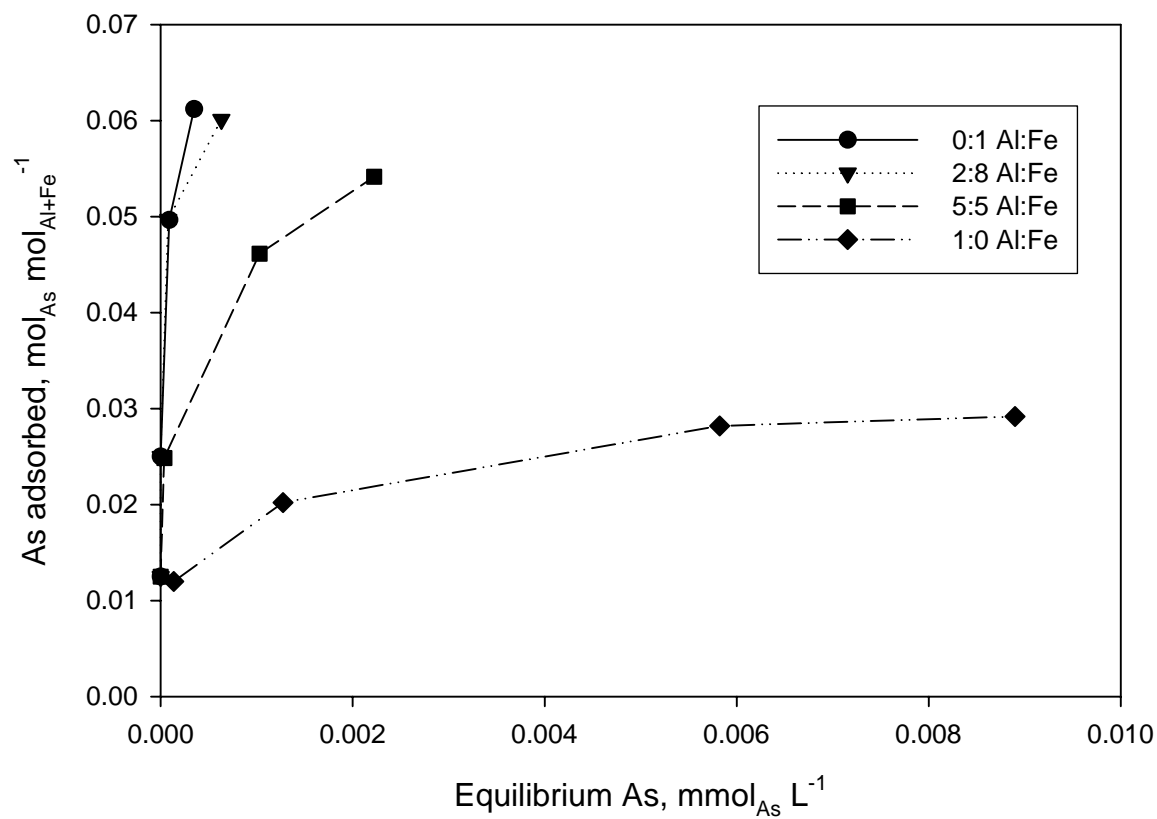
Figure 29. Adsorption isotherms of As^V at low equilibrium As^V concentrations at pH 8 on precipitated products of various Al:Fe molar ratio.

higher capacity to adsorb As^V, regardless of pH, at any As:(Al+Fe) molar ratio (Figure 26

and Figure 27). A slightly higher retention of As^V was observed with the 0:1 Al:Fe

hydroxide than with the 2:8 Al:Fe hydroxide; however, the statistical significance was

uncertain.

As^V is usually considered to be more effectively removed by Fe than by Al

coagulation (Cheng et al., 1994; Edwards, 1994; Gulledge and O'Connor, 1973; Hering et

al., 1997; Tokunaga et al., 1999), even though the As^V adsorption mechanism is

predominately inner-sphere complexation with both Al and Fe oxyhydroxides (Arai et al.,

2001; Fendorf et al., 1997; Goldberg and Johnson, 2001; Harrison and Berkheiser, 1982;

Manceau, 1995; Manning et al., 1998; Sun and Doner, 1996; Waychunas et al., 1993).

The generally lower efficiencies of As^V removal in the case of Al hydroxide might have

been influenced by the relatively inert structure of the crystalline Al hydroxide minerals,

gibbsite and bayerite, which are likely produced during the coagulation processes.

As^{III} was not quantitatively adsorbed regardless of adsorbent and pH (Figures 30 –

33). Adsorption of As^{III} decreased as Al substitution was increased, and adsorption of

As^{III} on the 1:0 Al:Fe hydroxide was negligible at all As:Al molar ratios, regardless of the

pH. This result indicates that As^{III} is strongly adsorbed only by the Fe^{3+} ion within the Al

substituted Fe hydroxides. Because the sum of Fe plus Al present in all suspensions was

consistent throughout this study, less Fe was likely available at surface adsorption sites as

Al substitution was increased.

Weak affinity for As^{III} adsorption on gibbsite and amorphous Al hydroxide and

relatively slow kinetics of As^{III} adsorption by gibbsite have been reported previously

(Goldberg and Johnson, 2001; Weerasooriya et al., 2003). Affinity of As^{III} by Al
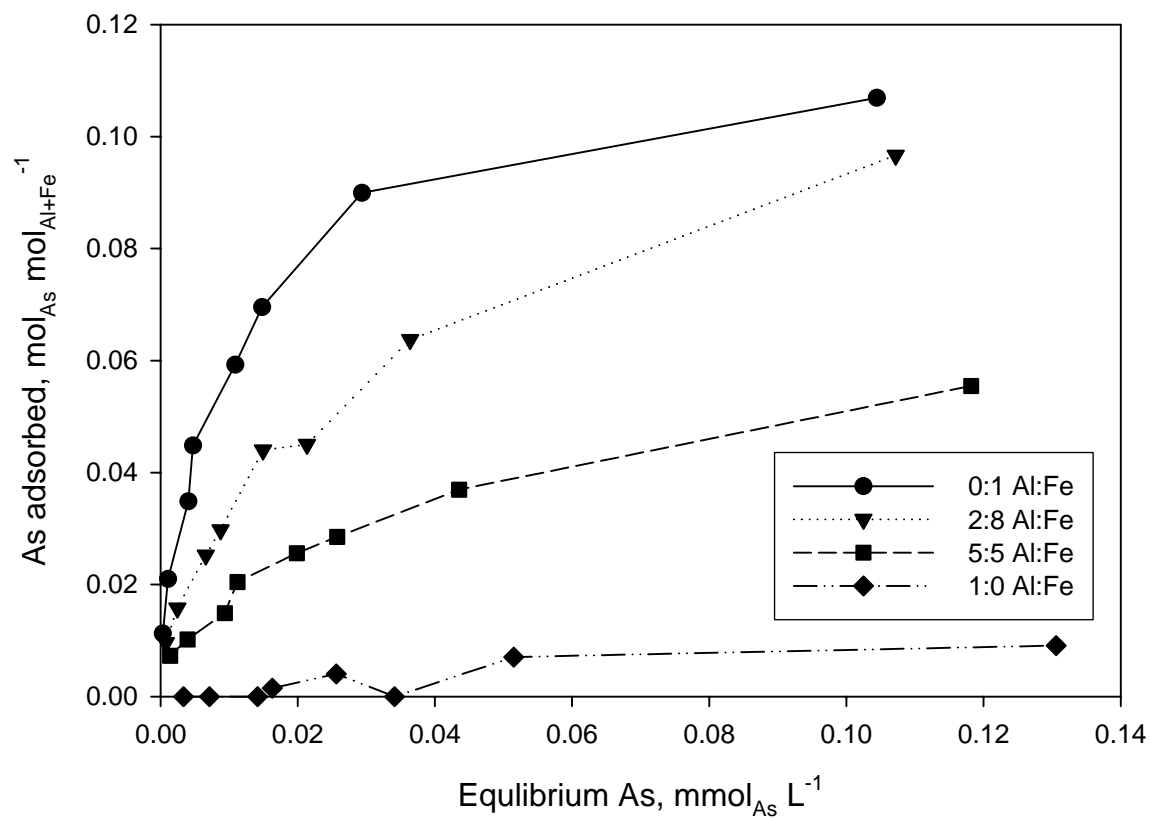
Figure 30. Adsorption isotherms of As^{III} at pH 5 on precipitated products of various Al:Fe molar ratio.
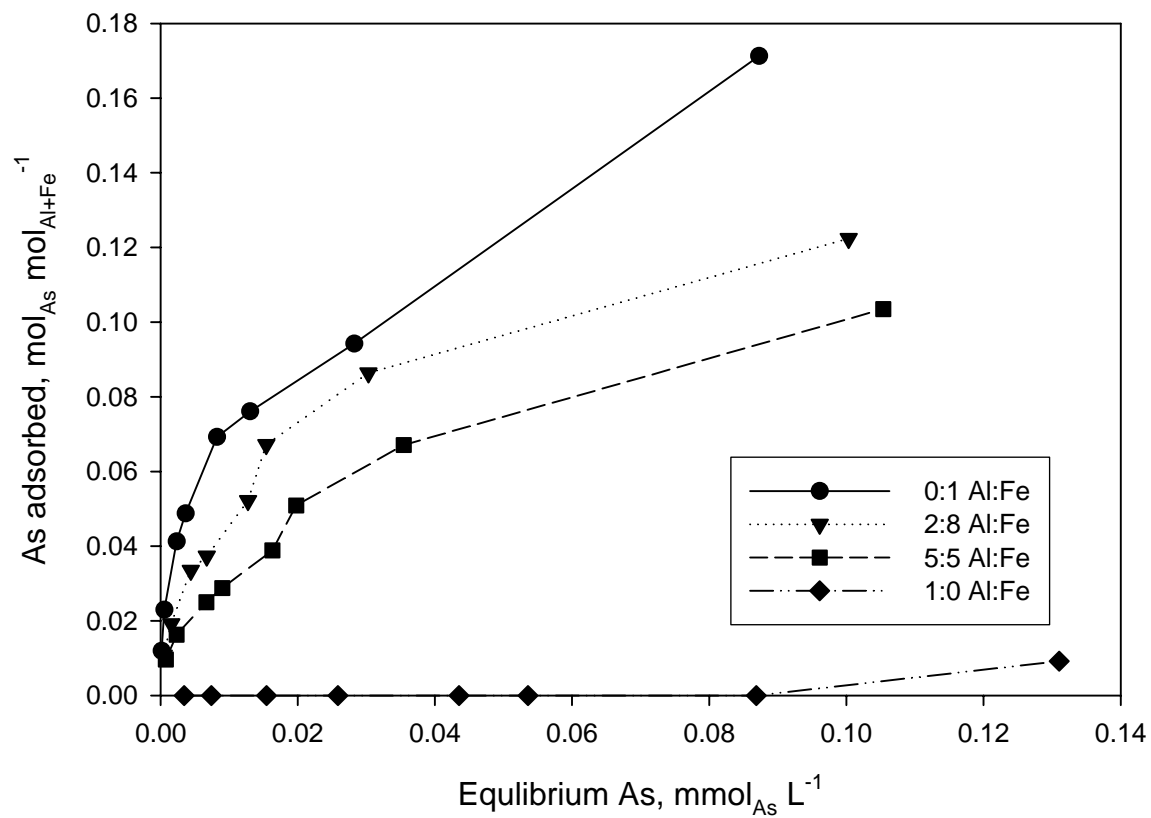
Figure 31. Adsorption isotherms of As^{III} at pH 8 on precipitated products of various Al:Fe molar ratio.
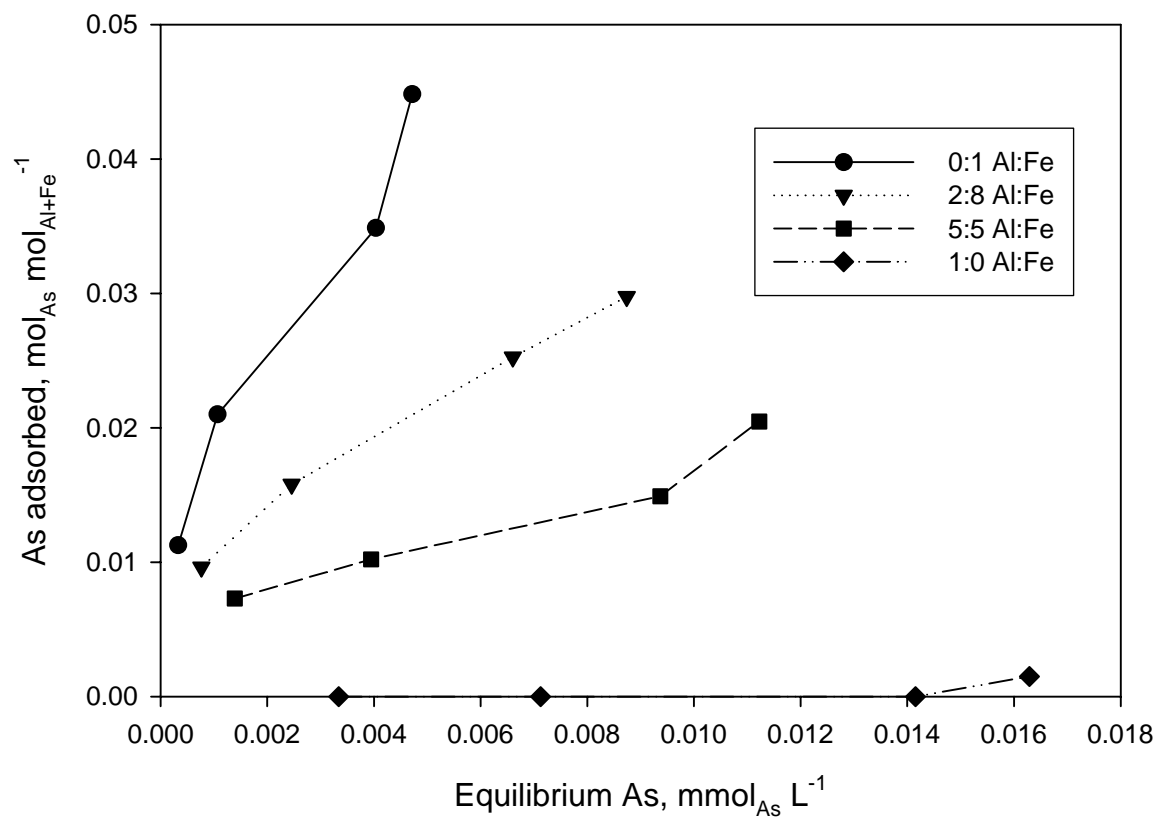
Figure 32. Adsorption isotherms of As^{III} at low equilibrium As^{III} concentrations at pH 5 on precipitated products of various Al:Fe molar ratio.
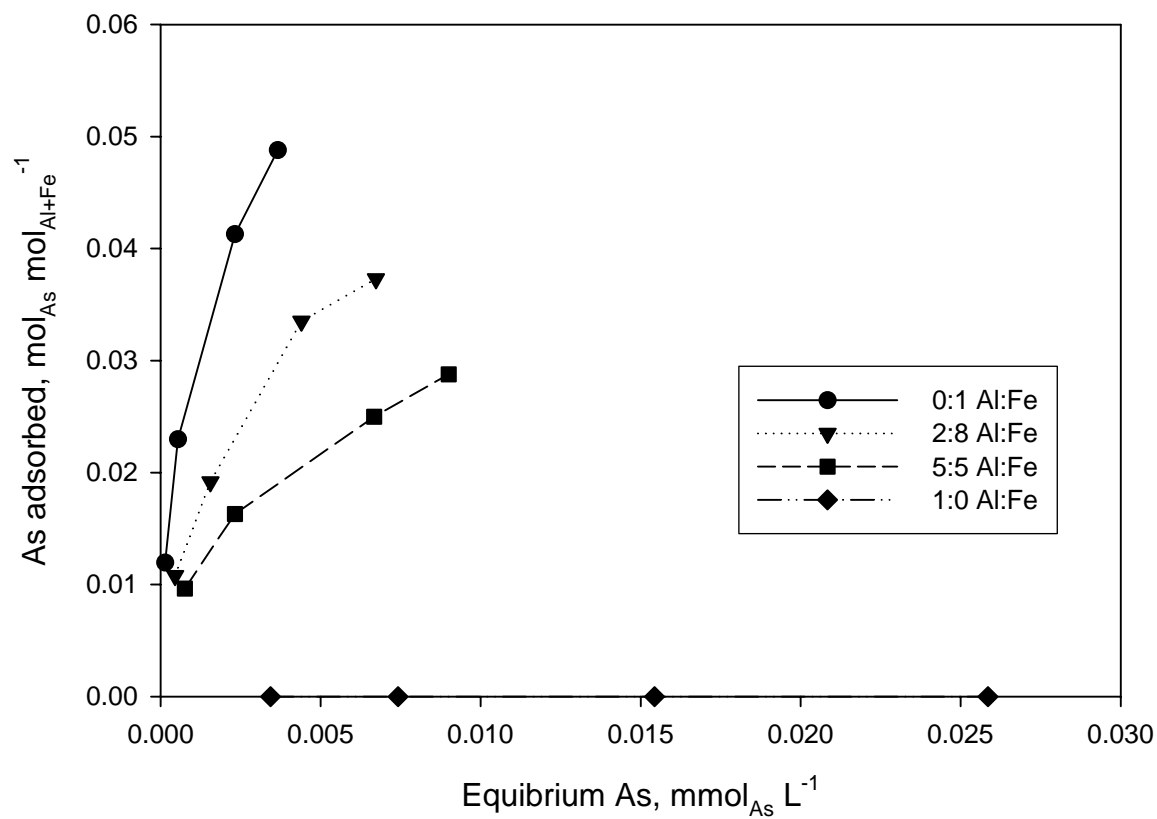
Figure 33. Adsorption isotherms of As^{III} at low equilibrium As^{III} concentrations at pH 8 on precipitated products of various Al:Fe molar ratio.

hydroxide is considerably weaker than that of As^V because the predominant mode of bonding of As^{III} on gibbsite and amorphous Al hydroxide is outer-sphere complexation, compared to the predominant inner-sphere bidentate-binuclear bonding of As^V on gibbsite.

Effect of pH

In general, more As^V was adsorbed at pH 5 than at pH 8, while higher quantities of As^{III} were adsorbed at pH 8 than at pH 5 (Figure 26 versus Figure 27 and Figure 30 versus Figure 31). Previously published data has also indicated greater adsorption of As^V at lower pH and As^{III} at higher pH (Raven et al., 1998). At pH 5, As^V exists mainly as $H_2AsO_4^-$ and As^{III} as neutral $H_3AsO_3^o$, while at pH 8, As^V exists as $HAsO_4^{2-}$ with a small fraction of $H_2AsO_4^-$, and As^{III} exists as neutral $H_3AsO_3^o$ with a small fraction of $H_2AsO_3^-$. The net charge of the hydroxide surface is positive at pH 5; however, the proportion of negative charge sites increase as pH increases. The higher affinity of As^V at pH 5 is predominately due to the impact of electrostatic attraction between the negatively charged As^V and the positively charged hydroxide surface on the overall ligand-exchange reaction. The higher affinity of As^{III} at pH 8 than at pH 5 might be attributable to the charge characteristics of As^{III} (pKa_1=9.22). Maximum adsorption or inflections in adsorption envelopes are often observed at or around the pKa of the oxyanion (Mott, 1981).

Arsenic Adsorption Models

Langmuir Adsorption Model

A set of Langmuir adsorption isotherms was constructed to illustrate the effect of change in variables (b and K_L) on Langmuir plots. Figure 34 illustrates three adsorption isotherms with identical adsorption maxima (b), but with varying binding strengths (K_L) as summarized in Table 5. Aqueous concentration at which adsorption reached a maximum increased as the K_L value was increased. When b is fixed, the slopes (1/b) of the linearly transformed Langmuir function, $C/q = (1 / K_L b) + (C / b)$ (Equation [2]), are identical; however, the intercept ($1/K_L b$) of the function increases as the aqueous concentration at which the adsorption maximum is achieved decreases (Figure 35).

Figure 36 illustrates three adsorption isotherms with identical intercepts ($1/K_L b$) of the linearly transformed Langmuir function and increasing adsorption maxima as summarized in Table 5. Because $1/K_L b$ was fixed, binding energy (K_L) decreased as adsorption maximum (b) was increased. The linearly transformed Langmuir functions exhibit an increase in slope (1/b) as adsorption maxima (b) was decreased (Figure 37).

Figure 38 illustrates three hypothetical adsorption isotherms at fixed binding strength (K_L) with varying adsorption maxima (b), as summarized in Table 5. As adsorption maxima (b) was increased both the slope (1/b) and intercept ($1/K_L b$) of the linearly transformed Langmuir equation decreased (Figure 39).

Table 5. Calculated adsorption maxima (b), binding constants (K_L), and linear Langmuir functions of three sets of hypothetical data.

Adsorbent	b	K_L	Linear equation
A	0.1	500	Y=10X+0.02
B	0.1	250	Y=10X+0.04
C	0.1	167	Y=10X+0.06
D	0.0833	600	Y=12X+0.02
E	0.0714	700	Y=14X+0.02
F	0.05	1000	Y=20X+0.02
G	0.1	500	Y=10X+0.02
H	0.08	500	Y=12.5X+0.025
I	0.05	500	Y=20X+0.04
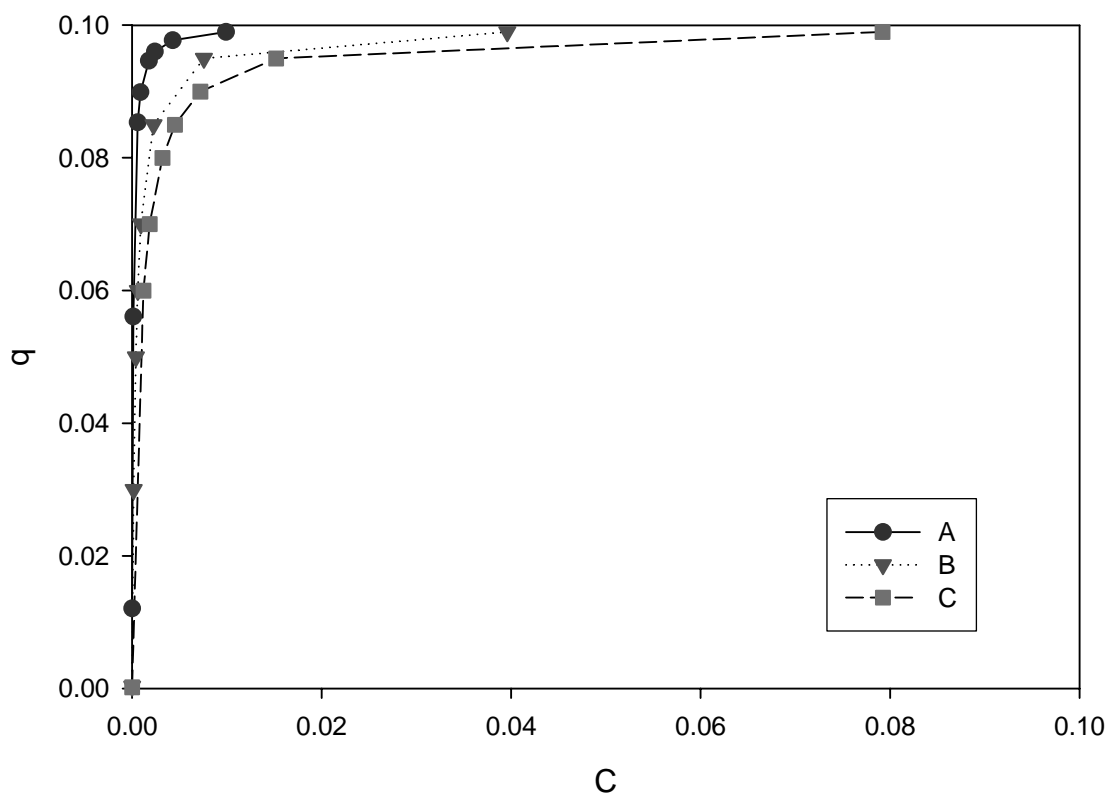
Figure 34. Langmuir adsorption isotherms for three sets of hypothetical data with fixed adsorption maxima (b) and varying bonding strength (K_L) as summarized in Table 5.
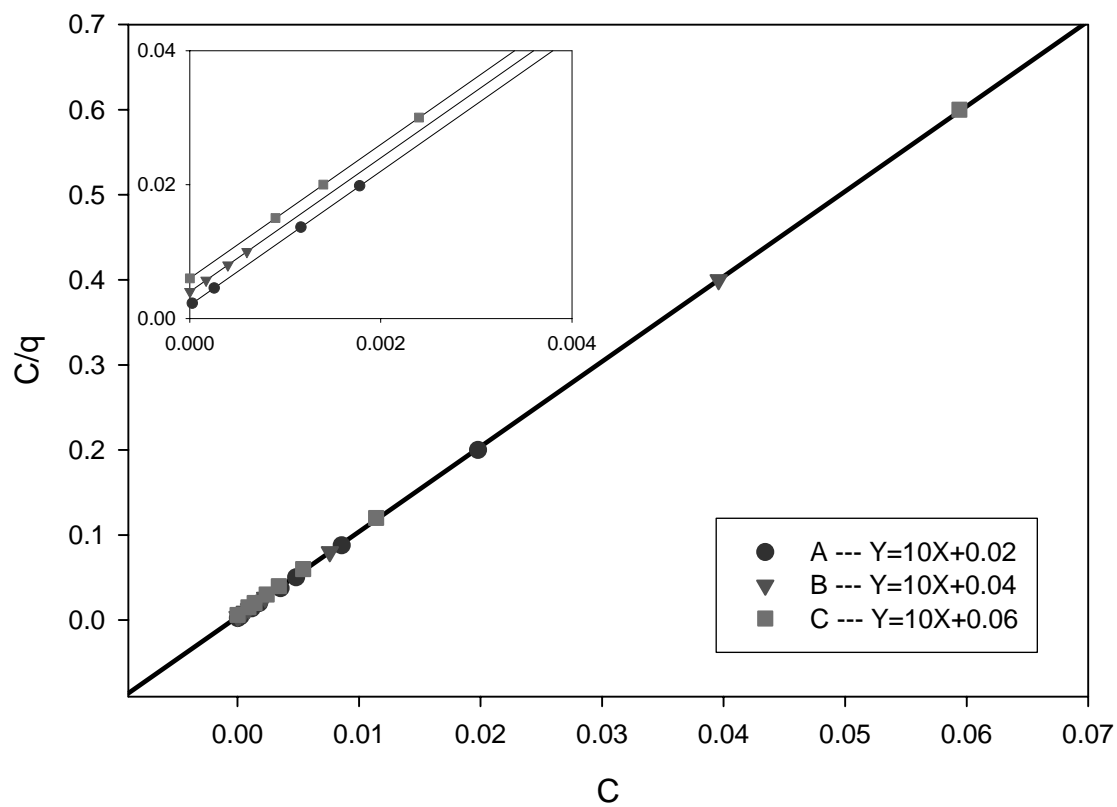
Figure 35. Linear regression using the linear form of the Langmuir equation for three sets of hypothetical data with fixed adsorption maxima (b) and varying bond strength (K_L), as summarized in Table 5.
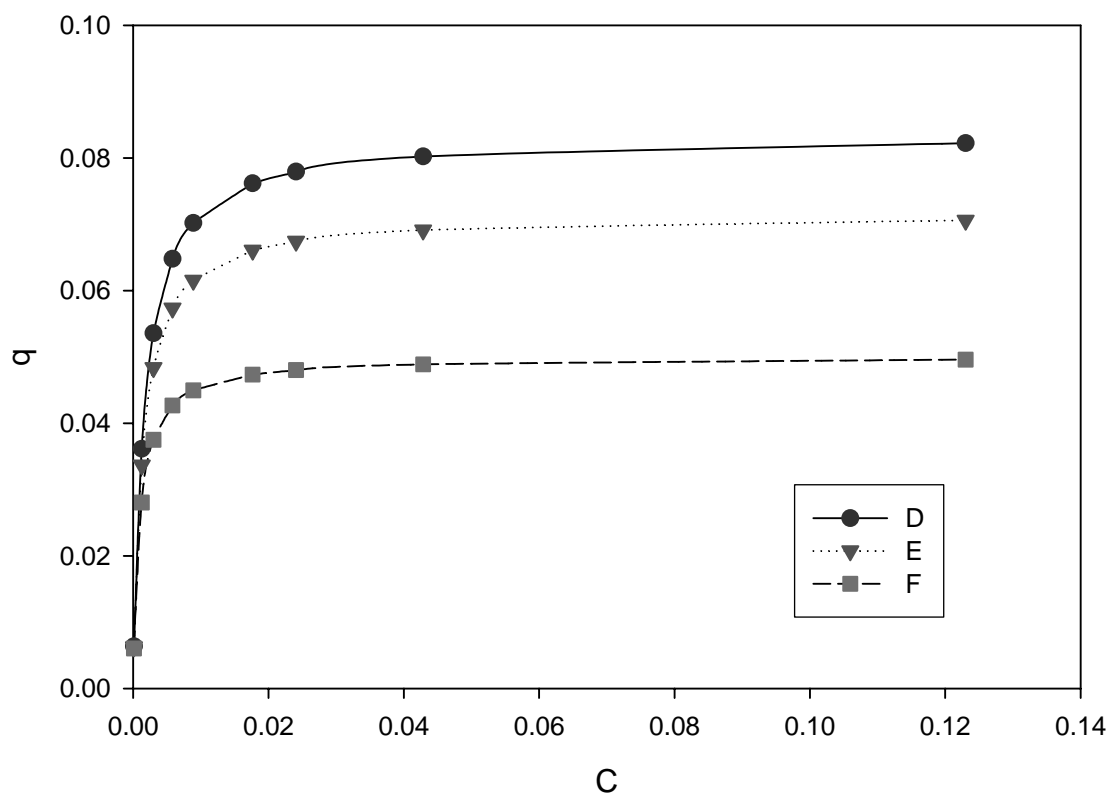
Figure 36. Langmuir adsorption isotherms of three sets of hypothetical data with fixed intercept of the linear Langmuir equation ($1/K_Lb$) and increasing adsorption maxima (b), as summarized in Table 5.
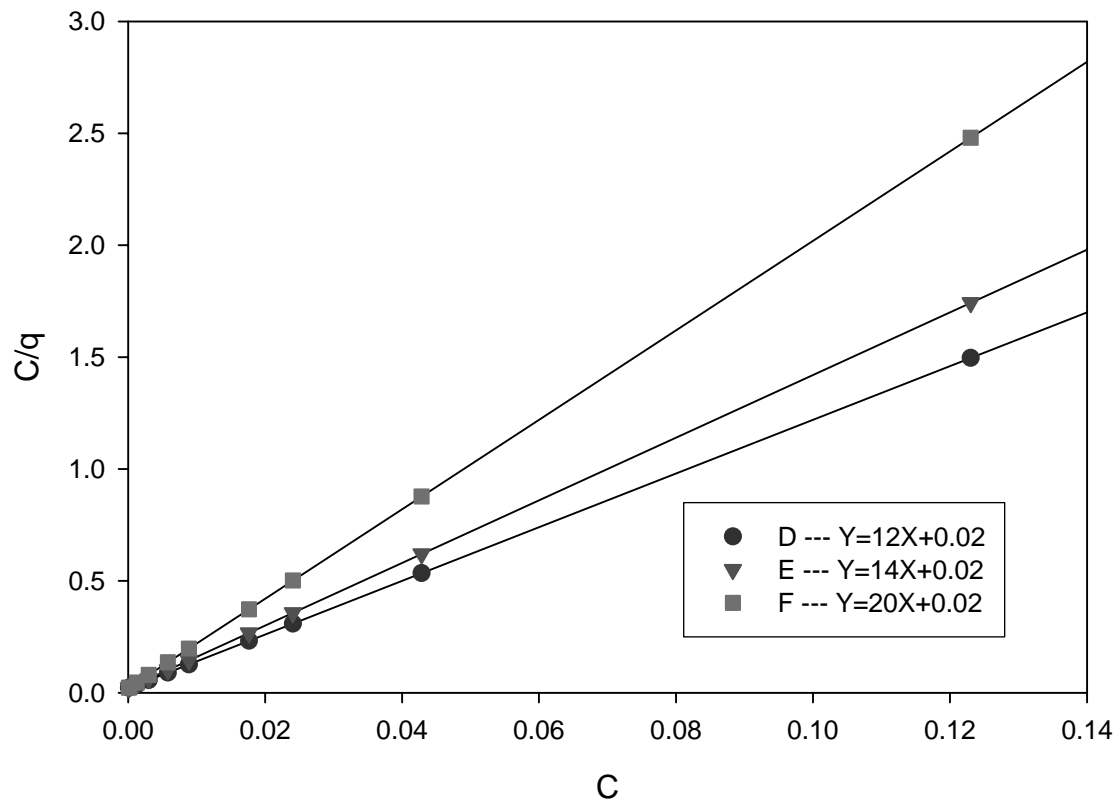
Figure 37. Linear regression using the linear form of Langmuir equation for three sets of hypothetical data with fixed intercept ($1/K_Lb$) and increasing adsorption maxima (b), as summarized in Table 5.
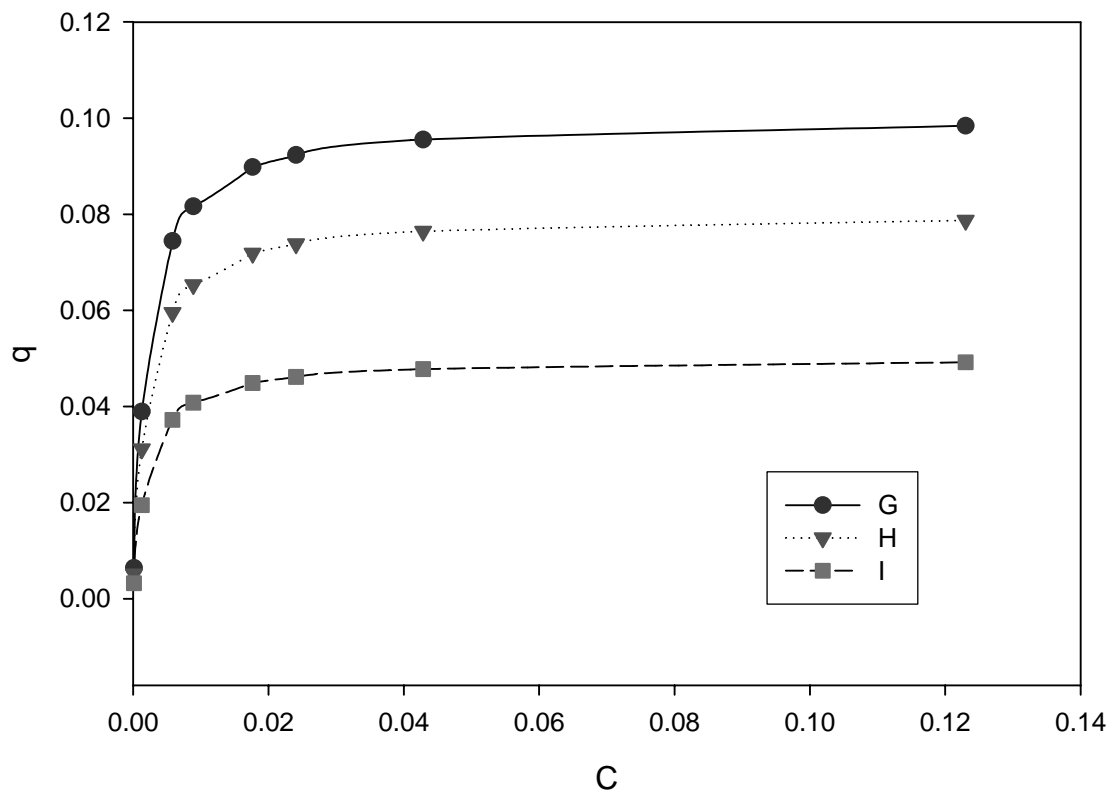
Figure 38. Langmuir adsorption isotherms of three sets of hypothetical data with fixed binding strength (K_L) and varying adsorption maxima (b), as summarized in Table 5.
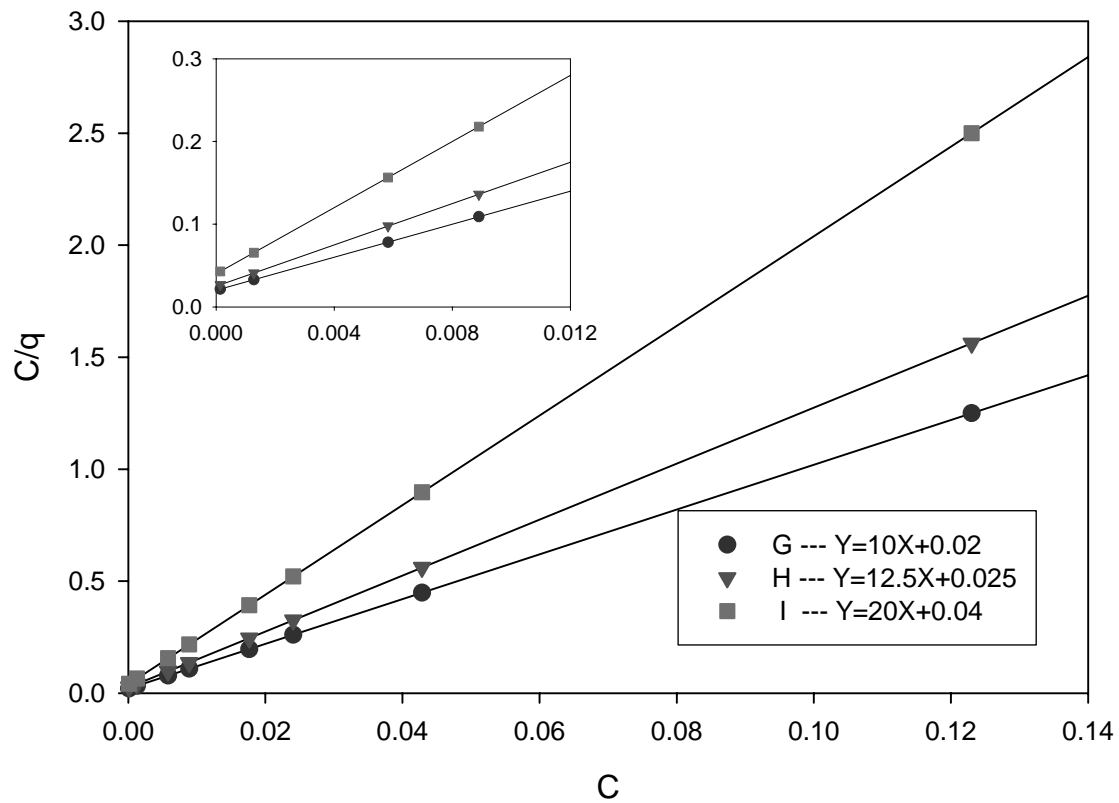
Figure 39. Linear regression using the linear form of the Langmuir equation for three sets of hypothetical data with fixed binding strength (K_L) and varying adsorption maxima (b), as summarized in Table 5.

The Langmuir parameters for the adsorption isotherms of As^V and As^{III} on the Al:Fe hydroxides are summarized in Table 6 and Table 7. In all cases, the linear Langmuir model described the data considerably better for As^V than for As^{III}. The b values indicate that the adsorption maxima of As^V were higher at pH 5 than at pH 8 for each of the Al:Fe molar ratios. Although the adsorption behavior of As^V on the 0:1 and 2:8 Al:Fe hydroxides were similar at both pH 5 and 8 (Figure 26 and Figure 27), the K_L values of the Langmuir adsorption isotherms indicate that As^V was more strongly adsorbed to the 0:1 Al:Fe hydroxide than the 2:8 Al:Fe hydroxide (Table 6, Figure 40, and Figure 41). The K_L values for adsorption of As^V on the 0:1 Al:Fe hydroxide were 23,000 at pH 5 and 14,000 at pH 8,while the K_L values for adsorption of As^V on the 2:8 Al:Fe hydroxide were 16,000 at pH 5 and 9,700 at pH 8 (Table 6). Also, the b values indicate slightly higher adsorption maximum with the 0:1 Al:Fe hydroxide compared to that of the 2:8 Al:Fe hydroxide.

In the case of As^{III}, the b and K_L values were higher at pH 8 than at pH 5, which is comparable with its adsorption behavior (Figure 30 and Figure 31). Adsorption of As^{III} was more highly affected by Al:Fe molar ratio than in the case of As^V (Figure 42 and Figure 43). The K_L values for adsorption of As^{III} on the 0:1 Al:Fe hydroxide were 288 at pH 5 and 565 at pH 8, while the K_L values for adsorption of As^{III} on the 2:8 Al:Fe hydroxide were 159 at pH 5 and 200 at pH 8 (Table 7). The decrease in adsorption maximum as affected by Al:Fe ratio was more severe with As^{III} than with As^V.

As^V exhibited higher K_L and b values than those of As^{III} under similar conditions. The adsorption maxima and bonding strengths of both of As^V and As^{III} increased as Al:Fe

Table 6. Coefficients of determination (r^2), calculated adsorption maxima (b), and binding constants (K_L) of As^V adsorption as affected by Al:Fe molar ratios derived by Langmuir linear functions.

Adsorbent	pH	r^2	b	K_L
0:1 Al:Fe	5	0.9985	0.1073	23298
	8	0.9996	0.0876	14266
2:8 Al:Fe	5	0.9968	0.1062	15691
	8	0.9989	0.0858	9713
5:5 Al:Fe	5	0.9971	0.0846	6219
	8	0.9973	0.0651	4652
1:0 Al:Fe	5	0.9971	0.0505	1376
	8	0.9957	0.0358	910

Table 7. Coefficients of determination (r^2), calculated adsorption maxima (b), and binding constants (K_L) of As^{III} adsorption as affected by Al:Fe molar ratios derived by Langmuir linear functions.

Adsorbent	pH	r^2	b	K_L
0:1 Al:Fe	5	0.9574	0.0812	288
	8	0.9824	0.0843	565
2:8 Al:Fe	5	0.946	0.0577	159
	8	0.905	0.0785	200
5:5 Al:Fe	5	0.9168	0.0377	104
	8	0.8828	0.0598	145
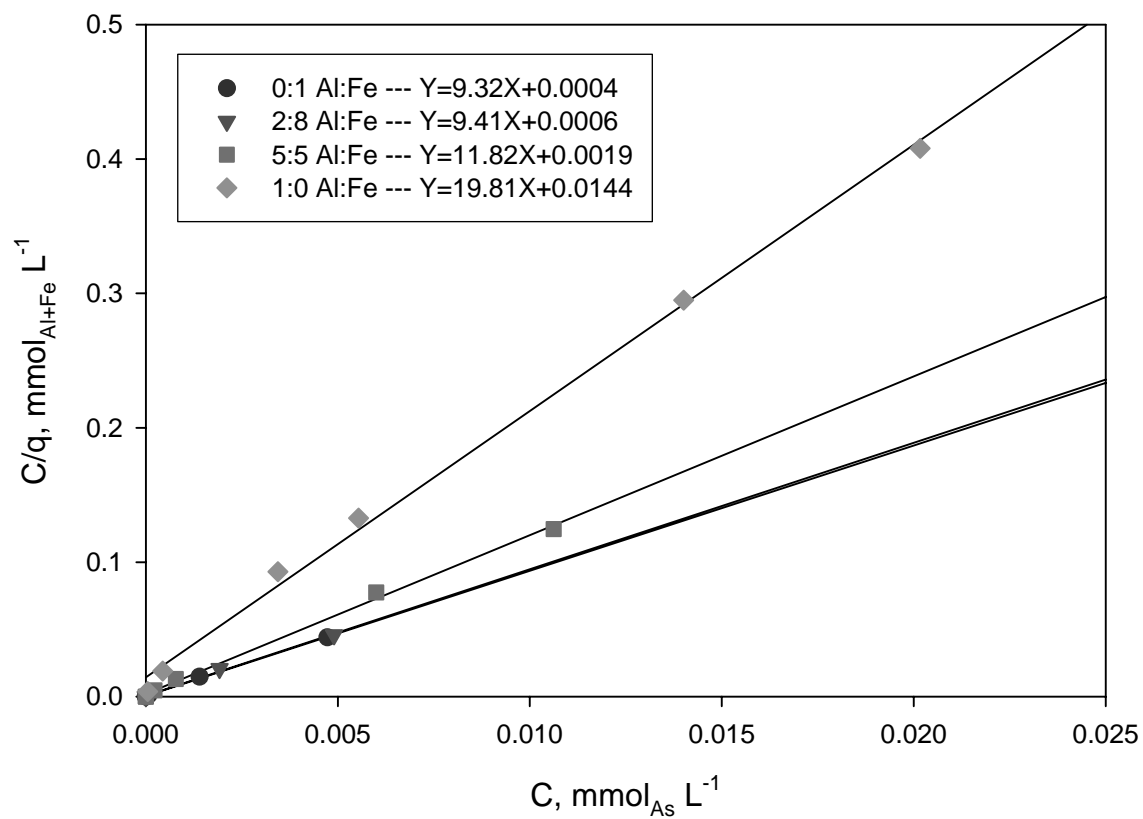
Figure 40. Linear regression using the linear form of the Langmuir equation for evaluation of adsorption of As^V by Al:Fe hydroxides at pH 5, as summarized in Table 6.
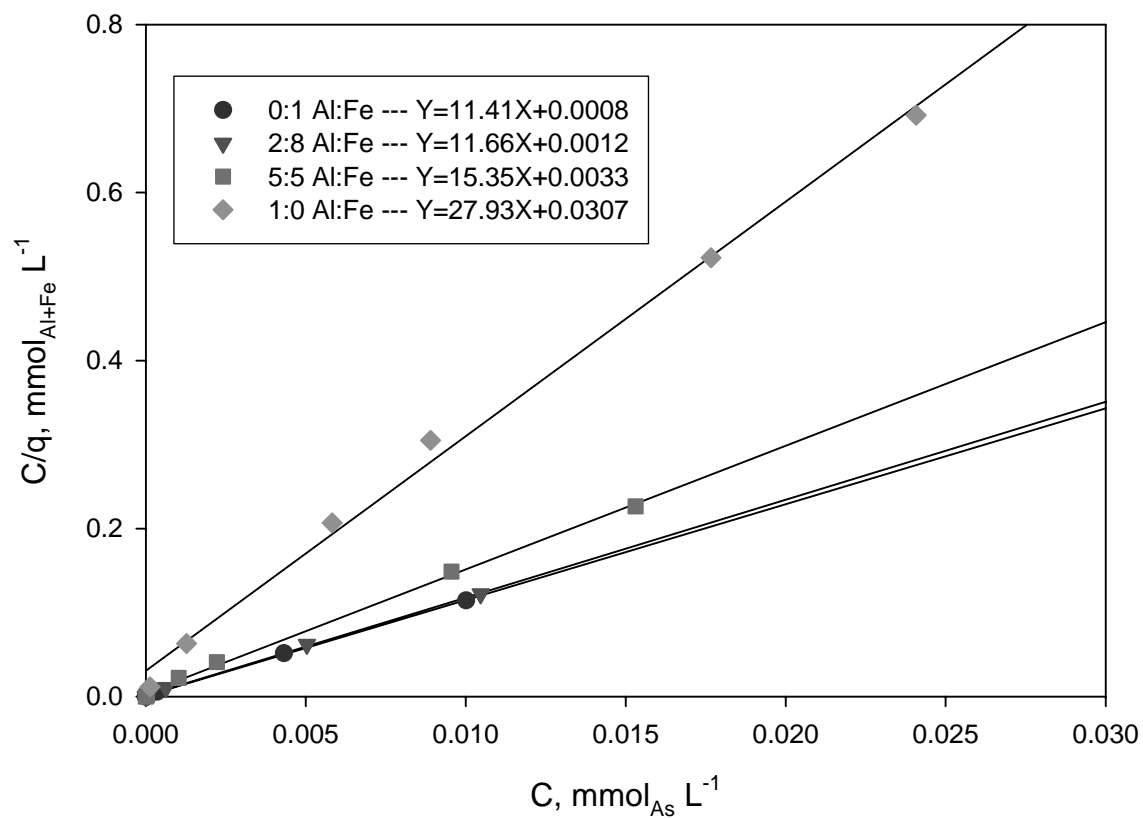
Figure 41. Linear regression using the linear form of the Langmuir equation for evaluation of adsorption of As^V by Al:Fe hydroxides at pH 8, as summarized in Table 6.
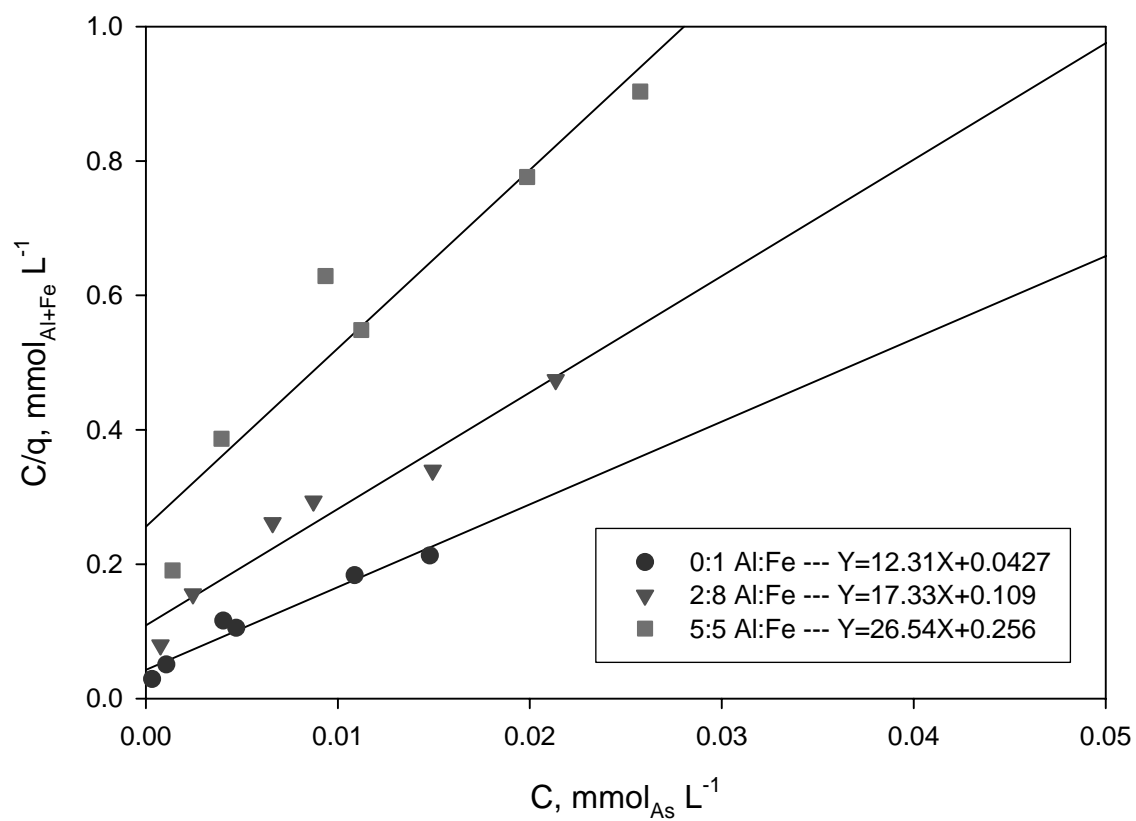
Figure 42. Linear regression using the linear form of the Langmuir equation for evaluation of adsorption of As[III] by Al:Fe hydroxides at pH 5, as summarized in Table 7.
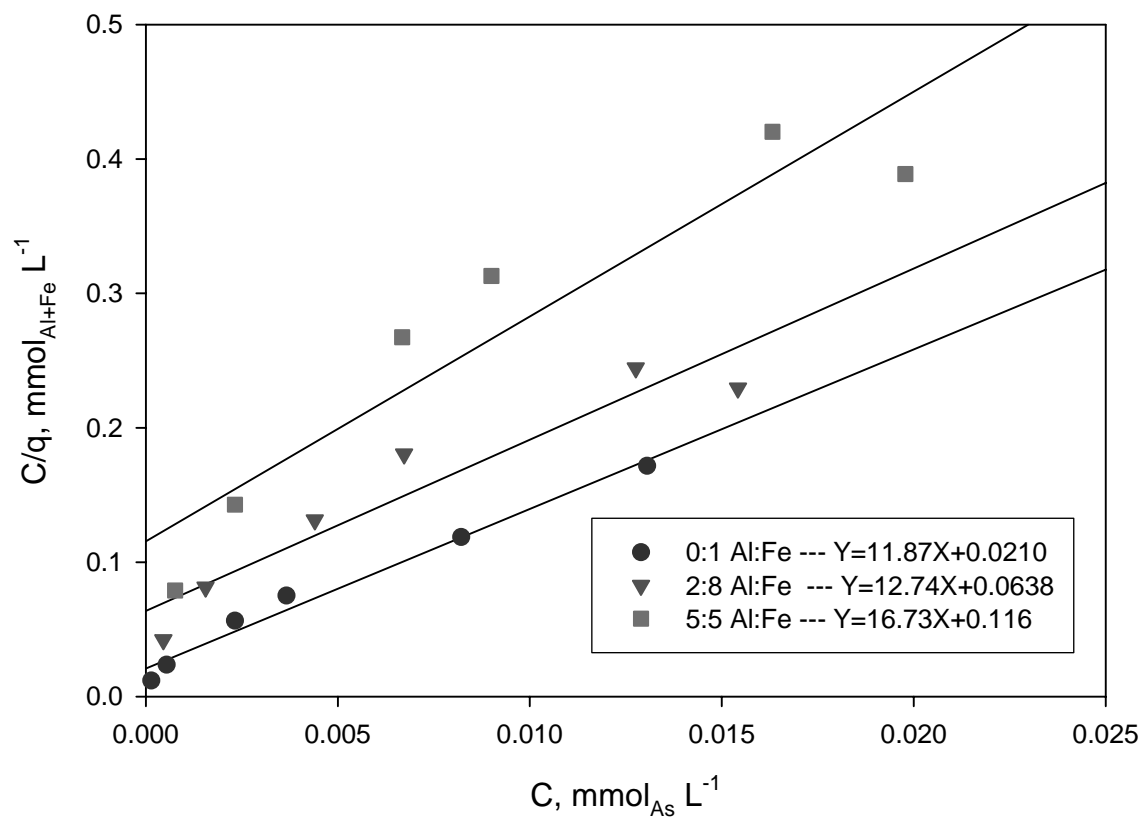
Figure 43. Linear regression using the linear form of the Langmuir equation for evaluation of adsorption of As^{III} by Al:Fe hydroxides at pH 8, as summarized in Table 7.

molar ratio decreased; however, this trend was more noticeable in the case of As^{III}. In general, these trends indicate the higher affinity of As^V on both Fe hydroxide and Al hydroxide compared to that of As^{III}, and higher retention of both As^V and As^{III} on Fe hydroxide compared to Al hydroxide.

Freundlich Adsorption Model

Sets of hypothetical Freundlich adsorption isotherms were constructed to illustrate the effects of the variables, N and K_F, on the Freundlich isotherm, $q = K_F C^N$ (Equation [3]), and its linear transformation, $\log q = N \log C + \log K_F$ (Equation [4]) with $0 \leq N \leq 1$. Figure 44 illustrates three hypothetical adsorption isotherms with identical K_F but varying N, as summarized in Table 8. When N is 1 (Figure 44 – C), the C-curve isotherm is obtained (Essington, 2004), that is, the slope of the Freundlich isotherm remains constant regardless of the surface coverage. As N is decreased, within the constraints of $0 \leq N \leq 1$, the initial slope of the adsorption isotherm is greater. N is most strongly influenced by the initial slope of the adsorption isotherm. A very small N value is indicative of quantitative adsorption at low C. The slope of the linearly transformed Freundlich equation increases with an increase in the N value, since N is the slope of the linear Freundlich function (Figure 45). Because K_F values were fixed in this example, the intercepts ($\log K_F$) of the linear Freundlich function are identical.

Table 8. Calculated N and K_F of Freundlich linear functions of two sets of hypothetical data.

Adsorbent	N	K_F	Linear equation
A	0.1	0.3162	Y=0.1X-0.2
B	0.5	0.3162	Y=0.5X-0.2
C	1	0.3162	Y=X-0.2
D	0.5	0.631	Y=0.5X-0.2
E	0.5	0.3162	Y=0.5X-0.5
F	0.5	0.1	Y=0.5X-1
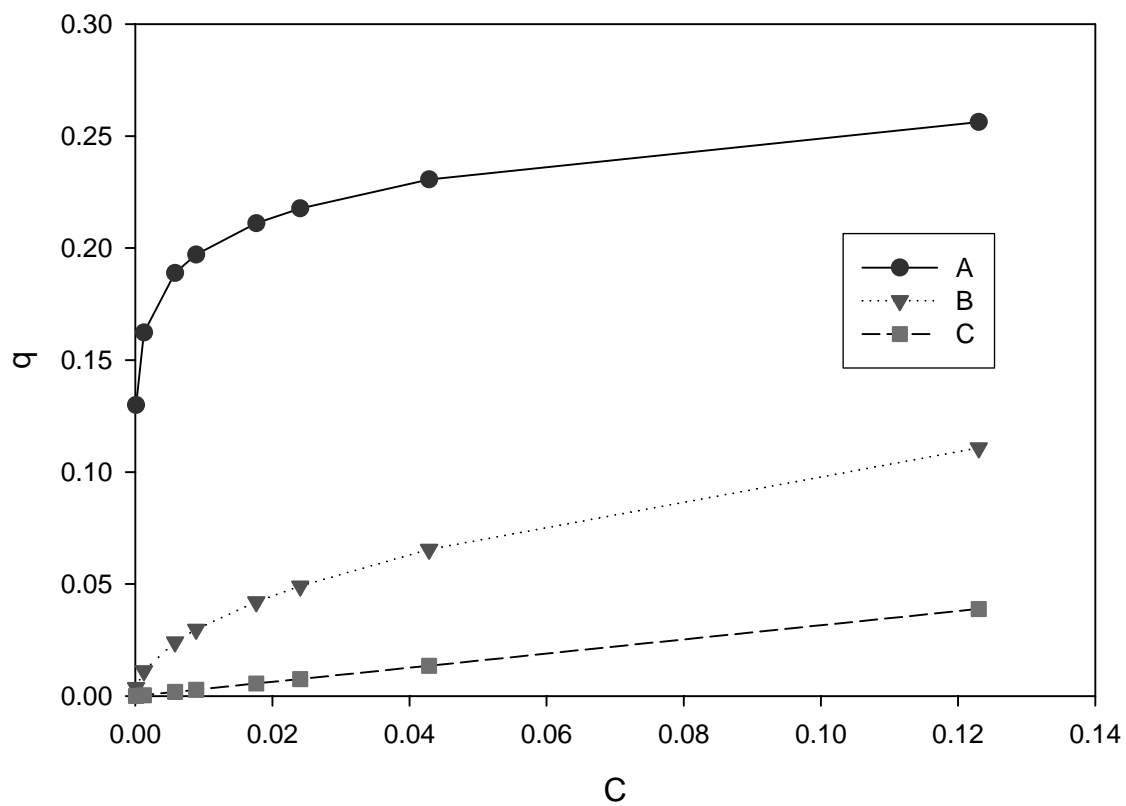
Figure 44. Freundlich adsorption isotherms, $q = K_F C^N$, for three sets of hypothetical data, with fixed K_F but with varying N, as summarized in Table 8.
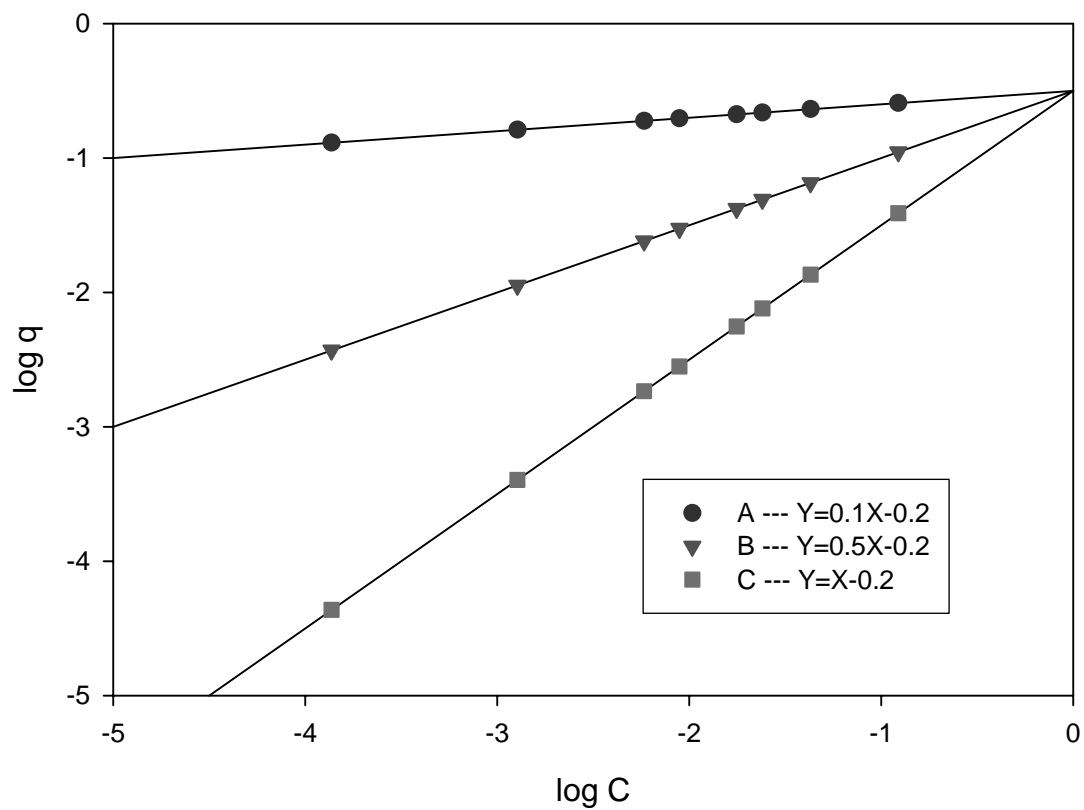
Figure 45. Linear regression lines of the Freundlich linear equation, log q = N log C + log K_F, for three sets of hypothetical data from Figure 44, with fixed K_F and varying N. The regression equations for these lines are summarized in Table 8.

Figure 46 illustrates three hypothetical adsorption isotherms with identical N but varying K_F, as summarized in Table 8. A higher K_F value also indicates a greater adsorption when N and C are fixed, as it is apparent from its mathematical relationship, $q = K_F C^N$. Linearly transformed Freundlich equations exhibit parallel lines as they have identical slopes, N (Figure 47). The intercepts, $\log K_F$, of these functions increase as the K_F value increases.

The Freundlich parameters, N and K_F, for the adsorption of As^V and As^{III} on the Al:Fe hydroxides are summarized in Table 9 and Table 10. With both As^V and As^{III} adsorption isotherms, calculated N values were not appreciably different at pH 5 than at pH 8, and were also not significantly affected by Al:Fe molar ratio (Table 9 and Table 10). The N values of As^V adsorption isotherms were similar, approximately 0.12 to 0.16; therefore, nearly parallel lines of the linearly transformed Freundlich lines were observed (Figure 48 and Figure 49). The N values of As^{III} adsorption isotherms were also similar, approximately 0.41 to 0.50, and approximately parallel lines of the linearly transformed Freundlich lines were also observed (Figure 50 and Figure 51). The similar values of N within the set of As^V adsorption isotherms and within the set of As^{III} adsorption isotherms indicate that the initial increase in adsorption followed similar trends at the various Al:Fe molar ratios, for both As^{III} and As^V.

The N values of As^V adsorption isotherms ($0.12 \leq N \leq 0.16$) were considerably smaller than those of As^{III} ($0.4137 \leq N \leq 0.497$). This trend indicates the greater slopes of adsorption isotherms at low C in the case of As^V compared to As^{III}, which indicates a higher affinity of As^V than As^{III} to the hydroxide surface. When As^V was quantitatively adsorbed at the lower As:(Al+Fe) molar ratios, the equilibrium concentration (C) was
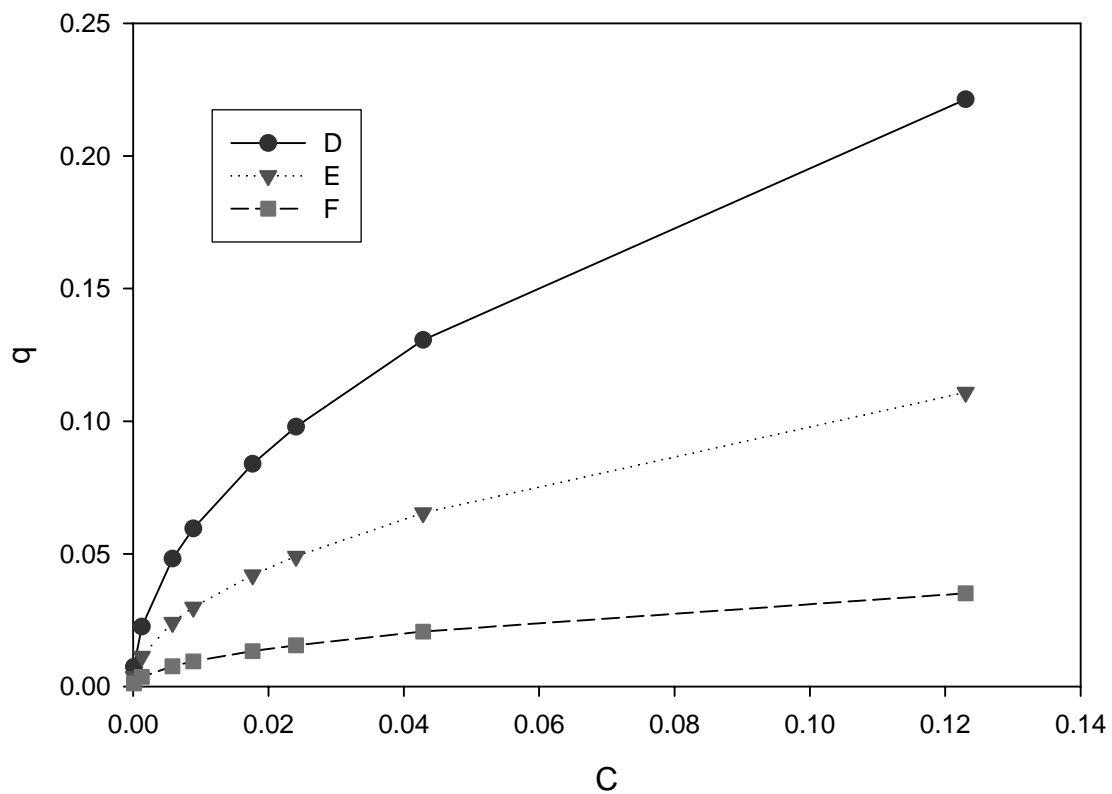
Figure 46. Freundlich adsorption isotherms, $q=K_F C^N$, for three sets of hypothetical data, with fixed N but with varying K_F, as summarized in Table 8.
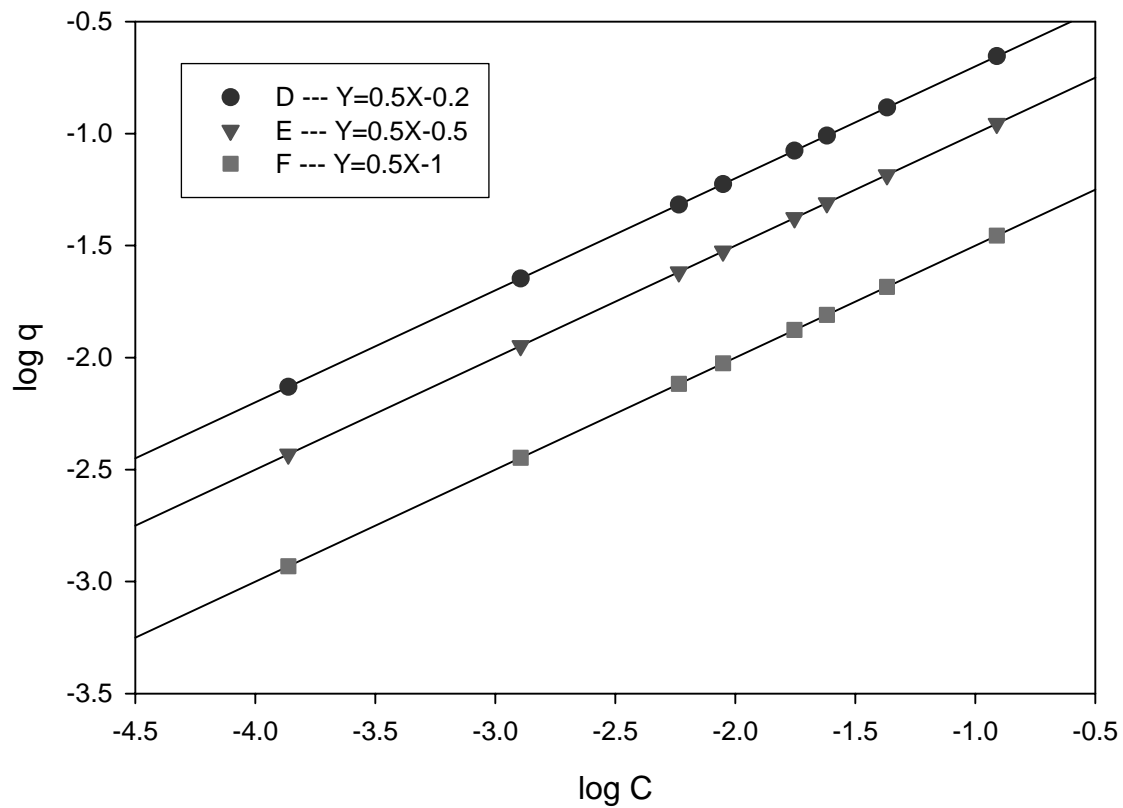
Figure 47. Linear regression lines of the Freundlich linear equation, $\log q = N \log C + \log K_F$, for three sets of hypothetical data from Figure 46, with fixed N and varying K_F, as summarized in Table 8.

Table 9. Coefficients of determination (r^2), and calculated N and K_F values for As^V adsorption by Al:Fe hydroxides, as derived using the Freundlich linear functions.

Adsorbent	pH	r^2	N	K_F
0:1 Al:Fe	5	0.9928	0.1433	0.2368
	8	0.9869	0.1226	0.1586
2:8 Al:Fe	5	0.9984	0.155	0.2443
	8	0.9894	0.116	0.1463
5:5 Al:Fe	5	0.9983	0.1403	0.1604
	8	0.9817	0.1372	0.1043
1:0 Al:Fe	5	0.9788	0.1586	0.0929
	8	0.9727	0.161	0.0638

Table 10. Coefficients of determination (r^2), and calculated N and K_F values for As^{III} adsorption by Al:Fe hydroxides, as derived using the Freundlich linear functions.

Adsorbent	pH	r^2	N	K_F
0:1 Al:Fe	5	0.9921	0.4724	0.5119
	8	0.9952	0.4137	0.4907
2:8 Al:Fe	5	0.9895	0.4859	0.3037
	8	0.9908	0.4966	0.4823
5:5 Al:Fe	5	0.9696	0.4867	0.1658
	8	0.9846	0.4795	0.2934
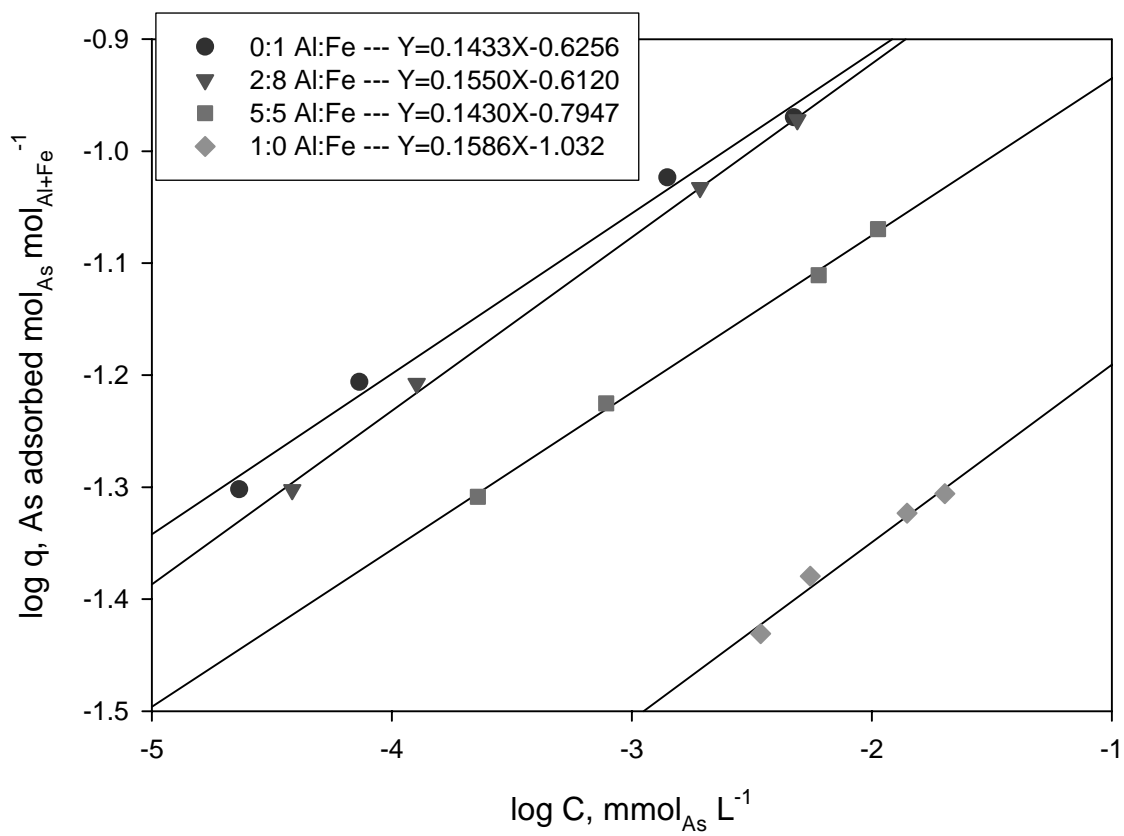
Figure 48. Linear regression lines of the linearly transformed Freundlich adsorption isotherms for adsorption of As^V by various Al:Fe hydroxides at pH 5, as summarized in Table 9.
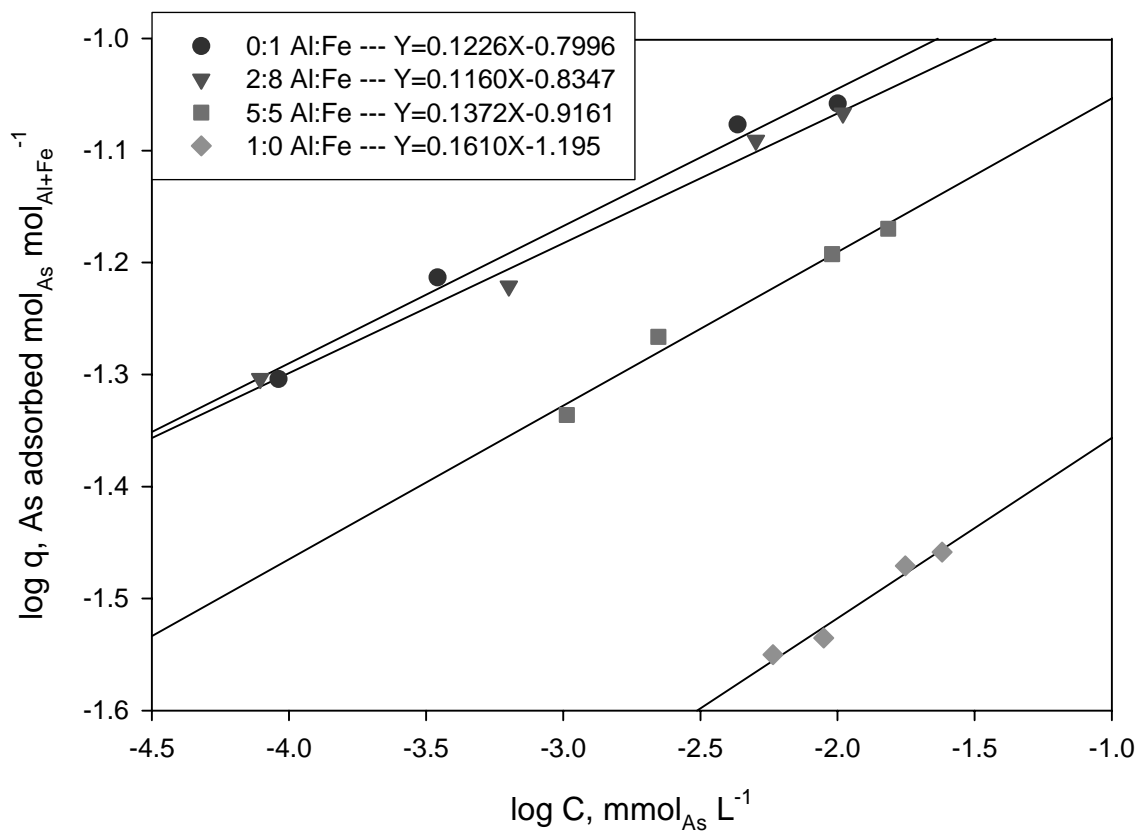
Figure 49. Linear regression lines of the linearly transformed Freundlich adsorption isotherms for adsorption of As^V by various Al:Fe hydroxides at pH 8, as summarized in Table 9.
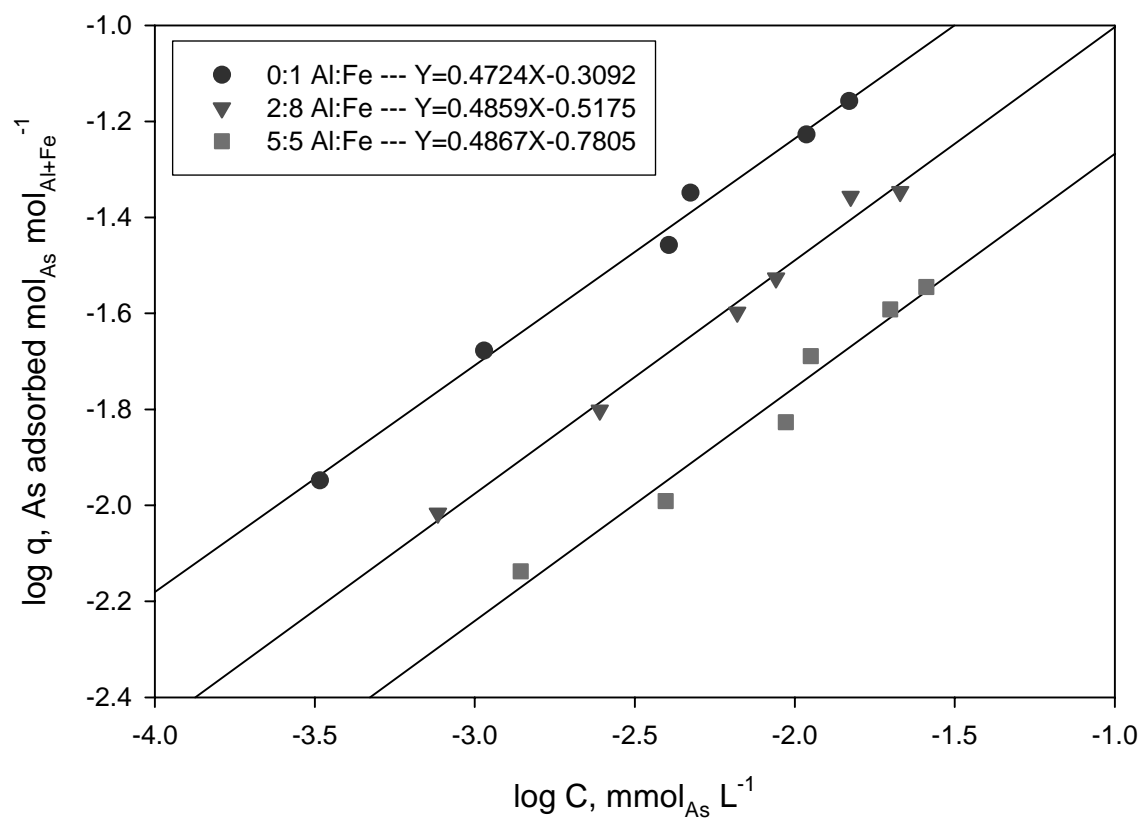
Figure 50. Linear regression lines of the linearly transformed Freundlich adsorption isotherms for adsorption of As[III] by various Al:Fe hydroxides at pH 5, as summarized in Table 10.
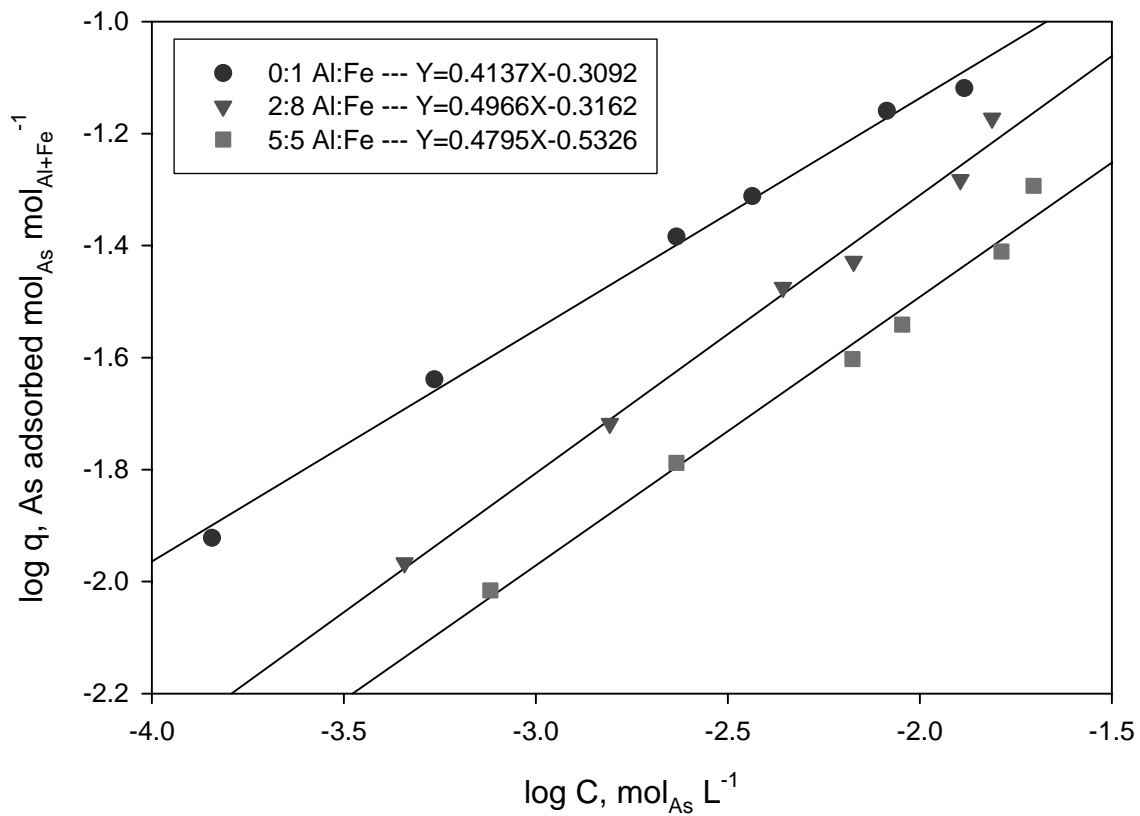
Figure 51. Linear regression lines of the linearly transformed Freundlich adsorption isotherms for adsorption of As^{III} by various Al:Fe hydroxides at pH 8 as summarized in Table 10.

zero. In determination of the linearly transformed Freundlich equation, $\log q = N \log C + \log K_F$ (Equation [3]), the data points in which the As^V was quantitatively adsorbed could not be considered, since log of zero is undefined. Because the points where As^V was quantitatively adsorbed were eliminated, the actual values of N are expected to be smaller than the calculated values.

Because the differences in N values within As^V or As^{III} were small, the differences between adsorption isotherms were mainly reflected by K_F rather than N. In general, there was a trend of higher K_F values with lower Al:Fe molar ratio with both As^V and As^{III}; however, K_F values were higher at pH 5 as opposed to pH 8 in case of As^V, and those of As^{III} were higher at pH 8 rather than pH 5. These trends indicate the greater adsorption of As^V at pH 5 compared to that at pH 8, and the greater adsorption of As^{III} at pH 8 as opposed to pH 5. The interpretation of the Freundlich parameters is compatible with the actual isotherms (Figure 26, Figure 27, Figure 30, and Figure 31).

The linearly transformed Freundlich functions of As^V adsorption isotherms with the 0:1 and 2:8 Al:Fe hydroxides nearly overlapped regardless of pH (Figure 48 and Figure 49), whereas, those of the As^{III} adsorption isotherms had significantly different intercepts with similar slopes (Figure 50, and Figure 51). This observation, along with the adsorption isotherms and the results of the Langmuir model indicate that As^V adsorption on the 0:1 and 2:8 Al:Fe hydroxides is comparable.

Adsorption isotherms of both As^V and As^{III} were described relatively well by the Freundlich model, since the correlation coefficients (r^2) were always greater than 0.97 (Table 9 and Table 10).

The Langmuir Model versus the Freundlich Model

Higher coefficients of determination (r^2) were observed with the Langmuir model than with the Freundlich model when they were used to describe the adsorption isotherms of As^V on the various hydroxides (Table 6 versus Table 9). However, higher coefficients of determination (r^2) were observed with the Freundlich model rather than the Langmuir model for the As^{III} adsorption isotherms (Table 7 and Table 10). In general, the Langmuir model better described As^V adsorption isotherms, and the Freundlich model better described As^{III} adsorption isotherms.

Arsenic Adsorption Envelopes

Adsorption of As^V followed the same general trends, with respect to pH, for the various Al:Fe hydroxides under the experimental conditions [As:(Al+Fe) = 0.05:1] utilized for the adsorption envelopes; however, adsorption of As^V on the 1:0 Al:Fe hydroxide was much less compared to that of the Fe-containing hydroxides (Figure 52). As^V was quantitatively adsorbed on 0:1, 2:8, and 5:5 Al:Fe hydroxides at pH 3 to 6.5. Electrostatic attraction between the negatively charged As^V and the positively charged hydroxide surface impacts the high affinity for As^V within this pH range. Adsorption of As^V decreased gradually with decreasing pH at pH > 7, as the repulsive potential between As^V and the hydroxide surface and the competition of OH^- for surface-adsorption sites increased. The negative charge of As^V increases at pH > 6 (Figure 2), because the pKa_2 of As^V is 6.97. As^V was never quantitatively adsorbed by the 1:0 Al:Fe hydroxide, and an adsorption maximum was observed at pH 5.2, with 76 % of total As^V adsorbed. The 1:0 Al:Fe hydroxide has a low concentration of adsorption sites compared to the Fe-containing hydroxides, due to the presence of the crystalline hydroxides, bayerite and

Figure 52. Adsorption envelopes of As^V in 0.1 M NaCl at an As:(Al+Fe) molar ratio of 0.05:1, at various Al:Fe molar ratios.

gibbsite, which were identified by XRD and TEM as major constituents of the precipitated hydroxide. A similar trend in As^V adsorption by amorphous Al hydroxide as a function of pH was observed by Anderson et al. (1976). This adsorption behavior might be influenced by the solubility of Al hydroxide. The 0:1 Al:Fe hydroxide is subject to enhanced dissolution at low pH (i.e. pH < 4.5; Lindsay, 1979), which contributes to the solubility of As^V (Figure 53). Though pzc of the Al hydroxide is typically around pH 9 (Hsu, 1989), a specifically adsorbed anion can shift the pzc of the hydroxide surface to lower pH values, making the surface charge at a given pH more negative (Mott, 1981). Anderson et al. (1976) observed that the pH of the isoelectric point decreased from 8.5 to 4.6 as increasing amounts of As^V were added to amorphous Al hydroxide. This trend explains the sharp decrease in As^V adsorption starting at pH 5.2. Electrostatic repulsion between As^V and the Al hydroxide increased because of the adsorbed As^V, and further adsorption was reduced. The pzc of Fe-containing hydroxides would also have been lowered due to the adsorbed As^V(Jain et al., 1999); however, the sharp decrease in adsorption was not observed because of the significantly higher concentration of adsorption sites per unit weight of adsorbent with the poorly crystalline Fe-containing hydroxides compared to the Al hydroxide that was dominated by gibbsite and bayerite (Figure 7).

Unlike As^V adsorption, As^{III} adsorption decreased substantially as Al:Fe molar ratio increased; however, 0:1, 2:8, and 5:5 Al:Fe hydroxides resulted in similar shapes of adsorption envelopes (Figure 54). Adsorption maxima of As^{III} were observed in the pH range of 8 to 9 with the 0:1, 2:8, and 5:5 Al:Fe hydroxides. As^{III} adsorption by the 1:0 Al:Fe hydroxide was negligible across the entire pH range of 3 to 11. At the adsorption
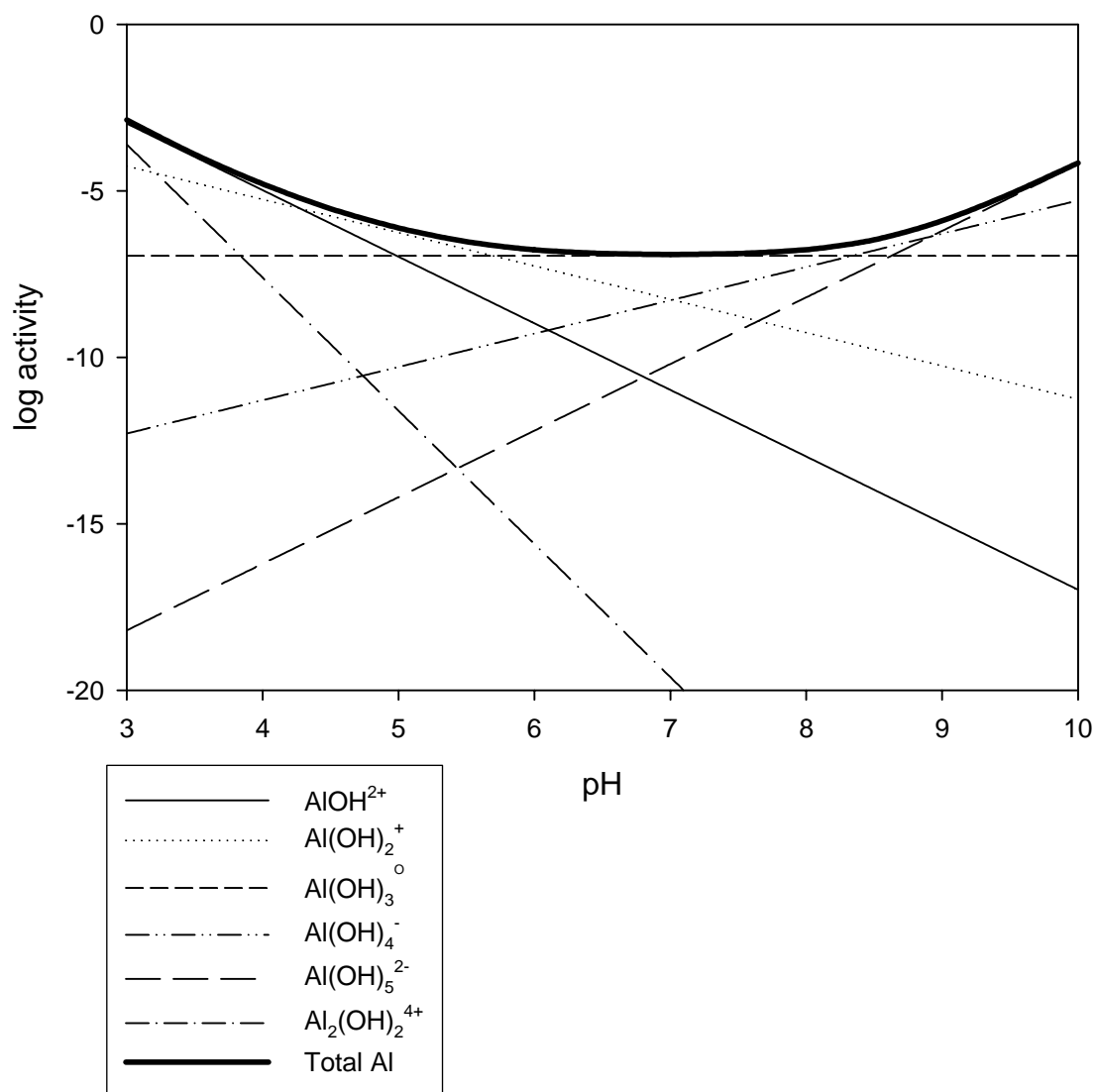
Figure 53. The hydrolysis species of Al^{3+} ion in equilibrium with gibbsite as a function of pH, calculated using thermodynamic constants tabulated in Lindsay (1979).
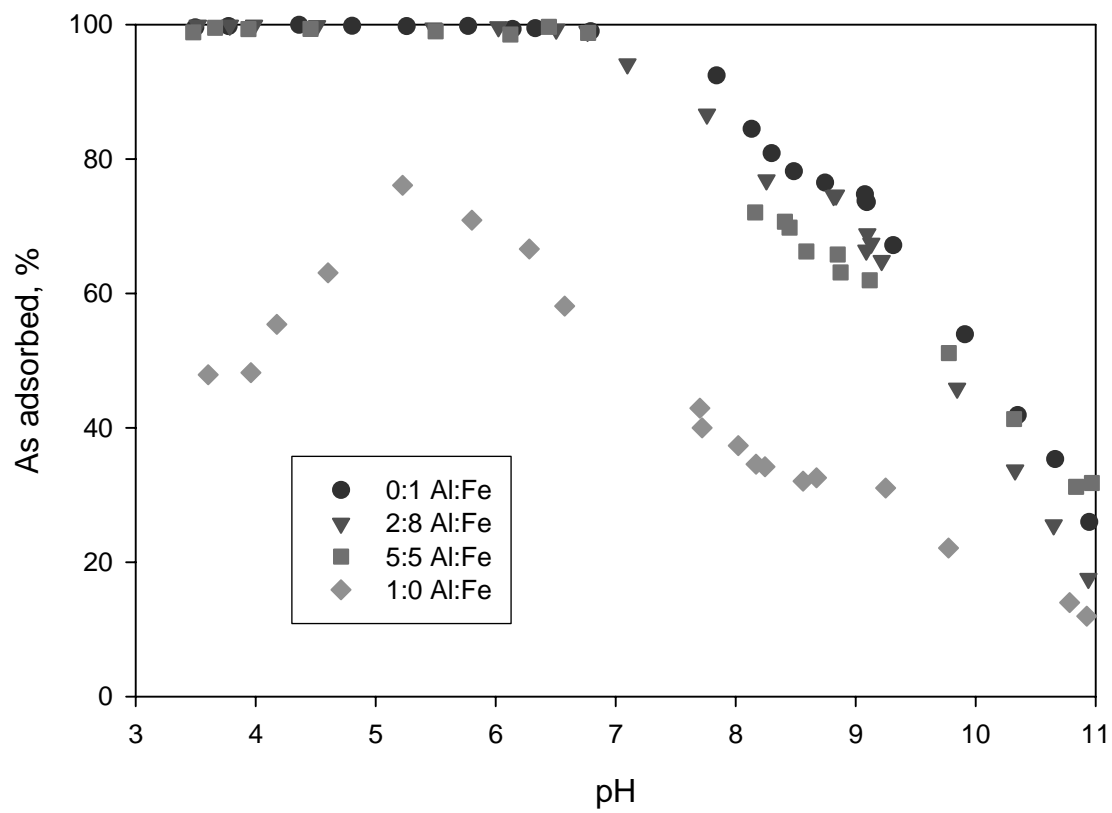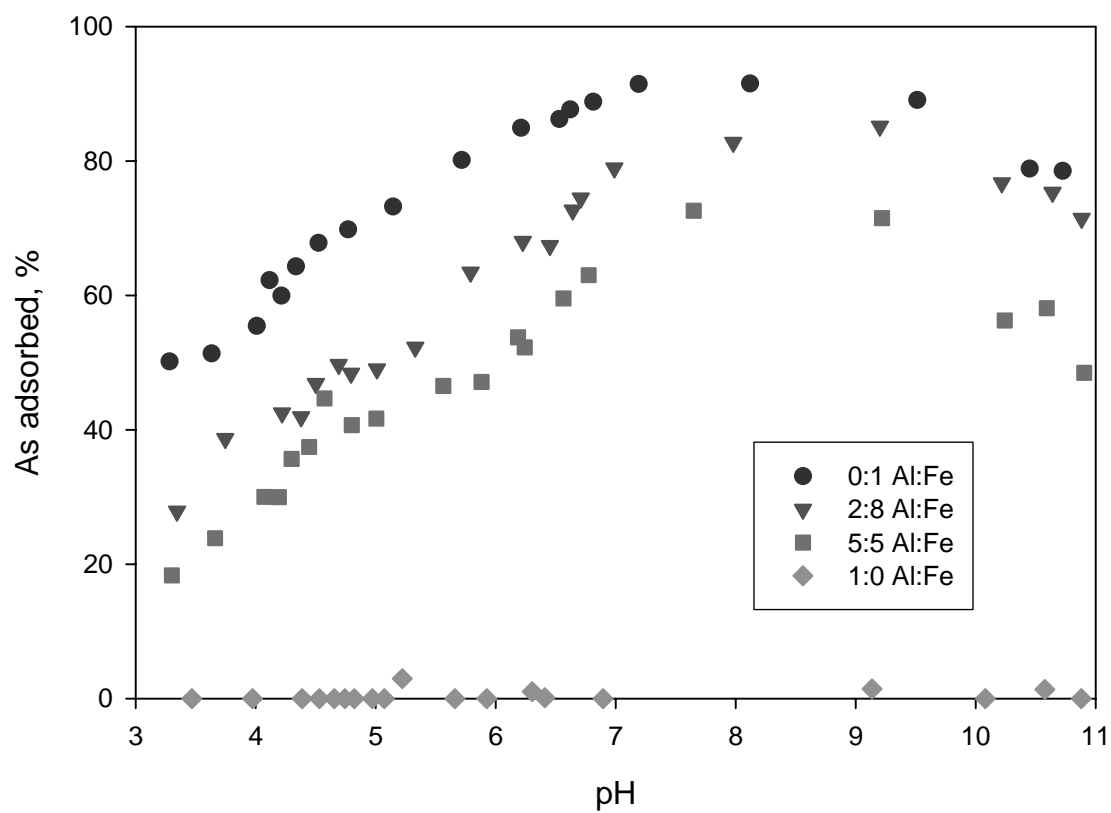
Figure 54. Adsorption envelopes of As^{III} in 0.1 M NaCl at an As:(Al+Fe) molar ratio of 0.05:1, at various Al:Fe molar ratios.

maxima, the 0:1, 2:8, and 5:5 Al:Fe hydroxides adsorbed 92, 85, and 73 %, respectively, of the initially added As^{III}. Adsorption of As^{III} decreased above pH 9 because the negatively charged species dominate above pH 9.22 (pKa_1), and the repulsive forces between As^{III} and the hydroxide surfaces are substantial and will increase with increasing pH. The decrease in As^{III} adsorption with Al substitution indicates the higher affinity of As^{III} by Fe^{3+} relative to Al^{3+}. This result is supported by the result of a previous study by Ferguson and Anderson (1974), in which it was also observed that As^{III} was not readily adsorbed by Al hydroxide.

Although the decrease in As^{III} adsorption was expected to occur in the same proportion as the increase in Al content due to the negligible As^{III} adsorption by Al hydroxide, the As^{III} adsorption maximum decreased by approximately 4 % with 10 % increase in Al content on average. This phenomenon might be due to a heterogeneous distribution of Al within the structure of the hydroxide. There is also a possibility that Fe^{3+} might be preferentially residing at the outer layer of the aggregates; although, Fe would be expected to hydrolyze first because the log Kº of the first Fe^{3+} hydrolysis is –2.19 and that of the first Al hydrolysis is –5.02 (Lindsay, 1979). It is also possible that Al^{3+} was able to adsorb some As^{III}, which might indicate a difference in the affinity of As^{III} to pure Al hydroxide surface sites compared to Al^{3+} sties at the Al:Fe hydroxide surface, i.e., the presence of structure Fe^{3+} might have influenced As^{III} adsorption at Al^{3+} surface sites.

Under the conditions of this experiment [As:(Al+Fe) = 0.05:1 in 0.1 M NaCl], As^{V} adsorption was not strongly influenced by Al substitution except with the 1:0 Al:Fe

hydroxides. Further work is needed to more fully evaluate the influence of pH on As^V adsorption at high As:(Al+Fe) molar ratios.

In the water treatment scenario, As^{III} removal by Al-substituted hydroxide might be problematic since its adsorption decreased with increase in Al substitution. However, As^V can be removed by Al-substituted hydroxides as efficiently as by pure Fe hydroxide when a sufficient amount of hydroxide is present.

Adsorption of Arsenic as Affected by Counterion

Adsorption Isotherms of As^V as Affected by Counterion

As^V was generally adsorbed on both the 0:1 and 2:8 Al:Fe hydroxides in larger amounts in the presence of Ca^{2+} than Na^+ (Figure 55 and Figure 56). At pH 5, As^V was quantitatively adsorbed by both 0:1 and 2:8 Al:Fe hydroxides up to approximately 0.10 As:(Al+Fe) molar ratio (Figure 55). Slightly higher retention of As^V was observed in the presence of Ca^{2+} compared to Na^+ as As:(Al+Fe) molar ratio was increased. At pH 8, As^V was adsorbed quantitatively by both 0:1 and 2:8 Al:Fe hydroxides up to approximately 0.06 As:(Al+Fe) molar ratio (Figure 56). Considerably higher retention of As^V was observed in the presence of Ca^{2+} compared to Na^+ as As:(Al+Fe) molar ratio was increased.

The differences in As^V retention due to pH can be explained by the electrostatic attraction of As^V and the surface-charge characteristics of the Al:Fe hydroxide. At pH 5, the attraction between the positively charged Al:Fe hydroxide surface and the negatively charged As^V species is so strong that As^V adsorption was favored regardless of counterion. At pH 8, the Al:Fe hydroxide surface is negatively charged as a result of both the pH dependent negative charge character of the variable charge mineral and the
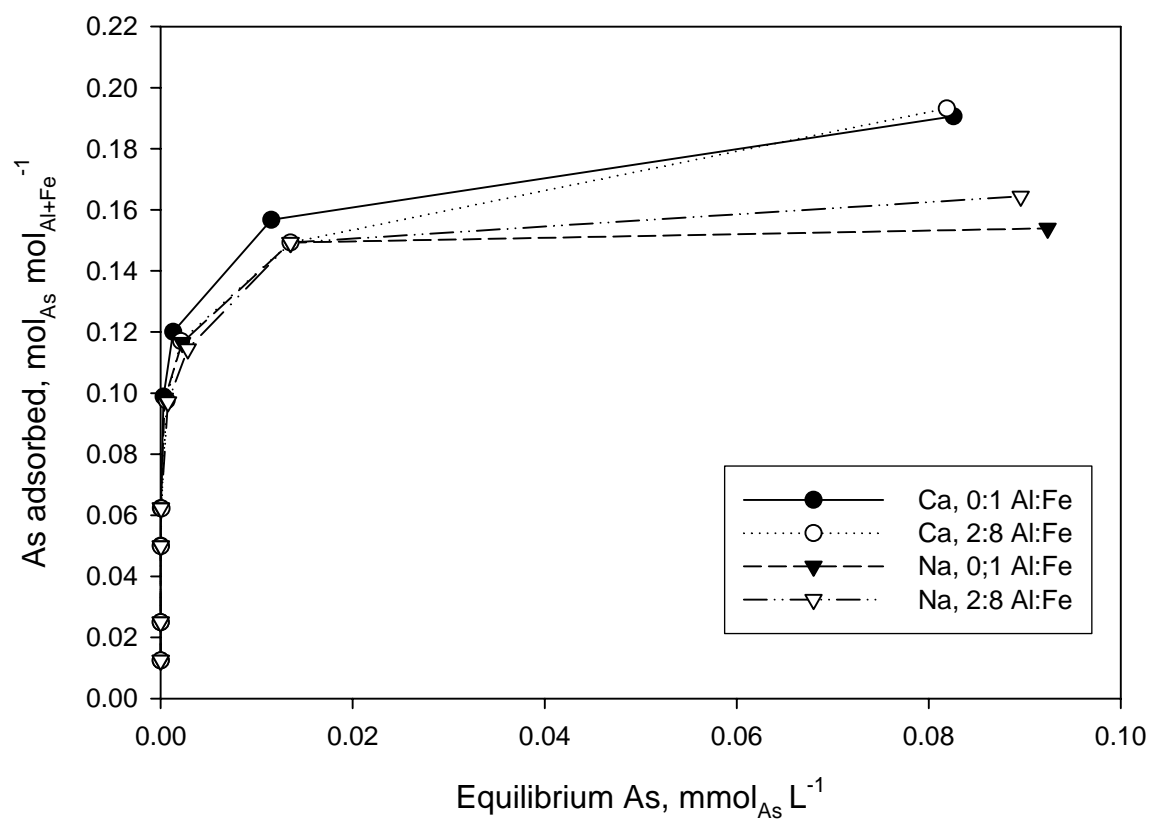
Figure 55. Adsorption isotherms of As^V in 0.1 mol$_{Ca}$ L^{-1} and 0.1 mol$_{Na}$ L^{-1} at pH 5 as affected by counterion and Al:Fe molar ratio.
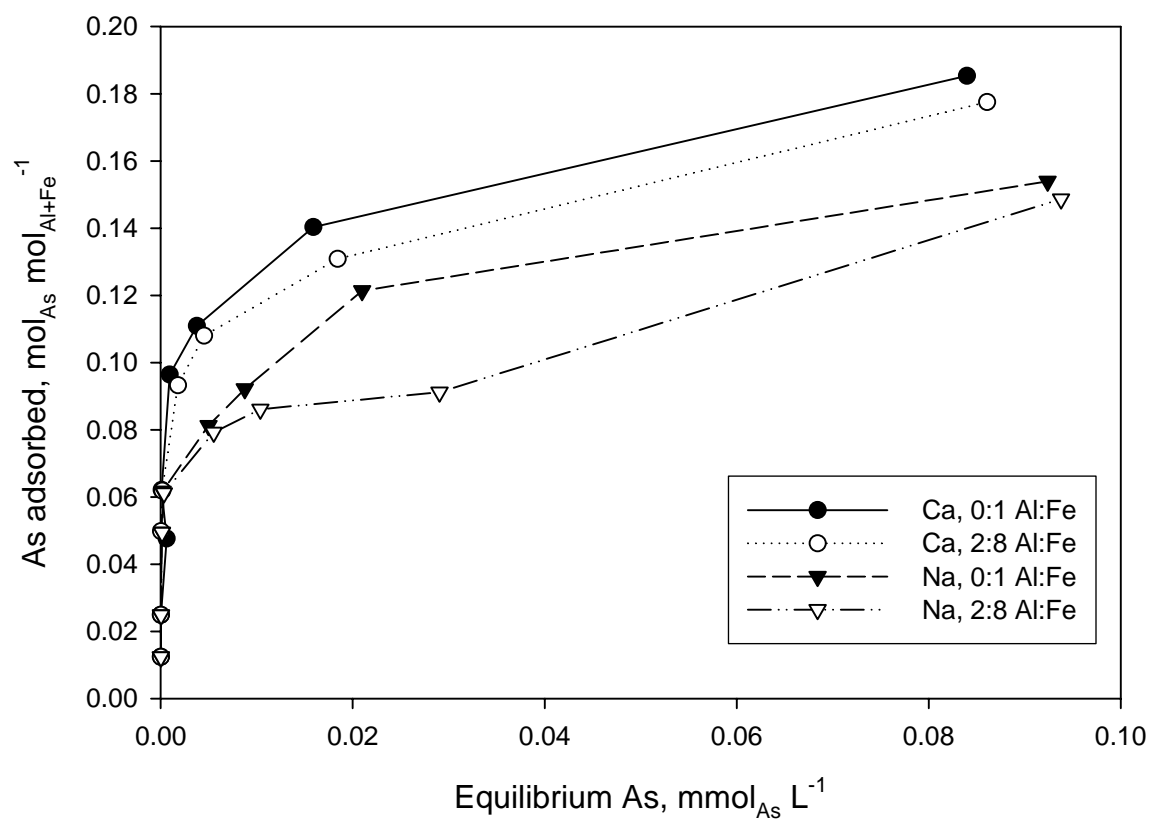
Figure 56. Adsorption isotherms of As^V in 0.1 mol$_{Ca}$ L^{-1} and 0.1 mol$_{Na}$ L^{-1} at pH 8 as affected by counterion and Al:Fe molar ratio.

specific adsorption of anionic As^V species (Mott, 1981); therefore, further adsorption of As^V was reduced. Because of the repulsive potential between the negatively charged hydroxide surface and the negatively charged As^V, a significant effect of divalent cation, Ca^{2+}, was observed at pH 8. Enhanced retention of As by soil and Al and Fe hydroxides in the presence of Ca^{2+} compared to Na^+ as the counterion has been reported by several investigators (Parks et al., 2003; Smith et al., 2002b). The possible scenarios by which Ca^{2+} could enhance the adsorption of As^V are discussed in the hypothesis section below.

Although significant differences in adsorption as affected by Al substitution were not observed at pH 5, slightly better retention of As^V by the 0:1 Al:Fe hydroxide was observed at pH 8 (Figure 55 and Figure 56). There is a possibility that Ca^{2+} can better enhance the retention of As^V without Al substitution; however, further study is needed, as there is also a chance of a potential error associated with the determination of adsorbed As^V concentration at high dissolved As^V concentrations.

Adsorption Envelopes of As^V as Affected by Counterion

Ca^{2+} vs. Na^+

The adsorption envelopes of As^V indicated that the adsorption maximum was in the pH range of approximately 3 to 5 at 0.1:1 As:(Al+Fe) molar ratio, while it was observed in the pH range of approximately 3 to 7.5 at 0.025:1 As:(Al+Fe) molar ratio, regardless of counterion (Figures 57 – 61). At pH above the adsorption maxima, As^V adsorption decreased gradually as pH increased in the presence of Ca^{2+} regardless of Al substitution and As:(Al+Fe) molar ratio, while retention of As^V decreased more rapidly as pH was increased in the presence of Na^+ (Figures 57 – 61). In summary, the retention of As^V was higher in the presence of Ca^{2+} than of Na^+ with both the 0:1 and 2:8
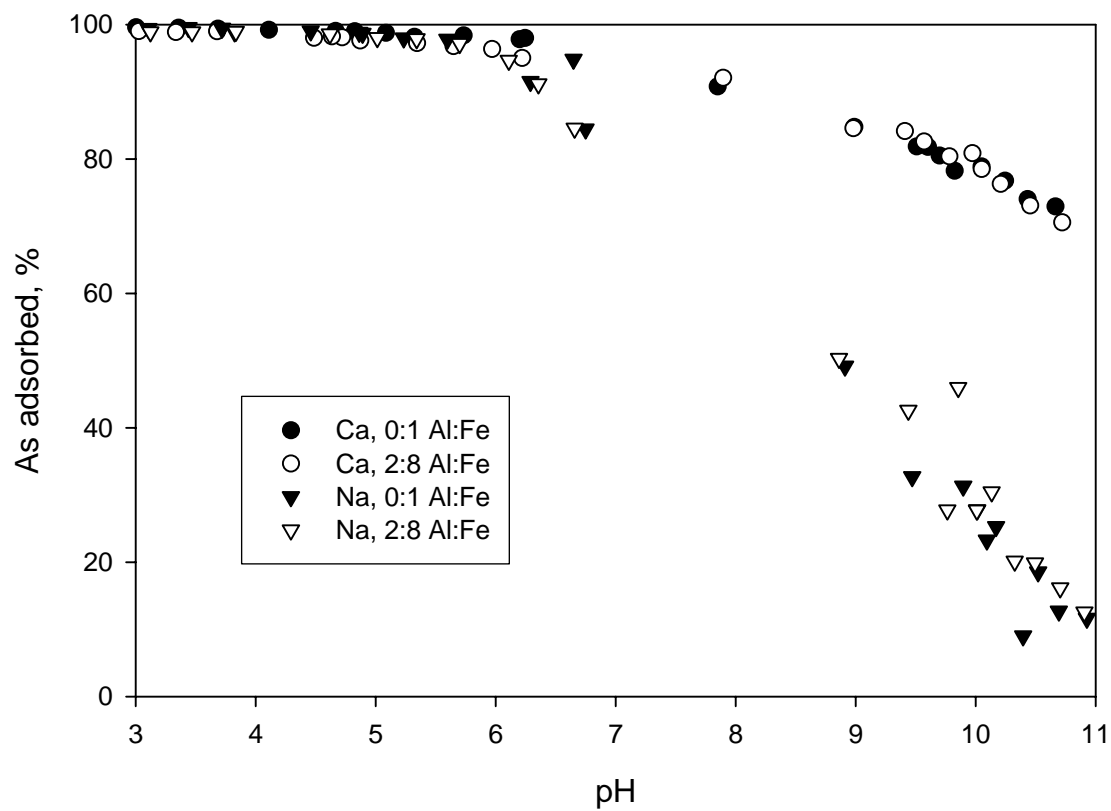
Figure 57. Adsorption envelopes of As^V in 0.1 mol$_{Ca}$ L^{-1} and 0.1 mol$_{Na}$ L^{-1} as affected by counterion and Al substitution at 0.1:1 As:(Al+Fe) molar ratio.
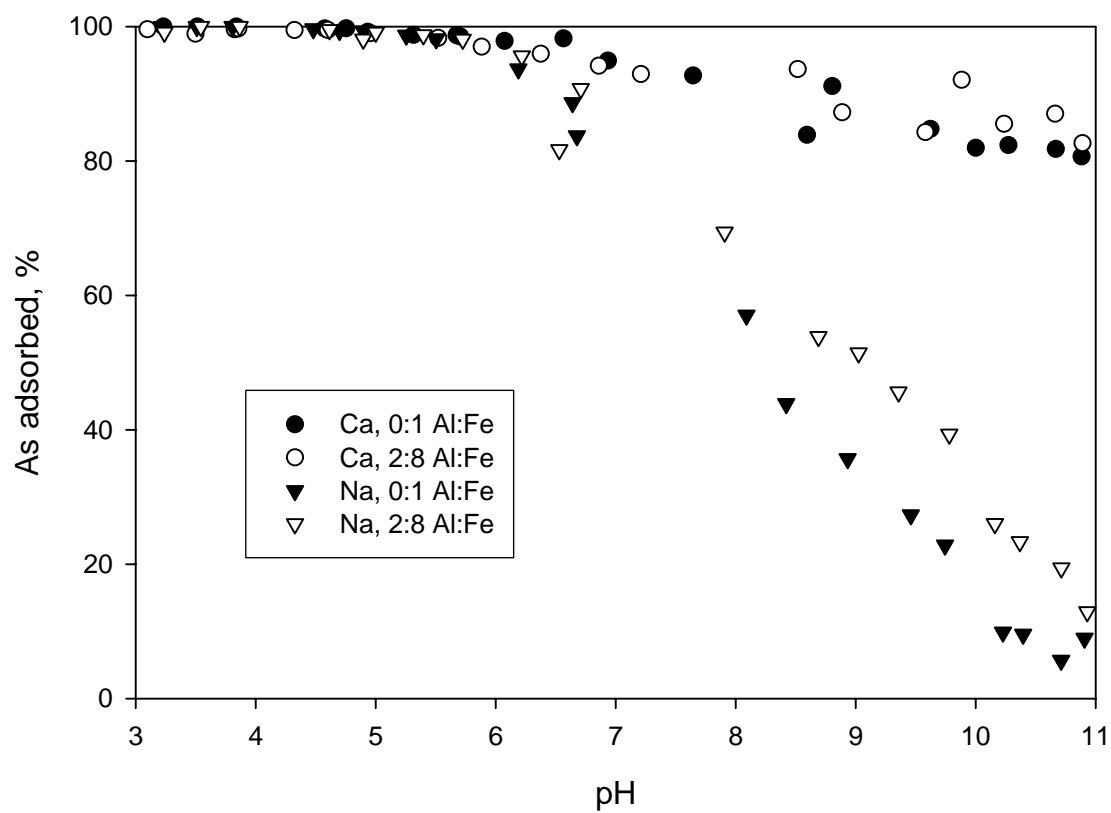
Figure 58. Adsorption envelopes of As^V in 0.01 mol_{Ca} L^{-1} and 0.01 mol_{Na} L^{-1} as affected by counterion and Al substitution at 0.1:1 As:(Al+Fe) molar ratio.
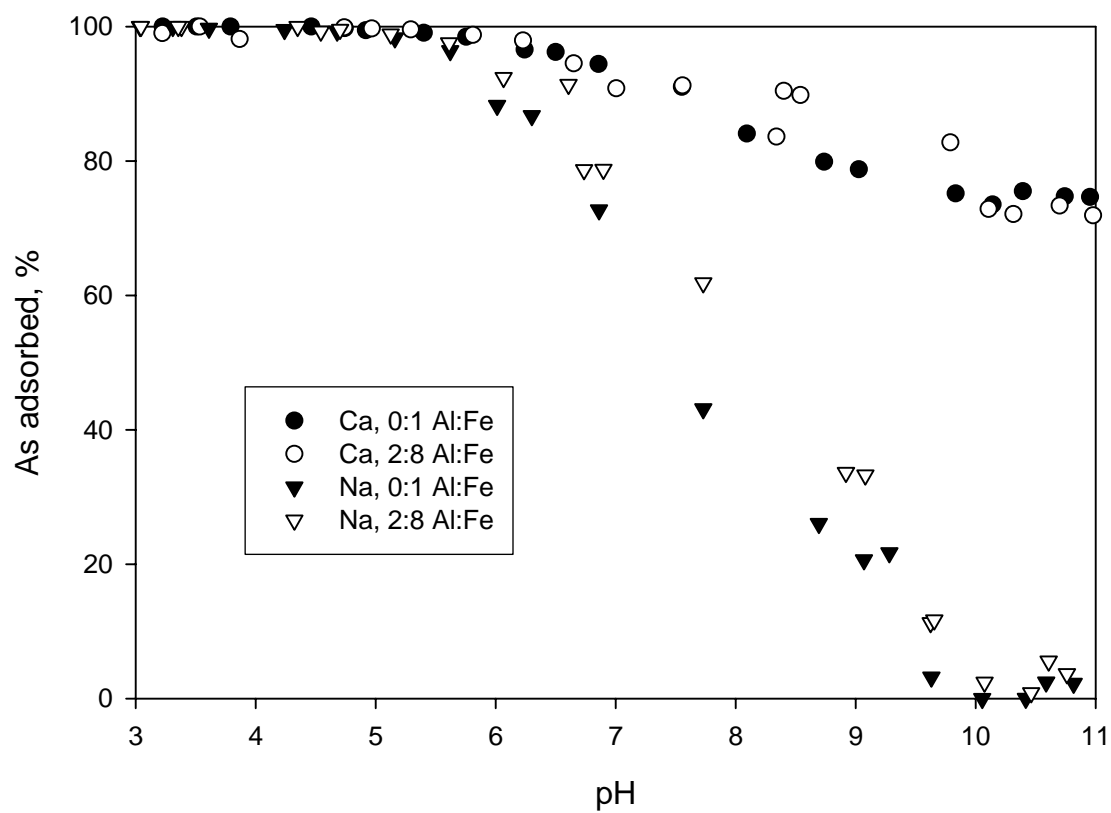
Figure 59. Adsorption envelopes of As^V in 0.001 mol$_{Ca}$ L^{-1} and 0.001 mol$_{Na}$ L^{-1}as affected by counterion and Al substitution at 0.1:1 As:(Al+Fe) molar ratio.
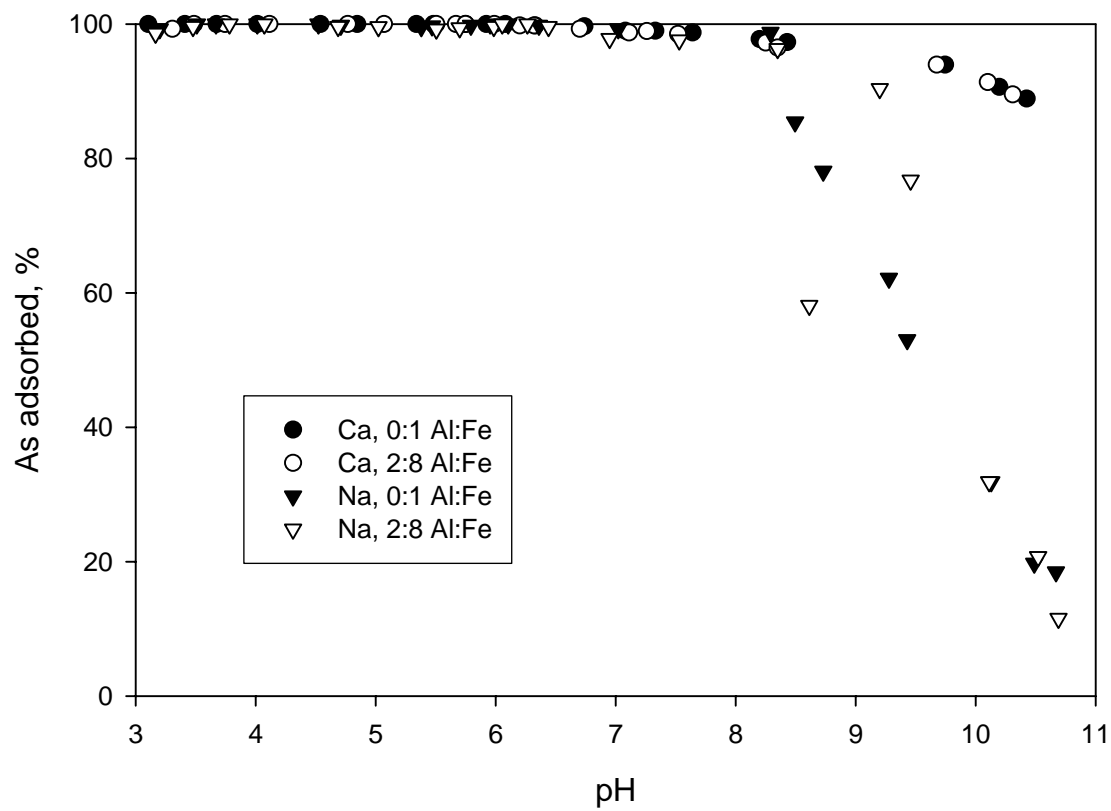
Figure 60. Adsorption envelopes of As^V in 0.1 mol$_{Ca}$ L^{-1} and 0.1 mol$_{Na}$ L^{-1} as affected by counterion and Al substitution at 0.025:1 As:(Al+Fe) molar ratio.
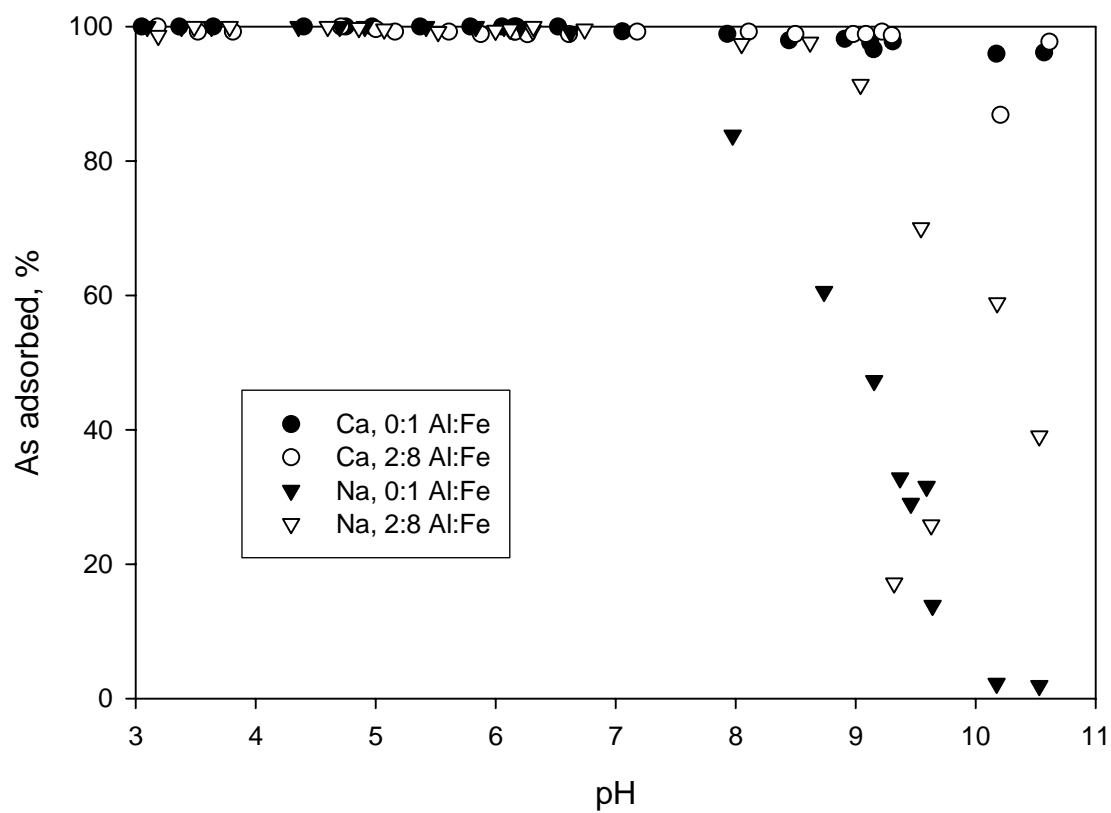
Figure 61. Adsorption envelopes of As^V in 0.01 mol$_{Ca}$ L^{-1} and 0.01 mol$_{Na}$ L^{-1} as affected by counterion and Al substitution at 0.025:1 As:(Al+Fe) molar ratio.

hydroxides, especially at pH>7; however, differences in adsorption maxima were not strongly influenced by either counterion or its concentration.

Counterion Concentration Effect

Similar trends in As^V adsorption envelopes were observed with 0.1, 0.01, and 0.001 $mol_{Ca}\ L^{-1}$ for both 0:1 and 2:8 Al:Fe hydroxides and at both 0.025:1 and 0.1:1 As:(Al+Fe) molar ratios (Figures 62 – 65). Also, similar trends in As^V adsorption were observed in 0.1, 0.01, and 0.001 $mol_{Na}\ L^{-1}$ with both hydroxides and at both the 0.025:1 and 0.1:1 As:(Al+Fe) molar ratios (Figures 66 – 69). Though As^V adsorption was strongly influenced by counterion, i.e., Ca^{2+} vs. Na^+, as discussed previously, adsorption was not strongly affected by counterion concentration at either the 0.025:1 or 0.1:1 As:(Al+Fe) molar ratio regardless of pH and Al:Fe molar ratio. The independence of As^V adsorption on counterion concentration indicates inner-sphere complexation as the As^V retention mechanism (McBride, 1997). The similar trends with both 0:1 and 2:8 hydroxides indicate the similar modes of bonding of As^V in these two systems. Independence of As^V adsorption from ionic strength was also observed by Goldberg and Johnson (2001), who studied As^V adsorption on amorphous Fe oxides in 0.01 to 1.0 M NaCl.

Al substitution

In general, adsorption envelopes of the 2:8 Al:Fe hydroxide overlapped with those of the 0:1 hydroxide regardless of experimental variables, which include counterion, counterion concentration, and pH (Figure 57 – 61). Adsorption of As^V by the 0:1 and 2:8 Al:Fe hydroxides was similarly enhanced in the presence of Ca^{2+}. Improved retention of
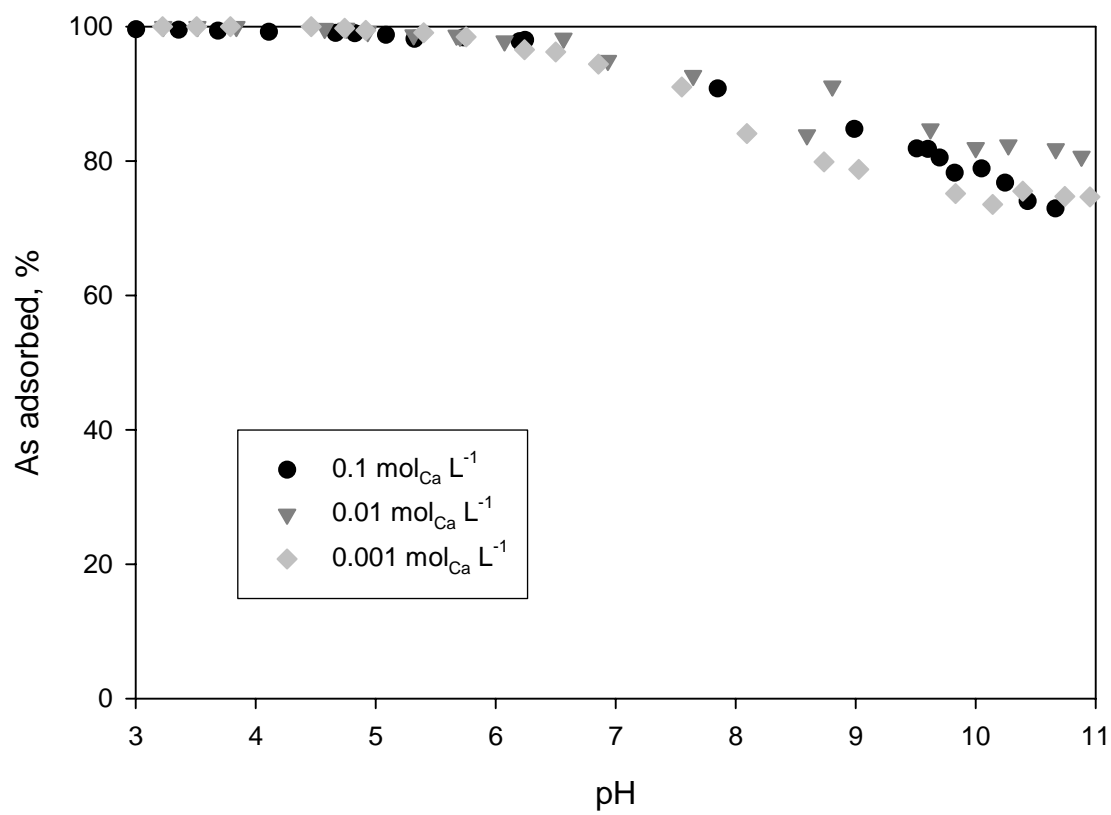
Figure 62. Adsorption envelopes of As^V with the 0:1 Al:Fe hydroxide at 0.1:1 As:(Al+Fe) molar ratio as affected by Ca counterion concentration.
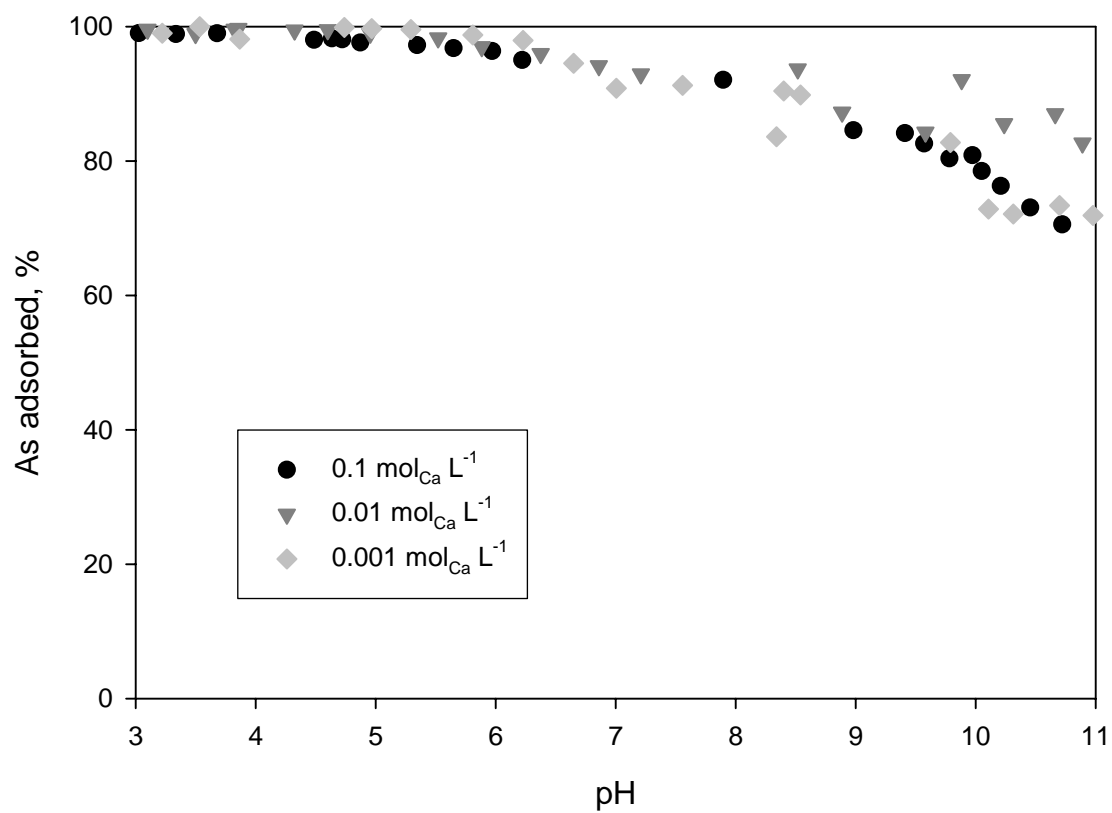
Figure 63. Adsorption envelopes of As^V with the 2:8 Al:Fe hydroxide at 0.1:1 As:(Al+Fe) molar ratio as affected by Ca counterion concentration.
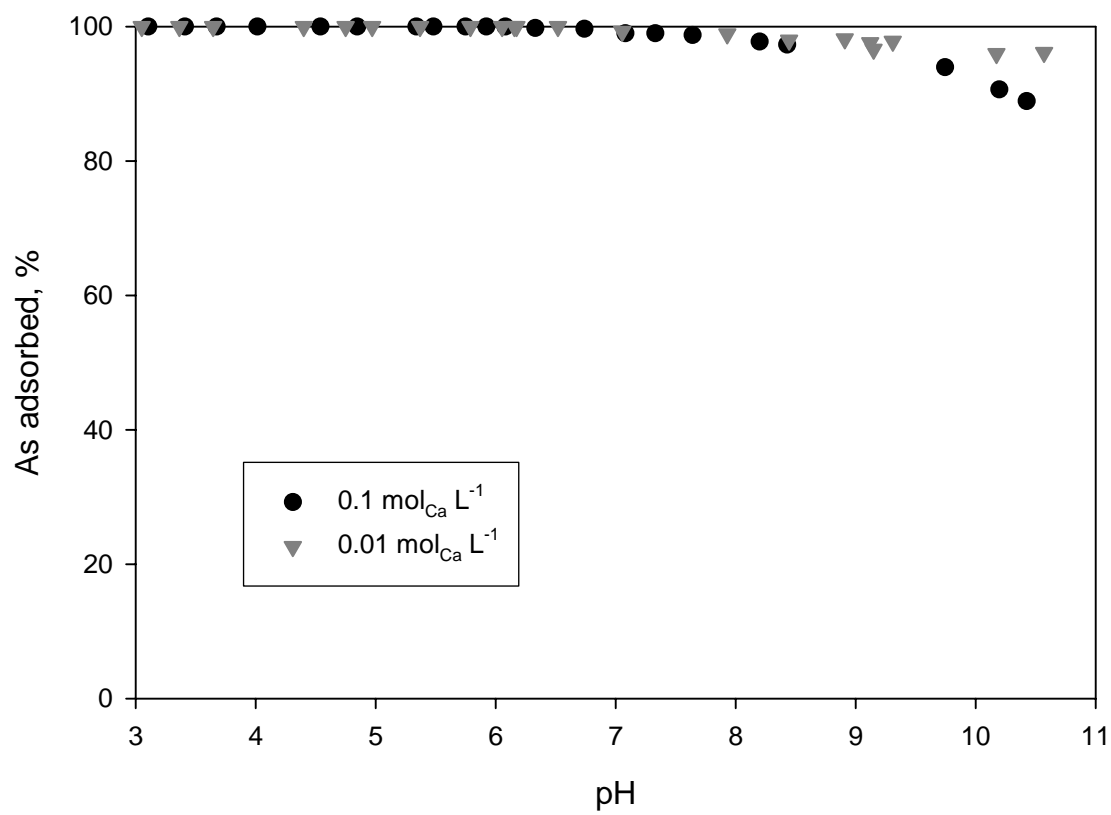
Figure 64. Adsorption envelopes of As^V with the 0:1 Al:Fe hydroxide at 0.025:1 As:(Fe+Al) molar ratio as affected by Ca counterion concentration.
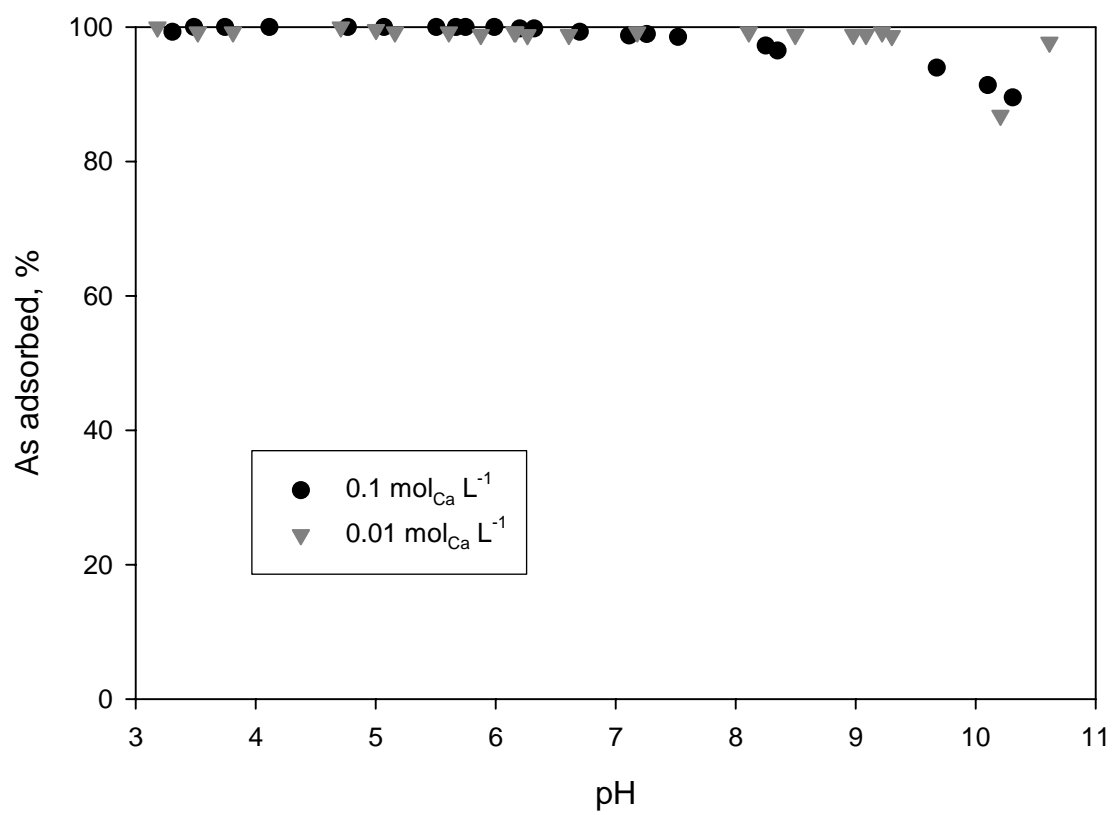
Figure 65. Adsorption envelopes of As^V with the 2:8 Al:Fe hydroxide at 0.025:1 As:(Fe+Al) molar ratio as affected by Ca counterion concentration.
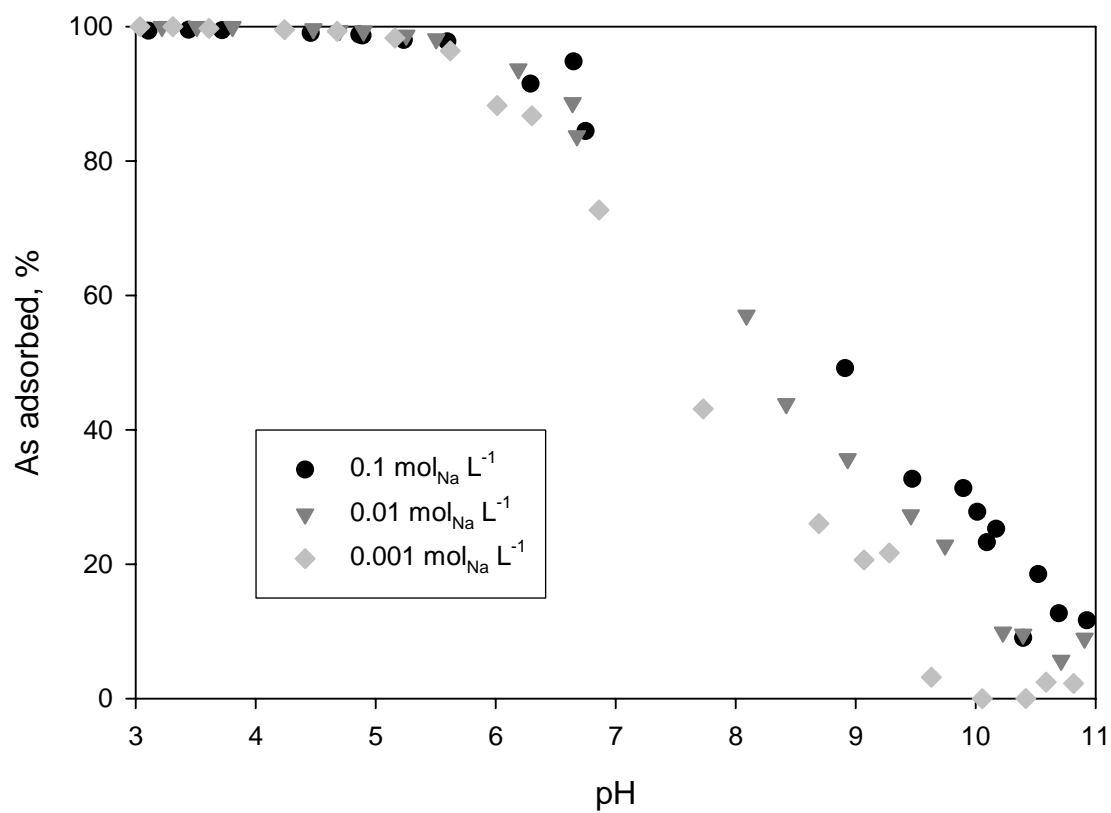
Figure 66. Adsorption envelopes of As^V with the 0:1 Al:Fe hydroxide at 0.1:1 As:(Fe+Al) molar ratio as affected by Na counterion concentration.
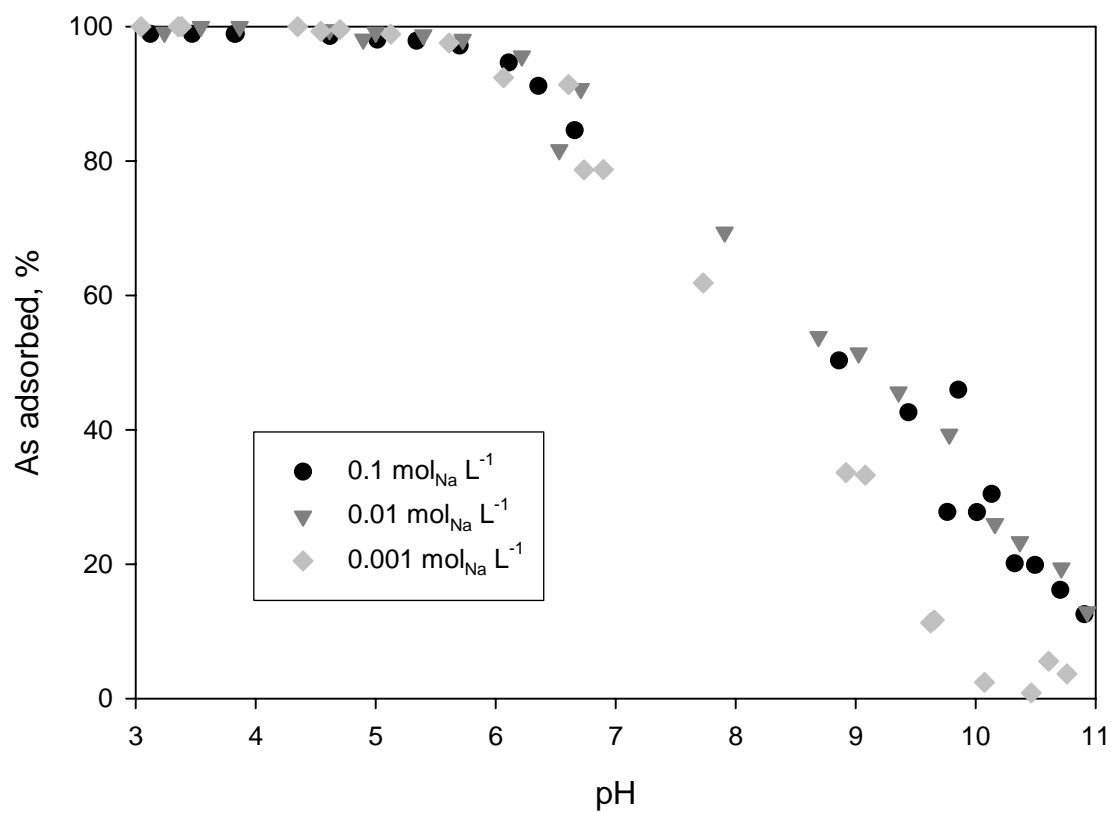
Figure 67. Adsorption envelopes of As^V with the 2:8 Al:Fe hydroxide at 0.1:1 As:(Fe+Al) molar ratio as affected by Na counterion concentration.
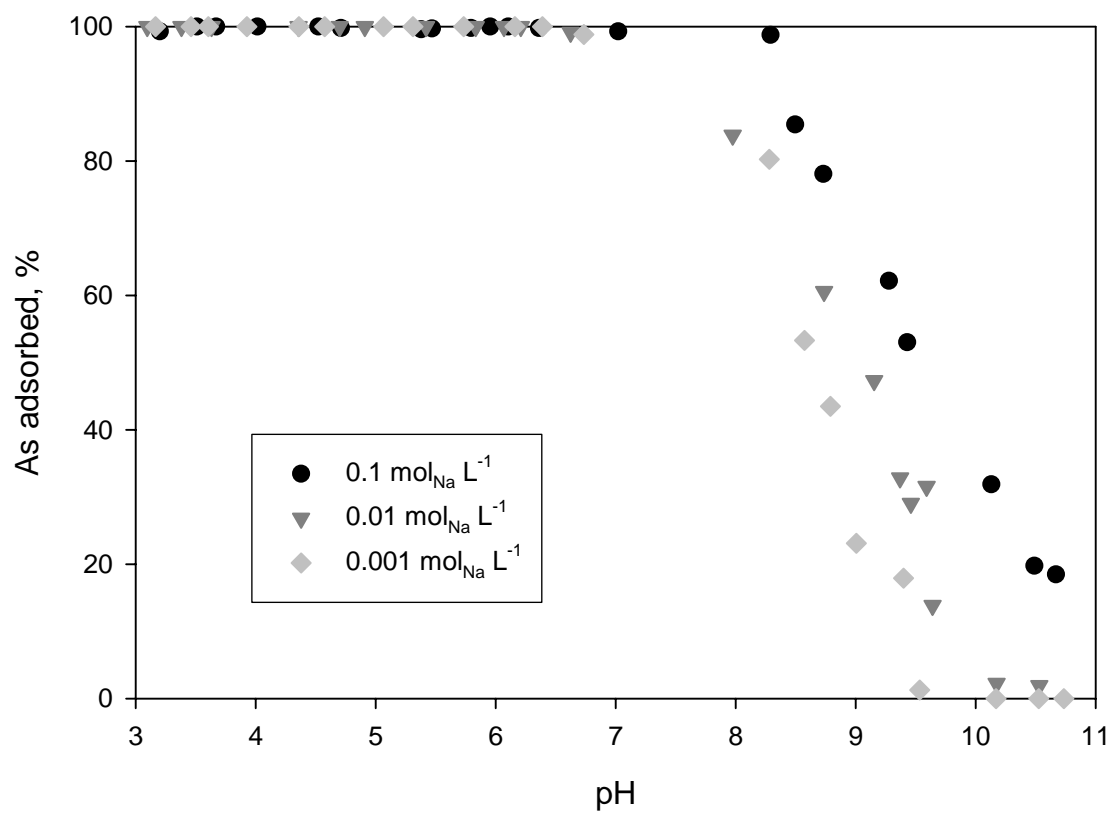
Figure 68. Adsorption envelopes of As^{V} with the 0:1 Al:Fe hydroxide at 0.025:1 As:(Fe+Al) molar ratio as affected by Na counterion concentration.
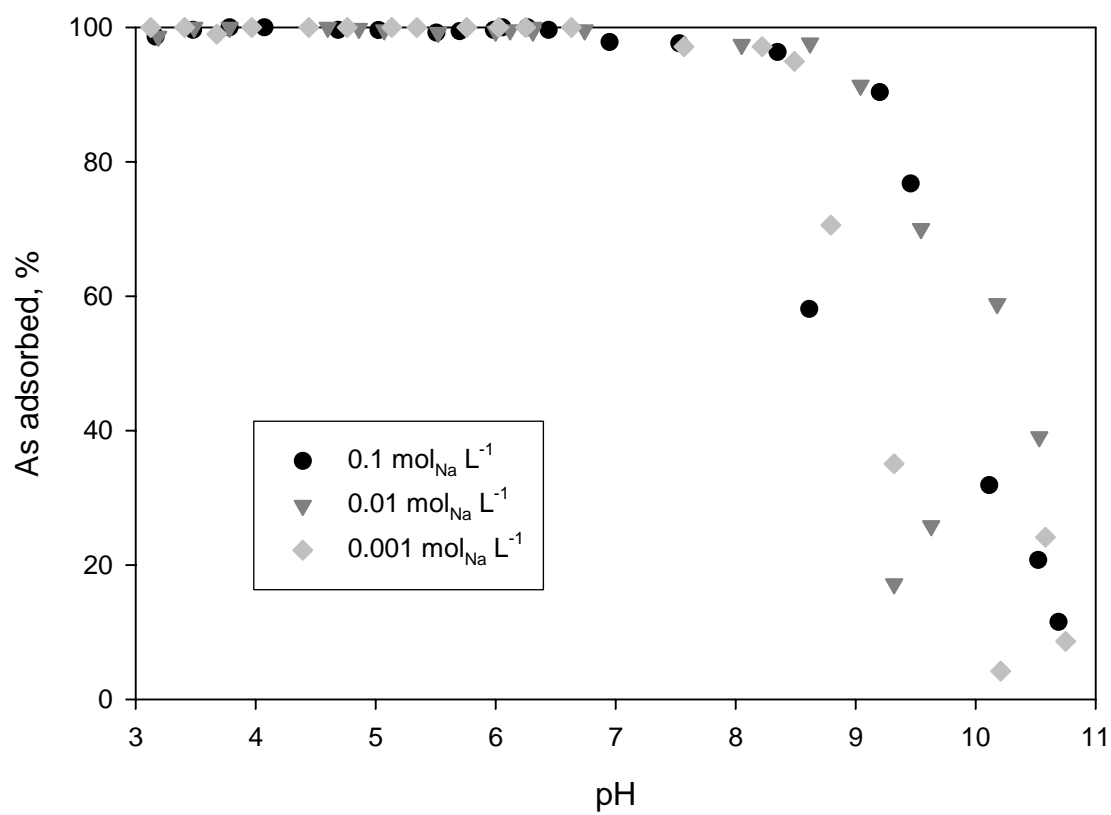
Figure 69. Adsorption envelopes of As^V with the 2:8 Al:Fe hydroxide at 0.025:1 As:(Fe+Al) molar ratio as affected by Na counterion concentration.

As^V by both Fe and Al hydroxides in the presence of Ca^{2+} was also reported by

(Goldberg and Johnson, 2001).

Hypotheses

There are three possible scenarios by which Ca^{2+} could enhance the adsorption of

As^V: (i) precipitation of Ca arsenate, (ii) cation bridging by Ca^{2+}, and (iii) reduced

repulsive potentials in the presence of counterion Ca^{2+}. The formation of Ca arsenate has

been reported at high pH (pH > 7.3) (Bothe and Brown, 1999). Jing et al. (2003)

observed the reduced mobility of As from cement treated Fe sludge at pH 11.32, due to

the formation of Ca arsenate. The formation of Ca arsenate has pH and Ca/As molar

ratio requirements as summarized in Table 3 (Bothe and Brown, 1999). For example, the

Ca/As molar ratio needs to be 1.5 −1.67 and pH needs to be in the range of 7.32 − 11.18

to form $Ca_3(AsO_4)_2 \cdot 32/3H_2O$ or $Ca_3(AsO_4)_2 \cdot 41/4H_2O$ (Bothe and Brown, 1999). Other

forms of Ca arsenate require even higher pH (pH > 9.77). In the current experiment, the

differences in As^V retention due counterion were observed to start at approximately pH 6.

When the net charge of the hydroxide surface is negative, Ca^{2+} could possibly

function as a bridge for the adsorption of negatively charged As^V (Figure 70). This

cation bridging could possibly enhance the retention of As^V; however, Parks et al. (2003)

eliminated this possibility by diffuse layer modeling. They concluded that the thinner

diffuse double layer formed by Ca^{2+} compared to Na^+ minimizes the repulsive potential

between the negatively charged hydroxide surface and the negatively charged As^V;

therefore, Ca^{2+} improves the retention of As^V on Al and Fe hydroxides (Figure 71).

Spectroscopic evidence will be required to verify the mechanism of enhanced As^V

retention in the presence of Ca^{2+}.

-

- Ca^{2+} ⋯⋯ $HAsO_4^{2-}$

-

-

-

- Ca^{2+} ⋯⋯ $H_2AsO_4^{-}$

-
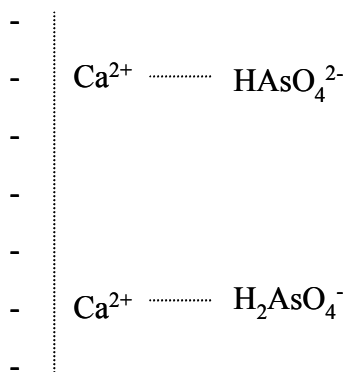
Figure 70. Cation bridging by Ca^{2+}.
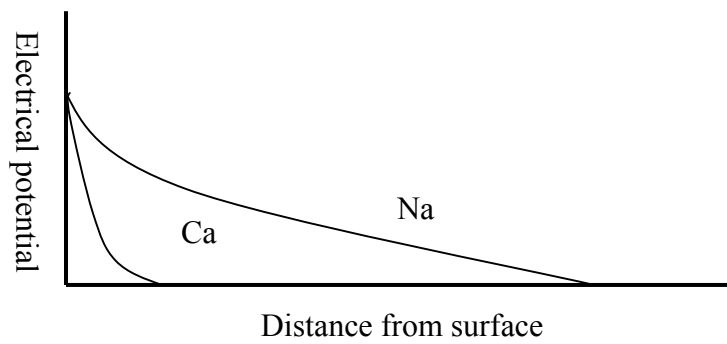
Figure 71. The diffuse double layers of Ca^{2+} vs. Na^{+}.

Desorption Envelopes of Arsenic

Desorption behavior of As^V and As^{III} with phosphate as the desorbing ion was studied at 375 : 0.05 : 1 P:As:(Al+Fe) molar ratio. Desorption of As^{III} from the 1:0 Al:Fe hydroxide was not studied because As^{III} was not adsorbed by the 1:0 Al:Fe hydroxides at any pH (Figure 54).

Most of the added As^V was adsorbed by the Fe-containing hydroxides during the adsorption stage of the experiment; however, only 49.4 % of the As^V was adsorbed on the 1:0 Al:Fe hydroxide (Table 11). Desorption of As^V by mechanical agitation of the aqueous suspension was negligible with the Fe-containing hydroxides; however, 1.2 % of the adsorbed As^V was desorbed from the 1:0 Al:Fe hydroxide during the 24 h shaking with deionized water (DIW). Adsorption of As^{III} was never 100 %, and As^{III} adsorption increased as Al:Fe molar ratio was decreased, as expected from the previous adsorption isotherm study. A significant amount of As^{III} was desorbed during mechanical agitation of the aqueous suspension, and As^{III} desorption in DIW increased as Al:Fe molar ratio was increased (Table 12). This trend reflects the differences in retention mechanism of As^V and As^{III} on Al and Fe hydroxides. The predominant mode of retention of As^V and As^{III} on Fe hydroxides is by formation of an inner-sphere bidentate binuclear surface complex (Manning et al., 1998; Waychunas et al., 1993), although outer-sphere complexation of As^{III} has also been observed (Goldberg and Johnson, 2001). As^V forms inner-sphere complexes with amorphous Al hydroxide, but As^{III} forms only outer-sphere complexes (Goldberg and Johnson, 2001).

Table 11. Proportion of As^V adsorbed during the 24 h adsorption reaction before phosphate desorption (A), proportion of adsorbed As^V after 24 h shaking with deionized water (DIW) (B), and proportion of As^V desorbed during 24 h shaking with deionized water.

Adsorbent Al:Fe	As^V adsorbed during 24 h adsorption (A)	As^V adsorbed after 24 h desorption with DIW (B)	As^V desorbed after 24 h desorption with DIW (A) - (B)
		%	
0:1	99.8	99.9	0
2:8	99.7	99.6	0.1
5:5	98.8	98.5	0.3
1:0	49.4	48.2	1.2

Table 12. Proportion of As^{III} adsorbed during the 24 h adsorption reaction before phosphate desorption (A), proportion of adsorbed As^{III} after 24 h shaking with deionized water (DIW) (B), and proportion of As^{III} desorbed during 24 h shaking with deionized water.

Adsorbent Al:Fe	As^{III} adsorbed during 24 h adsorption (A)	As^{III} adsorbed after 24 h desorption with DIW (B)	As^{III} desorbed after 24 h desorption with DIW (A) - (B)
		%	
0:1	91	88.3	2.7
2:8	79.5	75.8	3.7
5:5	66.4	57.3	9.1

Neither As^V nor As^{III} was completely desorbed by phosphate from the Fe-containing hydroxides, at any Al:Fe molar ratio and at any pH value within the range of 3 to 11; however, As desorption was always > 50% (Figure 72 and Figure 73). In general, As^V exhibited similar desorption patterns regardless of Al:Fe molar ratio, except that the most As^V was desorbed from the 1:0 Al:Fe hydroxide at each pH (Figure 72). Minimum As^V desorption was observed in the pH range of 5 to 9 with, increasing desorption at both lower and higher pH values. Desorption of As^V increased slightly as Al:Fe molar ratio was increased. The adsorption envelopes (Figure 52) indicated that adsorption of As^V was approximately quantitative in the pH range of 3 to 6.5 at the identical As:(Al+Fe) molar ratio as used in this experiment; therefore, surface sites were available for quantitative As^V adsorption under this condition. Phosphate and As^V have similar chemical characteristics. For example, H_3PO_4 and H_3AsO_4 have similar pKa values: the pKa values of H_3PO_4 are 2.15, 7.20, and 12.35, and those of H_3AsO_4 are 2.20, 6.97, and 11.53. At pH >8, As^V desorption might have been influenced by electrostatic repulsion as the negative charge character of both the hydroxide surface and the As^V species were increasing.

The As^{III} desorption trend was relatively independent of Al:Fe molar ratio; however, As^{III} desorption slightly increased as Al:Fe molar ratio was increased (Figure 73). The similar desorption trends might be attributable to the probability that in all cases the As^{III} was likely adsorbed to surface Fe^{III}, according to the previous adsorption isotherm study. The minimum desorption of As^{III} was observed at approximately pH 9.5, which corresponds with the pH of maximum As^{III} adsorption by Fe hydroxide (Figure 54; also, Ferguson and Anderson, 1974, and Raven et al., 1998). Both the adsorption
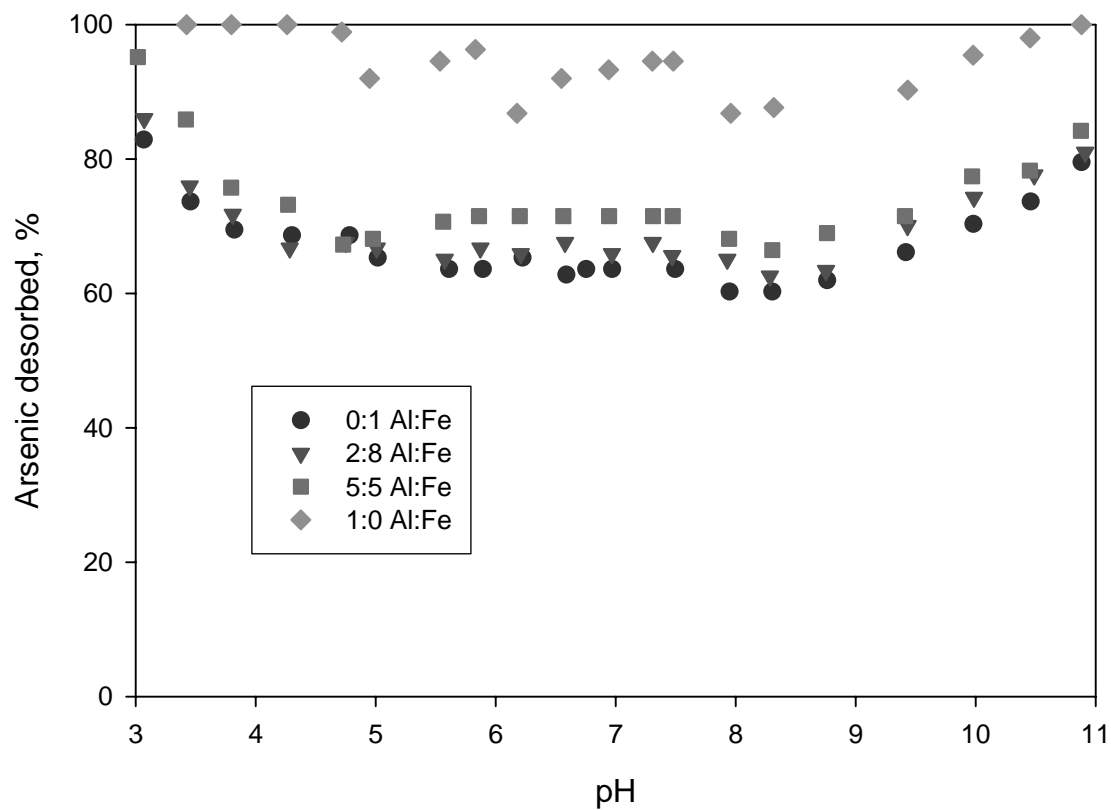
Figure 72. Desorption envelopes of As^V with sodium phosphate solution at 375 : 0.05 : 1 P:As:(Al+Fe) molar ratio, as affected by Al:Fe molar ratios.
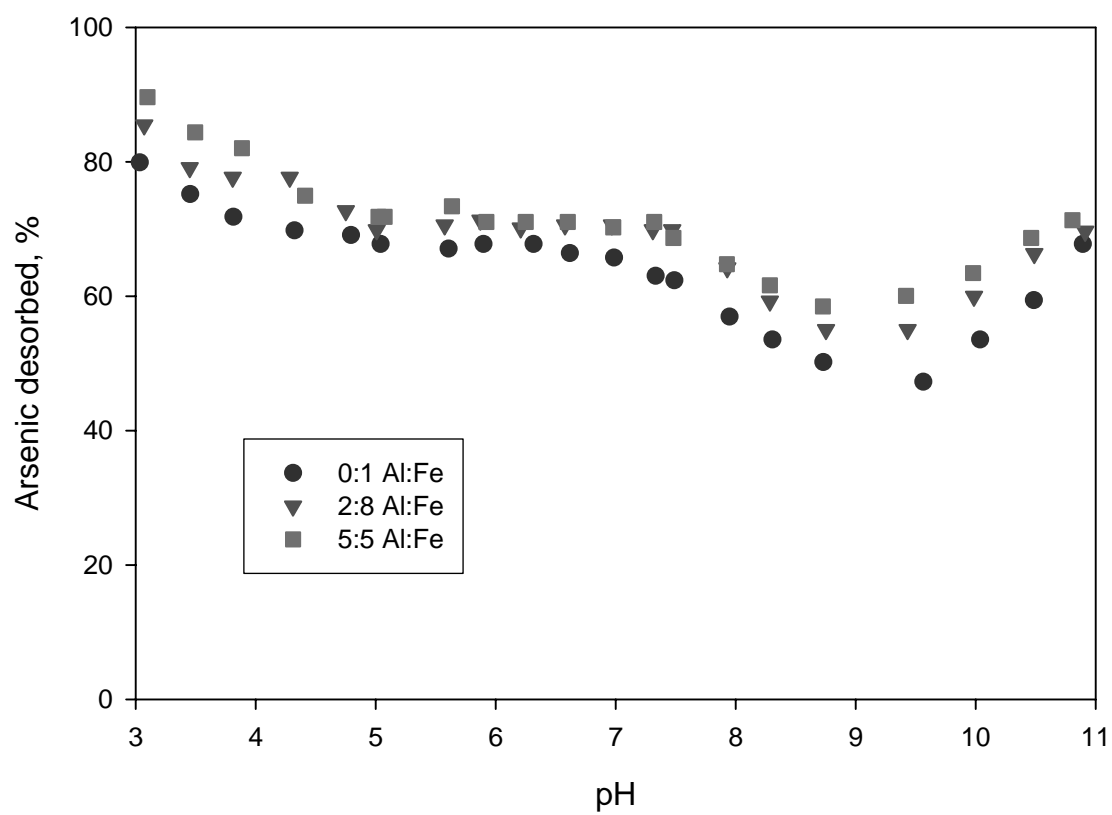
Figure 73. Desorption envelopes of As^{III} with sodium phosphate solution at 375 : 0.05 : 1 P:As:(Al+Fe) molar ratio, as affected by Al:Fe molar ratios.

maximum and the desorption minimum of As^{III} correspond approximately with the pKa_1

of As^{III} of 9.2. In general, As^V was desorbed more readily than As^{III} above pH 7.5;

whereas, As^{III} was desorbed more efficiently below pH 7.5 (Figures 74 –76).
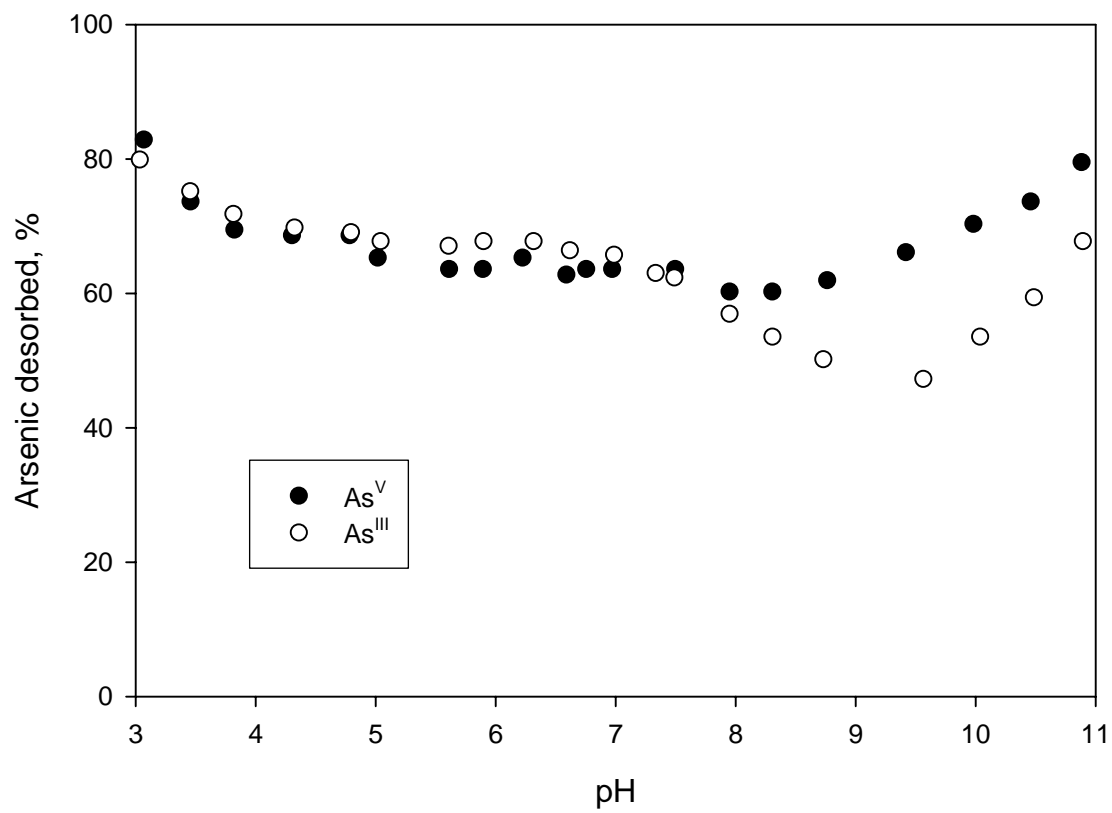
Figure 74. Desorption envelopes of As^V and As^{III} with sodium phosphate solution at 375 : 0.05 : 1 P:As:Fe molar ratio with the 0:1 Al:Fe hydroxide.
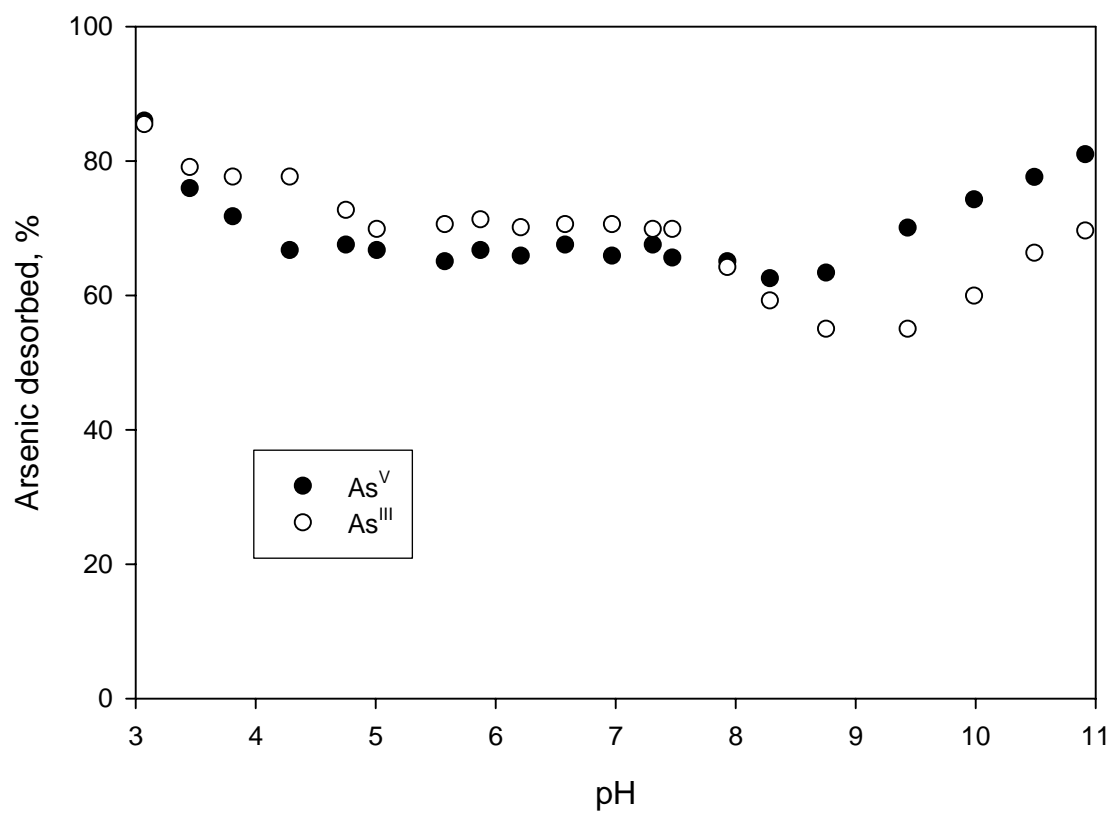
Figure 75. Desorption envelopes of As^{V} and As^{III} with sodium phosphate solution at 375 : 0.05 : 1 P:As:(Fe+Al) molar ratio with the 2:8 Al:Fe hydroxide.
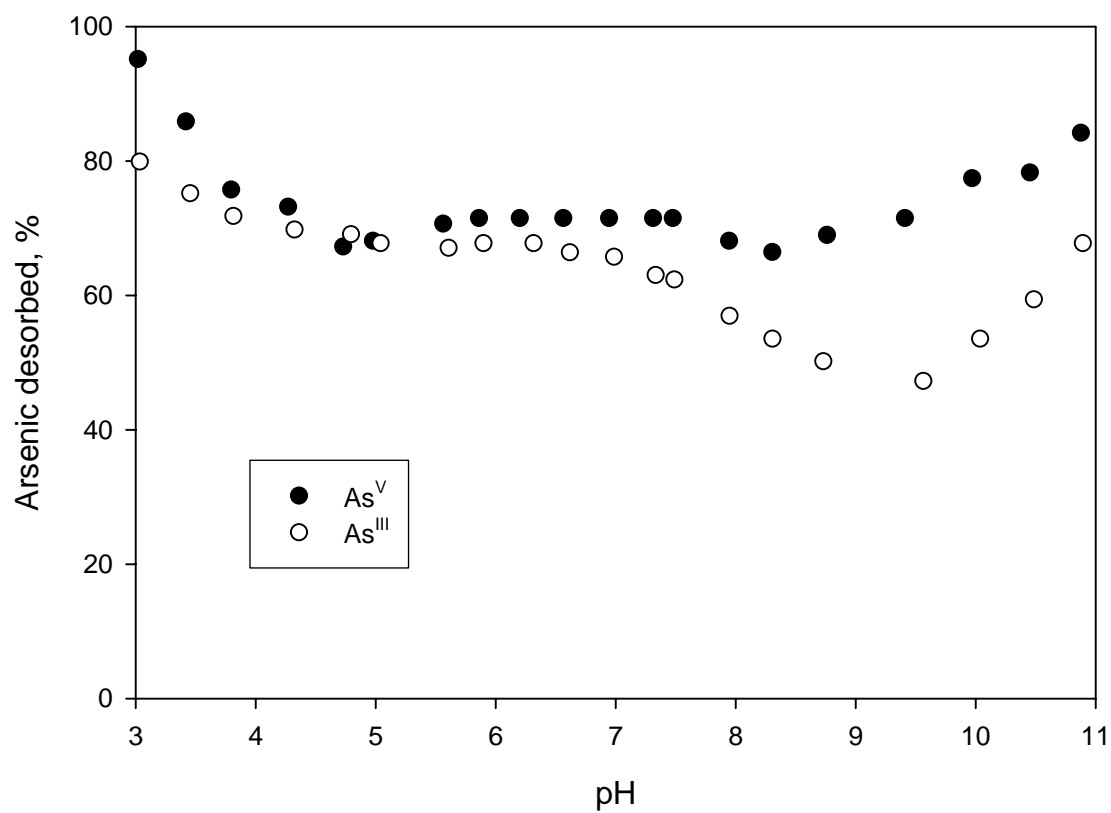
Figure 76 . Desorption envelopes of As^V and As^{III} with sodium phosphate solution at 375 : 0.05 : 1 P:As:(Fe+Al) molar ratio with the 5:5 Al:Fe hydroxide.

CONCLUSIONS

Mineralogy and Stability of the Hydroxides as Affected by Al:Fe Molar Ratio

Particle size, crystallinity, and morphology of aggregates are affected by Al:Fe molar ratio. Data collected in XRD and TEM studies indicated that Al substitution in ferrihydrite results in smaller particle size and less dense aggregates compared to pure ferrihydrite. The maximum quantitative Al substitution in the poorly crystalline ferrihydrite structure was up to approximately 20 %. The relative stability of the 2:8 Al:Fe hydroxide relative to pure ferrihydrite indicates that maximum stability of ferrihydrite might be achieved when the structure is slightly relaxed because of the smaller size of Al^{3+} than Fe^{3+}. Once the Al content exceeded the maximum substitution level, gibbsite and bayerite are formed. Location of Al in the ferrihydrite structure might greatly affect the adsorption of As; therefore, further study of the local distribution of Al is needed. In soils in which most of the ferrihydrite is Al substituted, Al in the structure is likely a major factor contributing to ferrihydrite solubility and its transformation into crystalline phases.

Adsorption of As^V and As^{III} as Affected by Al:Fe Molar Ratio

Differences in adsorption of As^V and As^{III} as affected by Al:Fe molar ratio of the hydroxide were observed. When Al was completely substituted in the poorly crystalline Fe hydroxide structure, the difference in As^V adsorption behavior compared to that of pure ferrihydrite was negligible. Adsorption of As^V decreased as Al:Fe molar ratio increased once the maximum Al substitution in ferrihydrite was achieved. Because gibbsite and bayerite were detected in the Al:Fe hydroxide with more than 30 % Al, the cause of decrease in As^V adsorption was the lower concentration of surface sites for

adsorption. Although higher surface area might be expected with 2:8 Al:Fe hydroxide compared to pure ferrihydrite, adsorption of As^V with the 2:8 Al:Fe hydroxide did not exceed that of pure ferrihydrite.

The adsorption maximum of As^{III} decreased approximately 4 % with a 10 % increase in Al content, even when Al was completely substituted in the structure of the ferrihydrite. This phenomenon is indicative of different modes of bonding on As^V and As^{III} on Al:Fe hydroxides. There might be a difference in bonding strength of As^{III} on Al within an Al:Fe hydroxide compared to pure Al hydroxides, since reduction of As^{III} adsorption should have been proportional to the increase in Al content. A possible heterogeneous distribution of Al in the structure might also influence the As^{III} adsorption behavior. A spectroscopic study would be useful to understand the local chemistry of bonding. In addition, a better understanding of the distribution of Al within ferrihydrite would help to elucidate the adsorption behavior of As^{III} on Al:Fe hydroxides.

The retention of As^V at pH > 7 was significantly improved in the presence of the counterion Ca^{2+} compared to Na^+, probably due to the more rapid decay in repulsive potential with distance from the surface with the former system. Counterion concentration did not significantly affect As^V adsorption. The negligible influence of counterion concentration is indicative of inner-sphere complexation.

Desorption of As^V and As^{III} as Affected by Al:Fe Molar Ratio

Phosphate desorbed both As^V and As^{III} from all Al:Fe hydroxides; however, quantitative desorption was never obtained. The efficiencies of As^V and As^{III} extraction by phosphate were lowest at pH 5 to 9 and pH 9.5, respectively. In general, more As^V was desorbed compared to As^{III} above pH 7.5; whereas, As^{III} was desorbed more

efficiently below pH 7.5. Desorption of both As^V and As^{III} increased slightly with increase in Al:Fe molar ratio, which indicates that As adsorbed on the Al portion of the hydroxide might be more readily desorbed. The results of this study indicate that phosphate significantly enhanced the release potential of both As^V and As^{III}. In order to understand As release in natural systems, desorption of As with other oxyanions such as sulfate might to useful.

<h3 style="text-align:center">Implications to the Water Treatment</h3>

Effective water treatment requires the efficient removal of As and the secure disposal of waste. Effective removal of As^V can be achieved using either ferrihydrite or coprecipitated 2:8 Al:Fe hydroxide, as their adsorption behaviors were similar; however, removal of As^{III} is more effective with the pure Fe system. When As^{III} is present, oxidation of As^{III} into As^V would be required to optimize the removal of As in the Al/Fe system. The 2:8 Al:Fe molar ratio adsorbent is less soluble and more stable against transformation into crystalline phases, which is advantageous for waste disposal.

In a reduced environment as might exist at a waste disposal site, both As^V and Fe^{III} are subject to be reduced into As^{III} and Fe^{II}, respectively. Because Fe^{II} is soluble, Al hydroxide will remain when an Al/Fe system is used; however, the weak affinity of As^{III} on Al hydroxide as shown in this study and other studies (Goldberg, 1986; Weerasooriya et al., 2003) could contribute to As release. An increase of As release potential in a reduced environment cannot be avoided whether pure ferrihydrite, pure Al hydroxide or Al:Fe hydroxides are used.

The mineralogy of the hydroxides and adsorption/desorption behavior indicate the possible utility of coprecipitated Al:Fe hydroxides in wastewater treatment. According to

the results of this study, 2:8 is a preferred Al:Fe molar ratio for As removal. Overall, the chemistry of As with Al:Fe hydroxides is complex; therefore, further research is required. It will be beneficial to study the retention of As that is coprecipitated with Al:Fe hydroxides, to simulate the water treatment scenario. In addition, the relative impacts of Al and Fe on the reduction of As^V should be more thoroughly investigated. The impact of structural Al on the rate of Fe^{III} reduction is not known. There is a possibility that Al might slow the rate of the reduction of Fe^{III} into Fe^{II} by retarding the ease of electron transfer within the system, because Al is not affected by redox processes.

4

REFERENCES

Alam, M.G.M., S. Tokunaga, and T. Maekawa. 2001. Extraction of arsenic in a synthetic arsenic-contaminated soil using phosphate. Chemosphere 43:1035-1041.

Anawar, H.M., J. Akai, K.M.G. Mostofa, S. Safiullah, and S.M. Tareq. 2002. Arsenic poisoning in groundwater-health risk and geochemical sources in Bangladesh. Environ. Int. 27:597-604.

Anderson, M.A., J.F. Ferguson, and J. Gavis. 1976. Arsenate adsorption on amorphous aluminum hydroxide. J. Colloid Interface Sci. 54:391-399.

Arai, Y., E.J. Elzinga, and D.L. Sparks. 2001. X-ray absorption spectroscopic investigation of arsenite and arsenate adsorption at the aluminum oxide-water interface. J. Colloid Interface Sci. 235:80-88.

Bothe, V.J., and P.W. Brown. 1999. Arsenic immobilization by calcium arsenate formation. Environ. Sci. Technol. 33:3806-3811.

Bowden, J.W., A.M. Posner, and J.P. Quirk. 1977. Ionic adsorption on variable charge mineral surfaces. Theoretical-charge development and titration curves. Aust. J. Soil Res. 15:121-136.

Carrero, P., A. Malave, J.L. Burguera, M. Burguera, and C. Rondon. 2001. Determination of various arsenic species by flow injection hydride generation atomic absorption spectrometry: Investigation of the effects of the acid concentration of different reaction media on the generation of arsines. Anal. Chim. Acta 438:195-204.

Cheng, R.C., S. Liang, H.C. Wang, and M.D. Beuhler. 1994. Enhanced coagulation for arsenic removal. J. Am. Water Works Assoc. 86:79-90.

Cherry, J.A., A.U. Shaikh, D.E. Tallman, and R.V. Nicholson. 1979. Arsenic species as an indicator of redox conditions in groundwater. J. Hydrol. 43:373-392.

Colombo, C., and A. Violante. 1996. Effect of time and temperature on the chemical composition and crystallization of mixed iron and aluminum species. Clays Clay Miner. 44:113-120.

Cullen, W.R., and K.J. Reimer. 1989. Arsenic speciation in the environment. Chem. Rev. 89:713-764.

Davenport, J.R., and F.J. Peryea. 1991. Phosphate fertilizers influence leaching of lead and arsenic in a soil contaminated with lead arsenate. Water Air Soil Pollut. 57:101-110.

Dixit, S., and J.G. Hering. 2003. Comparison of arsenic(V) and arsenic(III) sorption onto iron oxide minerals: Implications for arsenic mobility. Environ. Sci. Technol. 37:4182-4189.

Edwards, M. 1994. Chemistry of arsenic removal during coagulation and Fe-Mn oxidation. J. Am. Water Works Assoc. 86:64-78.

Essington, M.E. 2004. Soil and water chemistry: An integrative approach. CRC Press, Boca Raton, FL.

Fendorf, S., M.J. Eick, P. Grossl, and D.L. Sparks. 1997. Arsenate and chromate retention mechanisms on goethite .1. Surface structure. Environ. Sci. Technol. 31:315-320.

Ferguson, J.F., and M.A. Anderson. 1974. Chemical forms of arsenic in water supplies and their removal, p. 137-158, *In* A. J. Rubin, (ed). Chemistry of water supply, treatment, and distribution. Ann Arbor, MI., Ann Arbor Science Publishers.

Fey, M.V., and J.B. Dixon. 1981. Synthesis and properties of poorly crystalline hydrated aluminous goethites. Clays Clay Miner. 29:91-100.

Francesconi, K., and D. Kuehnelt. 2002. Arsenic compounds in the environment, p. 51-94, *In* W. T. Frankenberger, (ed). Environmental chemistry of arsenic. Marcel Dekker, Inc., New York.

Goldberg, S. 1986. Chemical modeling of arsenate adsorption on aluminum and iron-oxide minerals, pp. 1154-1157 Soil Sci. Soc. Am. J., Vol. 50.

Goldberg, S., and C.T. Johnson. 2001. Mechanisms of arsenic adsorption on amorphous oxides evaluated using macroscopic measurements, vibrational spectroscopy, and surface complexation modeling. J. Colloid Interface Sci. 234:204-216.

Goyer, R.A., and T.W. Clarkson. 2001. Toxic effect of metals, p. 811-867, *In* C. D. Kalaassen, (ed). Casarett & Doull's Toxicology: The basic science of poisons, 6 ed. The McGraw-Hill Companies, Inc., New York.

Gulledge, J.H., and J.T. O'Connor. 1973. Removal of arsenic(V) from water by adsorption on aluminum and ferric hydroxides. J. Am. Water Works Assoc. 65:548-552.

Gupta, S.K., and K.Y. Chen. 1978. Arsenic removal by adsorption. J. Water Pollut. Control Fed. 50:493-506.

Hammer, M.J., and M.J.J. Hammer. 2001. Water and wastewater technology. 4 ed. Princeton-Hall, Inc., Upper Saddle River, NJ.

Harrison, J.B., and V.E. Berkheiser. 1982. Anion interactions with freshly prepared hydrous iron-oxides. Clays Clay Miner. 30:97-102.

Hering, J.G., P.Y. Chen, J.A. Wilkie, and M. Elimelech. 1997. Arsenic removal from drinking water during coagulation. J. Environ. Eng. 123:800-806.

Hering, J.G., P.Y. Chen, J.A. Wilkie, M. Elimelech, and S. Liang. 1996. Arsenic removal by ferric chloride. J. Am. Water Works Assoc. 88:155-167.

Hingston, F.J., A.M. Posner, and J.P. Quirk. 1971. Competitive adsorption of negatively charged ligands on oxide surfaces. Discuss. Faraday Soc. 52:334-342.

Hsia, T.H., S.L. Lo, and C.F. Lin. 1992. As(V) adsorption on amorphous iron oxide: triple layer modeling. Chemosphere 25:1825-1837.

Hsu, P.H. 1989. Aluminum hydroxides and oxyhydroxides, p. 331-378, *In* J. B. Dixon and S. B. Weed, (eds). Minerals in soil environments, 2 ed. SSSA, Madison, WI.

Huang, P.M., M.K. Wang, N. Kampf, and D.G. Schulze. 2002. Aluminum hydroxides, p. 261-289, *In* J. B. Dixon and D. G. Schulze, (eds). Soil mineralogy with environmental applications. SSSA, Madison, WI.

Inskeep, W.P., T.R. McDermott, and S. Fendorf. 2002. Arsenic (V)/(III) cycling in soils and natural water: Chemical and microbiological processes, p. 183-215, *In* W. T. Frankenberger, (ed). Environmental chemistry of arsenic. Marcel Dekker, New York.

Jackson, B.P., and W.P. Miller. 2000. Effectiveness of phosphate and hydroxide for desorption of arsenic and selenium species from iron oxides. Soil Sci. Soc. Am. J. 64:1616-1622.

Jain, A., and R.H. Loeppert. 2000. Effect of competing anions on the adsorption of arsenate and arsenite by ferrihydrite. J. Environ. Qual. 29:1422-1430.

Jain, A., K.P. Raven, and R.H. Loeppert. 1999. Response to comment on Arsenite and Arsenate adsorption on ferrihydrite: Surface charge reduction and net OH-release stochiometry. Environ. Sci. Technol. 33:3696-3696.

Jing, C.Y., G.P. Korfiatis, and X.G. Meng. 2003. Immobilization mechanisms of arsenate in iron hydroxide sludge stabilized with cement. Environ. Sci. Tchnol. 37:5050-5056.

Kosmas, C.S., D.P. Franzmeier, and D.G. Schulze. 1986. Relationship among derivative spectroscopy, color, crystallite dimensions, and Al substitution of synthetic goethites and hematites. Clays Clay Miner. 34:625-634.

Leist, M., R.J. Casey, and D. Caridi. 2000. The management of arsenic wastes: Problems and prospects. J. Hazardous Materials 76:125-138.

Lindsay, W.L. 1979. Chemical equilibria in soils. John Wiley & Sons, New York.

Liu, F., A. De Cristofaro, and A. Violante. 2001. Effect of pH, phosphate and oxalate on the adsorption/desorption of arsenate on/from goethite. Soil Sci. 166:197-208.

Loeppert, R.H., and W.P. Inskeep. 1996. Iron, *In* D. L. Sparks, (ed). Methods of soil analysis, part 3, chemical methods, Vol. 5, 3 ed. SSSA, Madison, WI.

Loeppert, R.H., A. Jain, M.A. Abd El-Haleem, and B.K. Biswas. 2002. Quantity and speciation of arsenic in soils by chemical extraction, *In* Y. Cai, (ed). Biogeochemistry of environmentally important elements. American Chemical Society, Washington, DC.

Manceau, A. 1995. The mechanism of anion adsorption on iron-oxides - evidence for the bonding of arsenate tetrahedra on free Fe(O,0H)(6) edges. Geochim. Cosmochim. Acta. 59:3647-3653.

Manning, B.A., and S. Goldberg. 1996. Modeling competitive adsorption of arsenate with phosphate and molybdate on oxide minerals. Soil Sci. Soc. Am. J. 60:121-131.

Manning, B.A., S.E. Fendorf, and S. Goldberg. 1998. Surface structures and stability of arsenic(III) on goethite: spectroscopic evidence for inner-sphere complexes. Environ. Sci. Technol. 32:2383-2388.

Masscheleyn, P.H., R.D. Delaune, and W.H. Patrick. 1991a. A hydride generation atomic absorption technique for arsenic speciation. J. Environ. Qual. 20:96-100.

Masscheleyn, P.H., R.D. Delaune, and W.H. Patrick. 1991b. Effect of redox potential and pH on arsenic speciation and solubility in a contaminated soil. Environ. Sci. Technol. 25:1414-1419.

McBride, B.C. 1997. A critique of diffuse double layer models applied to colloid and surface chemistry. Clays Clay Miner. 45:598-608.

McBride, M.B. 1994. Environmental chemistry of soils. Oxford University Press, New York.

Meng, X., G.P. Korfiatis, C. Jing, and C. Christodoulatos. 2001. Redox transformations of arsenic and iron in water treatment sludge during aging and TCLP extraction. Environ. Sci. Technol. 35:3476-3481.

Mott, C.J.B. 1981. Anion and ligand exchange, p. 179-219, *In* D. J. Greenland and M. H. B. Hayes, (eds). The chemistry of soil processes. John Wiley & Sons Ltd, Chichester, UK.

NRC. (National Research Council) 2001. Arsenic in drinking water National Academic Press, Washington, DC.

Nriagu, J.O. 2002. Arsenic poisoning through the ages, p. 1-26, *In* W. T. Frankenberger, (ed). Environmental chemistry of arsenic. Marcel Dekker, Inc., New York.

Paige, C.R., W.J. Snodgrass, R.V. Nicholson, and J.M. Scharer. 1996. The crystallization of arsenate-contaminated iron hydroxide solids at high pH. Water Environ. Res. 68:981-987.

Parks, J.L., J. Novak, M. Macphee, C. Itle, and M. Edwards. 2003. Effect of Ca on As release from ferric and alum residuals. J. Am. Water Works Assoc. 95:108-118.

Pierce, M.L., and C.B. Moore. 1982. Adsorption of arsenite and arsenate on amorphous iron hydroxide. Water Res. 16:1247-1253.

Raven, K.P., A. Jain, and R.H. Loeppert. 1998. Arsenite and arsenate adsorption on ferrihydrite: kinetics, equilibrium, and adsorption envelopes. Environ. Sci. Technol. 32:344-349.

Reed, B.E., and M.R. Matsumoto. 1993. Modeling cadmium adsorption by activated carbon using the Langmuir and Freundlich isotherm expressions. Separation science and technology. 28:2179-2195.

Sadiq, M. 1997. Arsenic chemistry in soils: An overview of thermodynamic predictions and field observations. Water Air Soil Pollut. 93:117-136.

Samanta, G., T.r. Chowdhury, B.K. Mandal, B.K. Biswas, U.K. Chowdhury, g.K. Basu, C.r. Chanda, D. Lodh, and D. Chakraborti. 1999. Flow injection hydride generation atomic absorption spectrometry for determination of arsenic in water and biological samples from arsenic-affected districts of West Bengal, India, and Bangladesh. Microchem. J. 62:174-191.

Schulze, D.G. 1984. The influence of aluminum on iron oxides. VIII. Unit-cell demensions of Al-substituted goethites and estimation of Al from them. Clays Clay Miner. 32:36-44.

Schulze, D.G., and U. Schwertmann. 1984. The influence of aluminum on iron oxides: X. Properties of Al-substituted goethite. Clay Miner. 19:521-539.

Schwertmann, S., and R.M. Taylor. 1989. Iron oxides, p. 379-438, *In* J. B. Dixon and S. B. Weed, (eds). Minerals in soil environment, 1 ed. SSSA, Madison, WI.

Schwertmann, U., and R.M. Cornell. 1991. Iron oxides in the laboratory: Preparation and characterization VCH, New York.

Schwertmann, U., and E. Murad. 1983. Effect of pH on the formation of goethite and hematite from ferrihydrite. Clays Clay Miner. 31:277-284.

Schwertmann, U., J. Friedl, H. Stanjek, and D.G. Schulze. 2000. The effect of Al on Fe oxides. XIX. Formation of Al-substituted hematite from ferrihydrite at 25°C and pH 4 to 7. Clays Clay Miner. 48:159-172.

Smedley, P.L., and D.G. Kinniburgh. 2002. A review of the source, behaviour and distribution of arsenic in natural waters. Appl. Geochem. 17:517-568.

Smith, A.H., P.A. Lopipero, M.N. Bates, and C.M. Steinmaus. 2002a. Public health - Arsenic epidemiology and drinking water standards. Science 296:2145-2146.

Smith, A.H., C. Hopenhayn-Rich, M.N. Bates, H.M. Goeden, I. Hertz-Picciotto, H.M. Duggan, R. Wood, M.J. Kosnett, and M.T. Smith. 1992. Cancer risks from arsenic in drinking water. Environ Health Persp. 97:259-267.

Smith, E., R. Naidu, and A.M. Alston. 2002b. Chemistry of inorganic arsenic in soils: II. Effect of phosphorous, sodium, and calcium on arsenic sorption. J. Environ. Qual. 31:557-563.

Sparks, D.L. 2003. Environmental soil chemistry. 2nd ed. Academic Press, San Diego, CA.

Sun, X.H., and H.E. Doner. 1996. An investigation of arsenate and arsenite bonding structure on goethite by FTIR. Soil Sci. 161:865-872.

Tokunaga, S., S. Yokoyama, and S.A. Wasay. 1999. Removal of Arsenic(III) and Arsenic(V) Ions from Aqueous Solutions with Lanthanum(III) Salt and Comparison with Aluminum(III), Calcium(II), and Iron(III) Salts. Water Environ. Res. 71:299-306.

USEPA. (United States Environmental Protection Agency) 2001. 40 CRF parts 9, 141, and 142, National Primary Drinking Water Regulations; Arsenic and Clarifications to Compliance and New Source Contaminant Monitoring; Proposed Rule. Fe Regist 66, Washington, DC.

Van Raij, B., and M. Peech. 1972. Electrochemical properties of some oxisols and alfisols of the tropics. Soil Sci. Soc. Am. Proc. 36:587-593.

Veith, J.A., and G. Sposito. 1977. On the use of the Langmuir equation in the interpretation of "adsorption" phenomena. Soil Sci. Soc. Am. J. 41:697-702.

Violante, A., P. Massimo, and R. Raffaella. 2002. Factors affecting arsenate adsorption/desorption on/from variable charge minerals and soils, Thailand.

Wagman, D.D., H.H. Evans, V.B. Parker, R.H. Schumm, I. Harlow, S.M. Bailey, K.L. Churney, and R.L.J. Butall. 1982. The NBS tables of chemical thermodynamic properties - selected values for inorganic and C-1 and C-2 organic-substances in SI units. J. Phys. Chem. Ref. Data 11:392.

Waychunas, G.A., B.A. Rea, C.C. Fuller, and J.A. Davis. 1993. Surface chemistry of ferrihydrite, Part l. EXAFS studies of the geometry of coprecipitated and adsorbed arsenate. Geochim. Cosmochim. Acta. 57:2251-69.

Weerasooriya, R., H.J. Tobschall, H.K.D.K. Wijesekara, E.K.I.A.U.K. Arachchige, and K.A.S. Pathiratne. 2003. On the mechanistic modeling of As(III) adsorption on gibbsite. Chemosphere 51:1001-1013.

Wefers, K., and G.B. Bell. 1972. Oxides and hydroxides of aluminum: Technical paper No. 19. Alcoa, East St. Louis, IL.

Woolson, E.A., J.H. Axley, and P.C. Kearne. 1973. Chemistry and phytotoxicity of arsenic in soils: Effects of time and phosphorous. Soil Sci. Soc. Am. J. 37:254-259.

Yang, C. 1998. Statistical mechanical study on the Freundlich isotherm equation. J. Colloid Interface Sci. 208:379-387.

VITA

Yoko Masue received her B.S. in plant and environmental soil sciences at Texas A&M University in College Station, Texas in August 2002. After graduating, she worked as a research assistant at Texas A&M University in pursuit of her M.S. degree in soil science under the direction of Dr. R. H. Loeppert. During her study, she taught undergraduate introductory soil science laboratories in 2003 under Dr. C.T. Hallmark. Additionally, she has presented her thesis research at the 7th International Conference on the Biogeochemistry of Trace Elements in Uppsala, Sweden, in June 2003, and the American Society of Agronomy meeting in Denver, Colorado in November 2003. In September 2004, she will begin work on her Ph.D. in geological and environmental sciences at Stanford University in Stanford, California.

Permanent Address: 1-12-3 Kanaiwanishi, Kanazawa-shi, Ishikawa-ken, 920-0337, Japan